AD-A185 716 ANALYTICAL INVESTIGATIONS OF BULK WAVE RESONATORS IN THE PIEZOELECTRIC TH..(U) RENSSELAER POLYTECHNIC INST TROY NY DEPT OF MECHANICAL ENGINE.. H F TIERSTEN 1/1

UNCLASSIFIED 20 JUL 87 AFOSR-TR-87-1233 $AFOSR-84-0351 F/G 9/5 NL

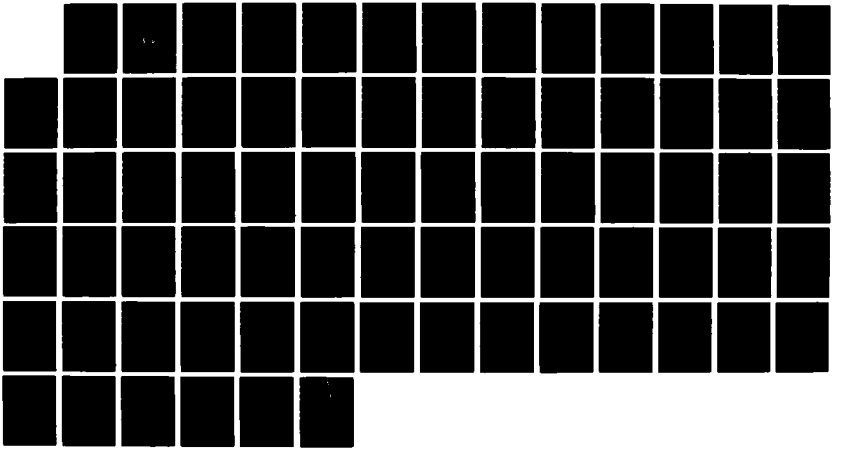

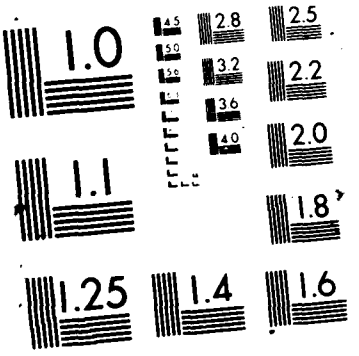
1.0
1.1
1.25
1.4
1.6
1.8
2.0
2.2
2.5
2.8
3.2
3.6
4.0
4.5
5.0
5.6

AFOSR-TR- 87-1233

Final Report on Analytical Investigations of Bulk Wave Resonators in the Piezoelectric Thin Film on Gallium-Arsenide Configuration

Harry F. Tiersten

July 1987

Unclassified

SECURITY CLASSIFICATION OF THIS PAGE

ADA185716

REPORT DOCUMENTATION PAGE

1a. REPORT SECURITY CLASSIFICATION: Unclassified	1b. RESTRICTIVE MARKINGS
2a. SECURITY CLASSIFICATION AUTHORITY	3. DISTRIBUTION/AVAILABILITY OF REPORT: Approved for public release; distribution unlimited.
2b. DECLASSIFICATION/DOWNGRADING SCHEDULE	
4. PERFORMING ORGANIZATION REPORT NUMBER(S)	5. MONITORING ORGANIZATION REPORT NUMBER(S): AFOSR-TR- 87-1233
6a. NAME OF PERFORMING ORGANIZATION: Rensselaer Polytechnic Institute; 6b. OFFICE SYMBOL (If applicable):	7a. NAME OF MONITORING ORGANIZATION: Air Force Office of Scientific Research
6c. ADDRESS (City, State and ZIP Code): Department of Mechanical Engineering, Aeronautical Engineering & Mechanics, Troy, NY 12180-3590	7b. ADDRESS (City, State and ZIP Code): Bolling Air Force Base, Bldg. 410, BAFB DC 20332
8a. NAME OF FUNDING/SPONSORING ORGANIZATION: AFOSR; 8b. OFFICE SYMBOL (If applicable): NE	9. PROCUREMENT INSTRUMENT IDENTIFICATION NUMBER: ~~Grant~~ No. AFOSR-84-0351
8c. ADDRESS (City, State and ZIP Code): Bolling Air Force Base, Bldg. 410, BAFB DC 20332	10. SOURCE OF FUNDING NOS.

PROGRAM ELEMENT NO.	PROJECT NO.	TASK NO.	WORK UNIT NO.
61102F	2306	B2	

11. TITLE (Include Security Classification) (over)

12. PERSONAL AUTHOR(S): Harry F. Tiersten

13a. TYPE OF REPORT	13b. TIME COVERED	14. DATE OF REPORT (Yr., Mo., Day)	15. PAGE COUNT
Final	FROM 9/1/84 TO 5/31/87	1987, July, 28	71

16. SUPPLEMENTARY NOTATION

17. COSATI CODES		
FIELD	GROUP	SUB. GR.

18. SUBJECT TERMS (Continue on reverse if necessary and identify by block number): Piezoelectricity; Elasticity; Resonators; Bulk Waves; Thin Films; Semiconductor Wafers; Composite Resonators; Energy Trapping; Radiation; Quality Factor; Plate Vibrations; (over)

19. ABSTRACT (Continue on reverse if necessary and identify by block number)

Trapped energy modes in the piezoelectric thin film on semiconductor composite resonator are explained and contrasted with modes that do not trap energy. The results of calculations of the quality factor of the fundamental essentially thickness-extensional mode in the composite resonator due to radiation into the bulk semiconductor wafer are discussed. The combination of materials considered was aluminum-nitride on gallium-arsenide. The calculations show that when trapping is not present the quality factor is a very rapidly varying function of the ratio of the composite resonator thickness to the wafer thickness and that the range of variation is very large, i.e., between one and two orders of magnitude. The calculations also reveal that when trapping is present the quality factor is always much larger and its range of variation with thickness ratio much smaller than when trapping is not present.

It is noted that the direct calculation procedure is extremely cumbersome to use, but that it is required to check the accuracy of a perturbation procedure which is much easier

20. DISTRIBUTION/AVAILABILITY OF ABSTRACT	21. ABSTRACT SECURITY CLASSIFICATION
UNCLASSIFIED/UNLIMITED ☐ SAME AS RPT. ☐ DTIC USERS ☐	Unclassified

22a. NAME OF RESPONSIBLE INDIVIDUAL	22b. TELEPHONE NUMBER (Include Area Code)	22c. OFFICE SYMBOL
Kevin J. Malloy	202-767-4931	NE

DD FORM 1473, 83 APR EDITION OF 1 JAN 73 IS OBSOLETE.

Unclassified

11. Analytical Investigations of Bulk Wave Resonators in the Piezoelectric Thin Film on Gallium-Arsenide Configuration

18. Forced Vibrations; Dispersion Relations; Variational Approximation; Perturbation Procedure; Strip Electrodes; Rectangular Electrodes; Strip Diaphragms; Rectangular Diaphragms; Thickness Extensional Vibrations; Gallium-Arsenide; Aluminum-Nitride

19. Abstract

to use. The perturbation procedure for the calculation of the quality factor of the composite resonator due to radiation into the semiconductor wafer is discussed and it is noted that the perturbation procedure enables calculations for the case of rectangular electrodes and diaphragms to be performed. It is further noted that for the strip case the calculations of the quality factor using the perturbation procedure are in good agreement with the results obtained from the earlier more cumbersome direct procedure.

1. Introduction

The composite resonator consists of a uniform thin layer etched in a small well-defined region of a semiconducting wafer to form a diaphragm, upon which is deposited a thin piezoelectric film along with the electrodes to form a resonant region directly on the wafer. Under this program the case of the aluminum-nitride film on gallium-arsenide was investigated.

Before proceeding with a discussion of the work performed under this program, it is essential for clarity that the meaning of the words "energy trapping" be understood. Since the pure thickness-extensional resonant frequencies are cutoff frequencies, there is usually a nearby frequency range in which the transverse mode shape is evanescent. There is also a nearby frequency range in which the transverse mode shape is trigonometric. Consequently, by the selection of the appropriate thickness-extensional overtone (or fundamental) and/or the appropriate adjustment of the geometry in the electroded and unelectroded regions, the transverse modal behavior can be made to decay with distance away from the electrodes in the unelectroded region. The resulting vibration is called a trapped energy mode, which radiates a controllably small amount of energy into the adjacent thick portion of the semiconducting wafer and, hence, results in the highest possible Q, albeit with many nearby spurious modes with high Q. Alternatively, the overtone and/or geometry can be selected so that the mode does not decay with distance away from the electrode in the unelectroded region and the resulting vibration is not a trapped energy mode. In this case much more energy is radiated into the adjacent thick portion of the semiconducting wafer and much lower Q's result. Although there are still many nearby spurious modes, they are less troublesome because the Q's are lower. Most experimental work on the composite resonator reported has been for this latter

case. On the other hand, before this program was started, a detailed analytical treatment of the composite resonator for the case when trapping is present appeared in the literature[1] along with a detailed discussion of when trapping is and is not present. Essentially motivated by work done under this program, experimental results obtained at Westinghouse when trapping is present have recently been reported in the literature[2]. However, the results are for a piezoelectric thin film on silicon rather than on gallium-arsenide.

2. Discussion of Work

It has been found that the fundamental essentially thickness-extensional mode will not trap for an aluminum-nitride film on a gallium-arsenide diaphragm in the flat plate configuration. However, the fundamental mode will trap if the gallium-arsenide diaphragm is appropriately notched a small amount in the electroded region, as shown in Fig. 9 of Ref. 1. In addition, we have found that the second essentially thickness-extensional mode will trap for the same film and substrate materials in the flat plate configuration for a ratio of film-thickness to diaphragm-thickness larger than .69.

An analysis of the vibrations of a composite resonator, which is driven by the application of an a.c. voltage across strip electrodes on the major surfaces of the film, has been performed. The analysis includes the pertinent waves in the active region of the composite resonator, as well as all radiating waves in the thick gallium-arsenide plate. The solution is obtained by satisfying the differential equations for the piezoelectric film and semiconductor as well as all boundary conditions on the major surfaces of the film and semiconductor exactly and using the appropriate variational principle to satisfy the remaining conditions along the minor interfaces approximately. The minor interfaces separate the electroded from the unelectroded regions of the resonator and the

thin region of the gallium-arsenide from the thick region. Both the configuration in which the film ends at the edges of the electrodes and in which it continues to the edges of the etched diaphragm have been considered when trapping is not present, along with the latter configuration when trapping is present. In each instance the Q at the resonance condition has been calculated.

In performing the aforementioned calculations we have found that it is imperative that all radiating plate waves in the thick region of the gallium-arsenide be included in order to achieve accuracy. Since at a given frequency the number of radiating waves in a plate goes up significantly with thickness, we have considered gallium-arsenide wafers no thicker than 8 mils at a frequency around 132 MHz, for which there are 30 radiating plate waves. Specifically, calculations have been performed for thicknesses ranging from 1.5 to 8 mils. The 1.5 mil case was considered at an early stage in the calculations to check the program with as small a number of dispersion curves as possible. All the definitive calculations were for a film thickness of 7 microns and a diaphragm thickness of 14 microns and the lateral dimensions were adjusted slightly to maintain the same resonant frequency for computational convenience. The major calculations were performed for wafer thicknesses ranging from 4 mils to 8 mils because this is considered to be within the practical range. The calculated Q is a very rapidly varying function of the wafer thickness. Consequently, calculations had to be performed for very small increments in thickness in order to get all the peaks and valleys in the interval.

In the absence of trapping in the case in which the film ends at the edges of the diaphragm, the highest Q obtained is about 5000 and the lowest is about 10 and there are about 10 peaks for thicknesses between 4 mils and 8 mils. The highest valley has a Q of 1000. The calculations were performed using an increment in thickness of 1 micron. In the case in which the film ends at the edges

of the electrode, the highest Q calculated is about 15,000 and the lowest Q is about 200. Calculations were performed when trapping was induced by notching the diaphragm under the electrode. As expected, the Q due to radiation can be made as high as we wish simply by extending the lateral dimensions of the film and diaphragm. We have calculated Q's higher than 200,000 for quite reasonable dimensions. In interpreting the foregoing information it should be remembered that the high Q's calculated should be higher than the actual Q's because the material Q and the Q due to radiation into the air are not included. The results discussed above mean that in order to obtain reasonably high Q when trapping is not present for a given wafer thickness, the thicknesses of the film and diaphragm must be very precisely selected. The aforementioned relative stability and instability in Q when trapping is and is not present has been observed at Westinghouse Defense and Electronics Center but with silicon diaphragms rather than gallium-arsenide.

A brief version of this work has been published as Ref. 3 and a more complete version has been published as Ref. 4. Both Refs. 3 and 4 are appended to this report.

The type of calculation performed in Refs. 3 and 4 is extremely cumbersome to perform and was preliminary to constructing a perturbation theory to calculate the Q due to radiation into the bulk semiconductor, which is much easier to use. The more cumbersome direct calculation is required in order to check the accuracy of the perturbation calculation.

A perturbation analysis of the Q due to radiation into the semiconductor wafer has been performed. This analysis is considerably less cumbersome to use than the earlier direct variational treatment[3,4] and is not restricted to the case of strip electrodes and diaphragms. In the treatment the resonant mode of interest is determined from the equation for transversely varying essentially

thickness-extensional modes in composite resonators[1] and simple approximate but very accurate conditions at the edge of the diaphragm. This resonant mode is then used to determine the radiation into the semiconductor wafer by means of a variational approximation procedure. Then the resonant mode and the radiation field are employed in a perturbation integral to calculate the Q. In this work only the configuration in which the film continues to the edges of the etched diaphragm is considered both when trapping is and is not present. However, in the latter work, the cases of rectangular electrodes and diaphragms are considered.

Of course, as in the earlier work[3,4], all radiating plate waves in the thick region of the gallium-arsenide must be included to achieve accuracy. Calculations utilizing the perturbation procedure have been performed for the case of strip electrodes for the same definitive geometries considered in the earlier work[3,4]. These geometries consist of wafer thicknesses ranging from 4 mils to 8 mils and a film thickness of 7 microns and diaphragm thickness of 14 microns. Although different lateral dimensions were considered in this work, for the strip case for comparison with the earlier work a diaphragm width of 500 microns was used when trapping is not present and 600, when trapping is present. The calculated results for the strip case are in good agreement with the earlier more cumbersome direct calculations[3,4]. When trapping is not present the highest Q's calculated are very nearly the same as those obtained in the earlier direct calculation[3,4], but the lowest Q's calculated by means of the perturbation procedure tend to be nearly an order of magnitude higher than those calculated by the earlier direct procedure[3,4]. We are not absolutely sure of the reason for this discrepancy, but there are two possibilities. The perturbation procedure might be tending to lose its accuracy for low Q because of the increased radiation or the resonant frequency might not have been sufficiently

precisely determined by means of the earlier direct procedure[3,4] for the accurate determination of the lowest Q values. However, the fact that the highest Q's calculated by the perturbation procedure are slightly higher than those calculated by the direct procedure seems to support the latter possibility. The location of the peaks and valleys of Q with wafer thickness determined by means of the perturbation procedure is in quite good agreement with those obtained from the earlier direct calculation. For the case of square electrodes and diaphragms, in the absence of trapping the calculated Q's are roughly between 1/2 to 2/3 of the values in the strip case. This is as expected because of the radiation in the two orthogonal directions for square diaphragms. When trapping is present the calculated Q's for both the strip and square cases increase very rapidly with the distance from the edge of the electrode to the edge of the diaphragm.

A brief version of this work has been published as Ref. 5 and a more complete version will be published as Ref. 6. Both Ref. 5 and a preprint of Ref. 6 are appended to this report.

References

1. H. F. Tiersten and D. S. Stevens, "An Analysis of Thickness-Extensional Trapped Energy Resonant Device Structures with Rectangular Electrodes in the Piezoelectric Thin Film on Silicon Configuration," J. Appl. Phys., 54, 5893 (1983).

2. J. Rosenbaum, H. Salvo, Jr. and S. V. Krishnaswamy, "Overtone Response of Composite Bulk Acoustic Resonators," Proceedings of the 4oth Annual Symposium on Frequency Control, U. S. Army Electronics Technology and Devices Laboratory, Fort Monmouth, New Jersey and Institute of Electrical and Electronics Engineers, New York, IEEE Cat. No. 86CH2330-9, 262 (1986), p. 206.

3. D. S. Stevens, H. F. Tiersten and D. V. Shick, "On the Reduction in Quality Factor of the Piezoelectric Thin Film on Semiconductor Composite Resonator Due to Radiation into the Bulk Semiconductor," 1985 Ultrasonics Symposium Proceedings, IEEE Cat. No. 85CH2209-5, Institute of Electrical and Electronics Engineers, New York (1985), p. 311.

4. D. V. Shick, D. S. Stevens and H. F. Tiersten, "Quality Factor of the Piezoelectric Thin Film on Semiconductor Composite Resonator Resulting from Radiation into the Semiconductor Wafer," J. Appl. Phys., 60, 2238 (1986).

5. D. V. Shick and H. F. Tiersten, "A Perturbation Calculation of the Quality Factor of the Piezoelectric Thin Film on Semiconductor Composite Resonator Due to Radiation into the Wafer," 1986 Ultrasonics Symposium Proceedings, IEEE Cat. No. 86CH2375-4, Institute of Electrical and Electronics Engineers, New York (1986), p.377.

6. D. V. Shick and H. F. Tiersten, "A Perturbation Calculation of the Quality Factor of the Piezoelectric Thin Film on Semiconductor Composite Resonator Resulting from Radiation into the Wafer," to be published in the Journal of Applied Physics (1987).

Publications

"On the Reduction in Quality Factor of the Piezoelectric Thin Film on Semiconductor Composite Resonator Due to Radiation into the Bulk Semiconductor," D. S. Stevens, H. F. Tiersten and D. V. Shick, 1985 Ultrasonics Symposium Proceedings, IEEE Catalog Number 85CH2209-5, Institute of Electrical and Electronics Engineers, New York, 311-318 (1985).

"Quality Factor of the Piezoelectric Thin Film on Semiconductor Composite Resonator Resulting from Radiation into the Semiconductor Wafer," D. V. Shick, D. S. Stevens and H. F. Tiersten, Journal of Applied Physics, 60, 2238-2249 (1986).

"A Perturbation Calculation of the Quality Factor of the Piezoelectric Thin Film on Semiconductor Composite Resonator Due to Radiation into the Wafer," D. V. Shick and H. F. Tiersten, 1986 Ultrasonics Symposium Proceedings, IEEE Catalog Number 86CH2375-4, Institute of Electrical and Electronics Engineers, New York, 377-382 (1986).

"A Perturbation Calculation of the Quality Factor of the Piezoelectric Thin Film on Semiconductor Composite Resonator Resulting from Radiation into the Wafer," D. V. Shick and H. F. Tiersten, to be published in the Journal of Applied Physics (1987).

ON THE REDUCTION IN QUALITY FACTOR OF THE PIEZOELECTRIC THIN FILM ON SEMICONDUCTOR COMPOSITE RESONATOR DUE TO RADIATION INTO THE BULK SEMICONDUCTOR

D.S. Stevens*, H.F. Tiersten and D.V. Shick

Rensselaer Polytechnic Institute
Troy, NY 12180-3590

I. Introduction

The composite resonator consists of a uniform thin layer etched in a small well-defined region of a semiconducting wafer to form a diaphragm, upon which is deposited a thin piezoelectric film along with the electrodes to form a resonant region directly on the wafer. In this work calculations are performed for the particular case of the aluminum-nitride film on gallium-arsenide.

Before proceeding with a discussion of this work, it is essential for clarity that we briefly explain the meaning of the words "energy trapping." Since the pure thickness-extensional resonant frequencies are cutoff frequencies, there is usually a nearby frequency range in which the transverse mode shape is evanescent. There is also a nearby frequency range in which the transverse mode shape is trigonometric. Consequently, by the selection of the appropriate thickness-extensional overtone (or fundamental) and/or the appropriate adjustment of the geometry in the electroded and unelectroded regions, the transverse modal behavior can be made to decay with distance away from the electrodes in the unelectroded region. The resulting vibration is called a trapped energy mode, which radiates a controllably small amount of energy into the adjacent thick portion of the semiconducting wafer and, hence, results in the highest possible Q, albeit with many nearby spurious modes with high Q. Alternatively, the overtone and/or geometry can be selected so that the mode does not decay with distance away from the electrode in the unelectroded region and the resulting vibration is not a trapped energy mode. In this case much more energy is radiated into the adjacent thick portion of the semiconducting wafer and much lower Q's result. Although there are still many nearby spurious modes, they are less troublesome because the Q's are lower. All experimental work on the composite resonator reported to date has been for this latter case[1-6]. On the other hand a detailed analytical treatment of the composite resonator for the case when trapping is present appears in the literature[7] along with a detailed discussion of when trapping is and is not present.

Using the existing[8] constants of aluminum-nitride, we have found that the fundamental essentially thickness-extensional mode will not trap for an aluminum-nitride film on a gallium-arsenide diaphragm in the flat plate configuration[5]. However, the fundamental mode will trap if the gallium-arsenide diaphragm is appropriately notched a small amount in the electroded region, as shown in Fig.9 of Ref.7. In addition, we have found that the second essentially thickness-extensional mode will trap in the flat plate configuration for the same film and substrate materials for any ratio of film-thickness to diaphragm-thickness.

In this work an analysis of the vibrations of a composite resonator, which is driven by the application of an a.c. voltage across strip electrodes on the major surfaces of the film, is performed. The analysis includes the pertinent waves in the active region of the composite resonator, as well as all radiating waves in the thick gallium-arsenide plate. All previous analytical work expressly ignores radiation into the bulk semiconductor except one treatment[10], which unrealistically ignores the junction between the etched diaphragm and the bulk semiconductor. The solution is obtained by satisfying the differential equations for the piezoelectric film and semiconductor as well as all boundary conditions on the major surfaces of the film and semiconductor exactly and using the appropriate variational principle[11] to satisfy the remaining conditions along the minor interfaces approximately. The minor interfaces separate the electroded from the unelectroded regions of the resonator and the thin region of the gallium-arsenide from the thick region. Past experience shows that this type of approximation yields extremely accurate results if all the proper waves are included[12,13]. Both the configuration in which the film ends at the edges of the electrodes and in which it continues to the edges of the etched diaphragm have been considered when trapping is not present, along with the latter configuration when trapping is present. In each instance the Q at the resonance condition is calculated.

II. Basic Equations

The differential equations of motion and electrostatics and linear piezoelectric constitutive equations for the piezoelectric film may be written in the tensor form[14,15]

* Present address: AT&T Bell Laboratories, 1600 Osgood St., North Andover, MA 01845.

0090-5607/85/0000-0311 $1.00 © 1985 IEEE

$$T^f_{ij,i} = \rho^f \ddot{u}^f_j, \quad D^f_{i,i} = 0, \tag{1}$$

$$T^f_{ij} = c^f_{ijk\ell} u^f_{k,\ell} + e^f_{kij} \varphi^f_{,k},$$

$$D^f_i = e^f_{ik\ell} u^f_{k,\ell} - \epsilon^f_{ik} \varphi^f_{,k}, \tag{2}$$

where the notation is conventional. The equations of motion and the linear elastic constitutive equations for the gallium-arsenide may be written in the tensor form[15,16]

$$T^s_{ij,i} = \rho^s \ddot{u}^s_j, \quad T^s_{ij} = c^s_{ijk\ell} u^s_{k,\ell}, \tag{3}$$

and we note that the equations are too cumbersome to write out in detail. At this point we introduce a Cartesian coordinate system x_1, x_2, x_3 with the x_3-axis normal to the major surfaces of the aluminum nitride film and along a cube axis of the gallium-arsenide. Since aluminum-nitride has small piezoelectric coupling, for small wave and decay numbers along the plate, which are the only ones of interest in the active region, we need retain only x_3-dependence of all electrical variables and we have

$$D^f_{3,3} = 0, \quad D^f_3 = e^f_{3k\ell} u^f_{k,\ell} - \epsilon^f_{33} \varphi^f_{,3}. \tag{4}$$

Figure 1 shows a schematic diagram of a cross section of a thin aluminum-nitride film on a thin gallium-arsenide layer composite trapped energy resonator for the configuration in which the film ends at the edge of the diaphragm. In the unelectroded regions the boundary conditions on the major surfaces are

$$T^f_{3j} = 0, \quad D_3 = 0 \quad \text{at } x_3 = h^f, \tag{5}$$

$$T^f_{3j} - T^s_{3j} = h' \rho' \ddot{u}^s_j, \quad u^f_j = u^s_j, \quad \varphi^f = 0 \text{ at } x_3 = 0, \tag{6}$$

$$T^s_{3j} = 0 \quad \text{at } x_3 = -h^s, \tag{7}$$

where the superscripts f and s stand for the thin film and semiconductor layer, respectively, and ρ' is the mass density of the ground electrode. The electrical condition in $(5)_2$ is a consequence of the fact that the x_1- and x_2-dependence of all electrical variables has been left out of account and the electrical potential in space is bounded at $x_3 = \infty$. Since the electrodes are much thinner than either the thin film or the layer, we have employed approximate thin plate equations[17] for the electrode plating in $(6)_1$, and we have made use of the fact that the mechanical stiffness of the very thin electrode plating is negligible for small wavenumbers along the plate. Similarly, on the major surfaces of the composite plate in the electroded region the boundary conditions are

$$T^f_{3j} = -\rho' h' \ddot{u}^f_j, \quad \varphi^f = V e^{i\omega t} \quad \text{at } x_3 = h^f, \tag{8}$$

$$\varphi^f = 0 \quad \text{at } x_3 = 0, \tag{9}$$

along with (6) and (7), which remain unchanged. The quantity ρ' is the mass density of the upper electrode.

Figure 2 shows a schematic diagram of a cross-section for the configuration in which the film ends at the edges of the electrodes. The boundary conditions on the major surfaces of the composite plate in the electroded region, which still contains the film, are exactly the same as in the previous case. However, the boundary conditions on the major surfaces of the unelectroded plate, which no longer contains the film, are much simpler than in the previous case and in place of (5) - (7) we have

$$T^s_{3j} = 0 \quad \text{at } x_3 = 0 \text{ and } x_3 = -h^s. \tag{10}$$

For either configuration the corresponding boundary conditions on the major surfaces in the region of the bulk semiconductor are

$$T^s_{3j} = 0 \quad \text{at } x_3 = 0 \text{ and } x_3 = -\hat{h}^s. \tag{11}$$

Since the piezoelectric coupling is small in aluminum-nitride, we may transform the inhomogeneity from the boundary conditions in $(8)_2$ into the differential equations by means of the transformation shown in Eqs.(3.26) of Ref.7, which is considered to be part of this work[15]. Furthermore, since we have replaced $(1)_2$ and $(2)_2$ by (4), no electrical conditions need be satisfied at a minor interface. Then the conditions that should be satisfied at each minor interface are the continuity of u_3, u_1, T_{13} and T_{11}. However, since in the approximation technique we employ the solution is written as a sum of eigensolutions, each of which satisfies the homogeneous differential equations and boundary conditions on the major surfaces for one of the three regions, i.e., the electroded composite, the unelectroded composite and the bulk semiconductor, exactly, we cannot satisfy the continuity conditions across the interfaces between the regions exactly. Nevertheless, the remaining continuity conditions across the interfaces may be satisfied approximately along with the inhomogeneous driving term resulting from the aforementioned transformation by satisfying the proper form of the appropriate variational principle[11] of linear piezoelectricity, in which all that remains is an integral over the inhomogeneous forcing term plus integrals over the interfaces because all other terms in that form of the variational principle vanish on account of the equations and conditions satisfied by the solution functions employed[18]. The form of the variational principle of interest here is given in Eq.(6.44) of Ref.11. Since the solution functions satisfy the aforementioned equations and conditions, all that remains of Eq.(6.44) of Ref.11 is

$$\int_0^{\ell} \int_0^{h^f} \left(-\rho^f \omega^2 \frac{e^f_{33}}{c^f_{33} h^f} V e^{i\omega t} \right) \delta \bar{u}^f_3 \, dx_3 dx_1$$

$$- \int_0^{h^f} \left(\bar{T}^f_{13} \delta \bar{u}^f_3 + \bar{T}^f_{11} \delta \bar{u}^f_1 \right) \Big|_{x_1 = d} dx_3$$

$$+ \int_{-\hat{h}^s}^{-h^s} (\hat{T}^s_{11}\delta\hat{u}^s_1 + \hat{T}^s_{13}\delta\hat{u}^s_3)\Big|_{x_1=d} dx_3 + \frac{1}{2}\int_{-\bar{h}^s}^{0} [T^s_{11} - \bar{T}^s_{11})(\delta\bar{u}^s_1 + \delta u^s_1) + (T^s_{13} - \bar{T}^s_{13})(\delta\bar{u}^s_3 + \delta u^s_3) + (\bar{u}^s_1 - u^s_1)(\delta\bar{T}^s_{11} + \delta T^s_{11}) + (\bar{u}^s_3 - u^s_3)(\delta\bar{T}^s_{13} + \delta T^s_{13})]_{x_1=\ell} dx_3 + \frac{1}{2}\int_{0}^{h^f} [(T^f_{11} - \bar{T}^f_{11})(\delta\bar{u}^f_1 + \delta u^f_1) + (T^f_{13} - \bar{T}^f_{13})(\delta\bar{u}^f_3 + \delta u^f_3) + (\bar{u}^f_1 - u^f_1)(\delta\bar{T}^f_{11} + \delta T^f_{11}) + (\bar{u}^f_3 - u^f_3)(\delta\bar{T}^f_{13} + \delta T^f_{13})]_{x_1=\ell} dx_3 + \frac{1}{2}\int_{-\hat{h}^s}^{0} [(\hat{T}^s_{11} - T^s_{11})(\delta u^s_1 + \delta\hat{u}^s_1) + (\hat{T}^s_{13} - T^s_{13})(\delta u^s_3 + \delta\hat{u}^s_3) + (u^s_1 - \hat{u}^s_1)(\delta T^s_{11} + \delta\hat{T}^s_{11}) + (u^s_3 - \hat{u}^s_3)(\delta T^s_{13} + \delta\hat{T}^s_{13})]_{x_1=d} dx_3 = 0 , \quad (12)$$

for the case when trapping is not present and the film extends over the entire diaphragm. When the film ends at the edges of the electrodes the fifth integral in (12) is not present and the second integral is replaced by

$$- \int_{0}^{h^f} (\bar{T}^f_{13}\delta\bar{u}^f_3 + \bar{T}^f_{11}\delta\bar{u}^f_1)\Big|_{x_1=\ell} dx_3 . \quad (13)$$

When trapping is present with a notch under the electroded region, as shown in Fig.3, the fourth integral is taken from $-\bar{h}^s$ to 0 (instead of $-h^s$ to 0) and there is an additional term

$$+ \int_{-h^s}^{-\bar{h}^s} (T^s_{11}\delta u^s_1 + T^s_{13}\delta u^s_3)\Big|_{x_1=\ell} dx_3 , \quad (14)$$

in Eq.(12).

III. Pure Thickness-Extensional Vibrations

Since in all cases the composite resonator will be operated at a frequency in the vicinity of one of the pure thickness-extensional resonances of the composite plate, the pure thickness-extensional resonant frequencies of the composite are of particular importance in this work. It is shown in Sec. III of Ref.7 that for the composite plate without a driving electrode but with a ground electrode, the pure thickness-extensional resonant frequencies are given by

$$\omega_e = (\bar{c}^f_{33}/\rho^f)^{1/2}\eta^o_f(1 - R''/G^o) , \quad (15)$$

where η^o_f is the appropriate root of

$$\tan \eta^o_f h^f + c^r\mu \tan \mu\sigma\eta^o_f h^f = 0 , \quad (16)$$

and

$$R'' = \frac{\rho''h''}{\rho^f h^f} , \quad G^o = \frac{1}{\cos^2\eta^o_f h^f} + \frac{c^r\mu^2\sigma}{\cos^2\mu\sigma\eta^o_f h^f} ,$$
$$\bar{c}^f_{33} = c^f_{33} + \frac{(e^f_{33})^2}{\epsilon^f_{33}} , \quad c^r = \frac{c^s_{33}}{\bar{c}^f_{33}} ,$$
$$\mu = \left(\frac{\bar{c}^f_{33}\rho^s}{c^s_{33}\rho^f}\right)^{1/2} , \quad \sigma = \frac{h^s}{h^f} . \quad (17)$$

Similarly, for the completely electroded composite plate driven by a voltage it has been shown that the pure thickness-extensional resonant frequencies are given by

$$\bar{\omega}_e = (\bar{c}^f_{33}/\rho^f)^{1/2}\bar{\eta}^o_f(1 + P^o/G^o) , \quad (18)$$

where

$$P^o = \frac{k^2}{(\bar{\eta}^o_f h^f)^2}\left(\frac{2}{\cos\bar{\eta}^o_f h^f} - 2 + c^r\mu \tan\mu\sigma\bar{\eta}^o_f h^f \tan\bar{\eta}^o_f h^f\right)$$
$$- R'' - R'(1 - c^r\mu \tan\eta^o_f h^f \tan\mu\sigma\bar{\eta}^o_f h^f) ,$$
$$k^2 = (e^f_{33})^2/\bar{c}^f_{33}\epsilon^f_{33}, \quad R' = \rho' h'/\rho^f h^f . \quad (19)$$

The difference between the resonant frequencies of pure thickness-extensional vibrations of the composite plate with and without a driving electrode, i.e., $\omega_e - \bar{\omega}_e$ for the same η^o_f, is very important when trapping is present.

IV. Straight-Crested Dispersion Relations

In this section we obtain the straight-crested dispersion relations for the composite plate, the thin diaphragm without the film and the bulk semiconductor because these determine the solution functions that are used in the variational condition (12). Since these eigensolutions in each region satisfy the homogeneous differential equations and boundary conditions on the major surfaces, they are too cumbersome to present here[5].

The solution for decaying waves in the unelectroded composite plate is presented in Eqs.(4.14) - (4.24) of Ref.7, which is considered to be part of this work. As noted in Ref.7, the solutions for traveling waves in the unelectroded and electroded composite plate can readily be obtained from the solution presented. The solutions for the simpler cases of the diaphragm without the film and the bulk semiconductor are not as cumbersome, but are also too lengthy to present here[5]. These types of solutions are presented in a number of places[18,19].

The pertinent dispersion curves for the aluminum-nitride film on the gallium-arsenide layer composite plate are shown in Fig.4. We do not distinguish between the electroded film with shorted

electrodes and the unelectroded film in the figure. This is done in great detail in Ref.7. Furthermore, when required, the difference between the two can be calculated from $(\omega^e - \bar{\omega}^e)$ given in the last section. The dispersion curves are for a film thickness of 7 microns and a diaphragm thickness of 14 microns. The pertinent dispersion curves for a 14 micron thick gallium-arsenide diaphragm are shown in Fig.5. The lowest 17 real dispersion curves for the bulk gallium-arsenide plate are shown in dimensionless form in Fig.6. For the fundamental essentially thickness-extensional resonance for the composite dimensions mentioned (around 132 MHz), this number of dispersion curves is for a gallium-arsenide wafer thickness of about 5 mils. In this work we perform calculations for wafer thicknesses up to 8 mils for which there are 30 real dispersion curves for a frequency of 132 MHz. However, we do not bother to show the figure for more than 17 in this work.

V. Forced Vibrations of Composite Resonator

In this section we determine the essentially thickness-extensional vibrations driven by the application of a steady-state driving voltage to the strip electrodes on the surfaces of the piezoelectric film of the composite resonator shown in any of Figs.1 - 3. Since we include radiation into the bulk semiconductor, we can use the solution to calculate the Q at resonance of the mode resulting from radiation into the bulk semiconductor.

In accordance with the earlier discussion we take the approximate solution in the form

$$u_a^f = \sum_{\beta=1}^{\bar{n}} \bar{K}^{(\beta)} \bar{u}_a^{f(\beta)} - \frac{e_{33}^f V x_3 e^{i\omega t}}{c_{33}^f h^f},$$

$$\bar{u}_a^s = \sum_{\beta=1}^{\bar{n}} \bar{K}^{(\beta)} \bar{u}_a^{s(\beta)}, \quad a = 1,3,$$

$$u_a^f = \sum_{\alpha=1}^{n} K^{(\alpha)} u_a^{f(\alpha)}, \quad u_a^s = \sum_{\alpha=1}^{n} K^{(\alpha)} u_a^{s(\alpha)},$$

$$\hat{u}_a^s = \sum_{\gamma=1}^{\hat{n}} \hat{K}^{(\gamma)} \hat{u}_a^{s(\gamma)}, \qquad (20)$$

where $\bar{n}$, n and $\hat{n}$ are the number of branches of the dispersion curves included in the electroded composite, unelectroded composite or diaphragm and bulk semiconductor, respectively, which are given in Figs.4 - 6. The eigensolution functions $\bar{u}_a^{f(\beta)}$, $\bar{u}_a^{s(\beta)}$, $u_a^{f(\alpha)}$, $u_a^{s(\alpha)}$, $\hat{u}_a^s$ denote the solution functions that satisfy the differential equations and the boundary conditions on the major surfaces for each of the respective regions and yield the dispersion curves shown in Figs.4 - 6 and which are too cumbersome to present here[15]. Since the solution functions in (20) are fixed, only the $\bar{K}^{(\beta)}$, $K^{(\alpha)}$ and $\hat{K}^{(\gamma)}$ are varied when (20) is substituted into (12). Accordingly, substituting from (20) into (12), employing $(2)_1$ and $(3)_2$ and performing the integrations, we obtain[15] an equation of the form

$$\sum_{\beta=1}^{\bar{n}} \delta\bar{K}^{(\beta)} V\bar{c}^{(\beta)} + \sum_{\beta=1}^{\bar{n}} \sum_{\delta=1}^{\bar{n}} \delta\bar{K}^{(\beta)} \bar{K}^{(\delta)} \bar{a}_{\beta\delta} + \sum_{\alpha=1}^{n} \sum_{\varepsilon=1}^{n} \delta K^{(\alpha)} K^{(\varepsilon)} a_{\alpha\varepsilon}$$

$$\sum_{\gamma=1}^{\hat{n}} \sum_{\zeta=1}^{\hat{n}} \delta\hat{K}^{(\gamma)} \hat{K}^{(\zeta)} \hat{a}_{\gamma\zeta} + \sum_{\beta=1}^{\bar{n}} \sum_{\alpha=1}^{n} (\delta\bar{K}^{(\beta)} K^{(\alpha)} \bar{b}_{\beta\alpha} + \delta K^{(\alpha)} \bar{K}^{(\beta)} \bar{b}_{\beta\alpha}$$

$$+ \sum_{\alpha=1}^{n} \sum_{\gamma=1}^{\hat{n}} \left(\delta K^{(\alpha)} \hat{K}^{(\gamma)} \hat{b}_{\alpha\gamma} + \delta\hat{K}^{(\gamma)} K^{(\alpha)} \hat{b}_{\alpha\gamma} \right) = 0, \qquad (21)$$

where the expressions for $\bar{c}^{(\beta)}$, $\bar{a}_{\beta\delta}$, $a_{\alpha\varepsilon}$, $\hat{a}_{\gamma\zeta}$, $\bar{b}_{\beta\alpha}$ and $\hat{b}_{\alpha\gamma}$ are too lengthy to present here. Since the variations in (21) are arbitrary, we obtain[15] the inhomogeneous linear equations for the $\bar{K}^{(\beta)}$, $K^{(\alpha)}$ and $\hat{K}^{(\gamma)}$ in the form

$$\sum_{\zeta=1}^{\bar{n}} \bar{K}^{(\zeta)} \bar{a}_{\beta\zeta} + \sum_{\alpha=1}^{n} K^{(\alpha)} \bar{b}_{\beta\alpha} = - V\bar{c}^{(\beta)}, \quad \beta = 1, \bar{n},$$

$$\sum_{\varepsilon=1}^{n} K^{(\varepsilon)} a_{\alpha\varepsilon} + \sum_{\beta=1}^{\bar{n}} \bar{K}^{(\beta)} \bar{b}_{\beta\alpha} + \sum_{\gamma=1}^{n} \hat{K}^{(\gamma)} \hat{b}_{\alpha\gamma} = 0, \quad \alpha = 1,n,$$

$$\sum_{\zeta=1}^{\hat{n}} \hat{K}^{(\zeta)} \hat{a}_{\gamma\zeta} + \sum_{\alpha=1}^{n} K^{(\alpha)} \hat{b}_{\alpha\gamma} = 0, \quad \gamma = 1,\hat{n}. \qquad (22)$$

VI. Quality Factor Resulting from Radiation

In this section we calculate the quality factor due to radiation into the bulk semiconductor for each of the three cases from the analysis presented in the previous section. Although the solution may be obtained from the analysis in the previous section at any driving frequency for which all the pertinent dispersion curves are available, in this work we are interested in the solution only at the fundamental essentially thickness-extensional resonance for each of the three configurations. It is clear from past experience[12,13] that under these circumstances we need consider only the essentially thickness-extensional branch in the composite region (either electroded or not) of the resonator, which is the curve labeled 1 in Fig.4. However, in the thin region of the semiconductor without the film and the bulk semiconductor all pertinent dispersion curves shown in the respective Figs.5 and 6 must be included to obtain accuracy. The use of only one branch for the composite region

means that we always have $\bar{n} = 1$ and $n = 1$ for the configuration shown in Figs.1 and 3 but not for the configuration shown in Fig.2, for which all curves shown in Fig.5 must be included.

As usual, the quality factor Q is defined by

$$Q = (K+U)/E^{tw}, \tag{23}$$

where

$$K = \frac{1}{T}\int_0^T dt\, \frac{1}{2}\,\mathrm{Re}\int_{-d}^{d} dx_1 \int_{-h^s}^{h^f} \frac{1}{2}\,\rho \dot{u}_a \dot{u}_a^* dx_3,$$

$$U = \frac{1}{T}\int_0^T dt\, \frac{1}{2}\,\mathrm{Re}\Big[\int_{-d}^{d} dx_1 \int_{-h^s}^{h^f} \frac{1}{2}\,(c_{11}u_{1,1}u_{1,1}^*$$

$$+ c_{33}u_{3,3}u_{3,3}^* + 2c_{13}u_{1,1}u_{3,3}^* + c_{44}(u_{1,3}$$

$$+ u_{3,1})(u_{1,3}^* + u_{3,1}^*)dx_3\Big],$$

$$E^{tw} = -2\int_0^T dt\, \frac{1}{2}\,\mathrm{Re}\int_{-h^s}^{s} (-\hat{T}_{1a}\dot{u}_a^*)_{x_1=d}\, dx_3, \tag{24}$$

in which T is the period of the vibration and we have taken the liberty of writing the integrals in $(24)_{1,2}$ over discontinuous functions[5] to achieve brevity. For a given geometry and mode, resonance is determined by obtaining Q over a (narrow) range of frequencies and finding the frequency for which Q is a maximum.

In performing the calculations we have found that it is imperative that all radiating plate waves in the thick region of the gallium-arsenide be included in order to achieve accuracy. Since at a given frequency the number of radiating waves in a plate goes up significantly with thickness, we have considered gallium-arsenide wafers no thicker than 8 mils at a frequency around 132 MHZ, for which there are 30 radiating plate waves. Results are presented for wafer thicknesses ranging from 4 mils to 8 mils because this is considered to be within the practical range. All the results presented are for a film thickness of 7 microns and a diaphragm thickness of 14 microns and the lateral dimensions of each configuration were adjusted slightly to maintain the same resonant frequency for computational convenience. Since the calculated Q is a very rapidly varying function of the wafer thickness, calculations had to be performed for very small increments in thickness, i.e., 1 micron, in order to get all the peaks and valleys in the interval.

In the absence of trapping, for the case shown in Fig.1 the results are plotted in Fig.7, which shows the aforementioned sharp variation in Q with wafer thickness. It can be seen from the figure that the highest Q obtained is about 4750 and the lowest is about 10 and there are about 10 peaks for thicknesses between 4 mils and 8 mils. The highest valleys have Q's of about 700 and 2000, respectively. For the case shown in Fig.2 the results are plotted in Fig.8, which shows variations in Q with wafer thickness similar to Fig.7, but in this case the Q's are considerably higher. It can be seen from the figure that the highest Q obtained is about 15,000 and the lowest Q is about 200. Calculations were performed when trapping was induced in the fundamental mode by notching the diaphragm under the electrode as shown in Fig.3. As expected, the Q due to radiation can be made as high as we wish simply by extending the lateral dimensions of the film and diaphragm. Figure 9 gives Q as a function of $(d - \ell)$, i.e., the distance from the edge of the electrode to the edge of the diaphragm. It can be seen from the figure that Q increases very rapidly with $(d - \ell)$ and at $d = 2\ell$, $Q = 70{,}000$ for this geometry. For these calculations the wafer thickness was 6 mils. Even when trapping is present the Q is a varying function of wafer thickness, but the range of the variation is less than 1/10 of that when trapping is not present, which is not of interest since the Q with trapping is so much higher than the Q without trapping. In interpreting the foregoing information it should be remembered that the high Q's calculated should be higher than the actual Q's because the material Q and the Q due to radiation into the air are not included. The results discussed above mean that in order to obtain reasonably high Q when trapping is not present, for a given wafer thickness the thicknesses of the film and diaphragm must be very precisely selected.

Since the variational condition in (12) does not expressly match the mode shape at the interfaces unless the solution is exact[5], the extent to which the calculated mode shape matches at the interfaces gives an indication of the accuracy of the approximate solution obtained. Typical plots of the u_3-displacement field, which is the large one for the essentially thickness-extensional modes considered here, for the configurations shown in Figs.1 and 2 are shown in Figs.10 and 11, respectively. It can be seen from the figures that the u_3-displacement field matches quite well at the interfaces. Consequently, we can conclude that the approximate solution obtained is quite accurate.

Acknowledgements

We wish to thank Dr. K.M. Lakin of Iowa State University for referring us to Ref.8 and acquainting us with the difficulty mentioned in Ref.9.

This work was supported in part by the Air Force Office of Scientific Research under Grant No. AFOSR-84-0351.

References

1. T.W. Grudkowski, J.F. Black, T.M. Reeder, D.E. Cullen and R.A. Wagner, "Fundamental-Mode VHF/UHF Miniature Acoustic Resonators and Filters on Silicon," Appl. Phys. Lett., 37, 993 (1980).

2. K.M. Lakin and J.S. Wang, "Acoustic Bulk Wave Composite Resonators," Appl. Phys. Lett., 38, 125 (1981).

3. K.H. Nakamura, H. Sasaki and H. Shimizu, "ZnO/SiO_2 Diaphragm Composite Resonator on a Silicon Wafer," Electronics Lett., 17, 507 (1981).

4 T.W. Grudowski, J.F. Black, G.W. Drake and D.E. Cullen, "Progress in the Development of Miniature Thin Film BAW Resonator and Filter Technology," Proceedings of the 36th Annual Symposium on Frequency Control, U.S. Army Electronics Research and Development Command, Fort Monmouth, New Jersey, 539 (1982).

5. J.S. Wang and K.M. Lakin, "Low Temperature Coefficient Bulk Wave Composite Resonators," Appl. Phys. Lett., 40, 308 (1982).

6. K.M. Lakin, J.S. Wang and A.R. Landin, "Aluminum Nitride Thin Film and Composite Bulk Wave Resonators," Proceedings of the 36th Annual Symposium on Frequency Control, U.S. Army Electronics Research and Development Command, Fort Monmouth, New Jersey, 517 (1982).

7. H.F. Tiersten and D.S. Stevens, "An Analysis of Thickness-Extensional Trapped Energy Resonant Device Structures with Rectangular Electrodes in the Piezoelectric Thin Film on Silicon Configuration," J. Appl. Phys., 54, 5893 (1983).

8. K. Tsubouchi, K. Sugai and N. Mikoshiba, "AlN Material Constants Evaluation and SAW Properties on AlN/Al_2O_3 and AlN/Si," 1981 Ultrasonics Symposium Proceedings, IEEE Cat. No. 81 CH1689-9, Institute of Electrical and Electronics Engineers, New York, 375 (1981).

9. The accuracy of the values of the material constants in the literature is open to some question because the published value of c_{33} yields resonant frequencies that differ significantly from measured resonant frequencies reported in the literature.

10. R.F. Milsom, J.E. Curran, S.L. Murray, S. Terry-Wood and M. Redwood, "The Effect of Mesa-Shaping on Spurious Modes in Zn-O/Si Bulk-Wave Composite Resonators," 1983 Ultrasonics Symposium Proceedings, IEEE Cat. No. 83 CH 1947-1, Institute of Electrical and Electronics Engineers, New York, 498 (1983). Some experimental work when trapping is present is reported in this reference.

11. H.F. Tiersten, Linear Piezoelectric Plate Vibrations (Plenum, New York, 1969), Chap.6, Sec.4.

12. H.F. Tiersten and B.K. Sinha, "An Analysis of Extensional Modes in High Coupling Trapped Energy Resonators," 1978 Ultrasonics Symposium Proceedings, IEEE Cat. No. 78 CH 1482-9, Institute of Electrical and Electronics Engineers, New York, 167 (1978).

13. D.V. Shick, H.F. Tiersten and B.K. Sinha, "Forced Thickness-Extensional Trapped Energy Vibrations of Piezoelectric Plates," 1981 Ultrasonics Symposium Proceedings, IEEE Cat. No. 81 CH 1689-9, Institute of Electrical and Electronics Engineers, New York, 452 (1981).

14. Ref.11, Eqs.(7.28) and (7.29).

15. For more detail see D.V. Shick, D.S. Stevens and H.F. Tiersten, "On the Quality Factor of the Piezoelectric Thin Film Semiconductor Composite Resonator Resulting from Radiation into the Semiconductor Wafer," to be issued as a technical report, Rensselaer Polytechnic Institute, Troy, New York 12180-3590.

16. B.A. Auld, Acoustic Fields and Waves in Solids (Wiley, New York, 1973), Vol.I, p.210.

17. Ref.11, Chap.14, Sec.4.

18. R.K. Kaul and R.D. Mindlin, "Vibrations of an Infinite Monoclinic Crystal Plate at High Frequencies and Long Wavelengths," J. Acoust. Soc. Am., 34, 1895 (1962).

19. Ref.11, Chap.10.

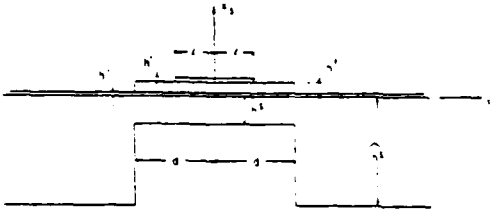

Figure 1 Cross-Section of a Composite Resonator Consisting of a Thin Piezoelectric Film on a Gallium-Arsenide Layer with the Film Covering the Entire Layer

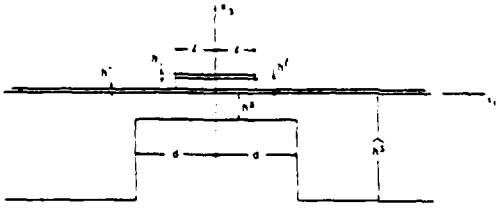

Figure 2 Cross-Section of a Composite Resonator with the Piezoelectric Film Ending at the Edge of the Electrodes

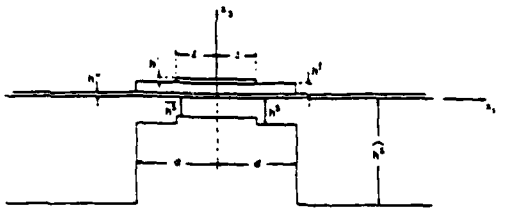

Figure 3 Cross-Section of a Composite Resonator with the Layer Notched under the Electrodes to Cause Trapping in the Fundamental Mode when it does not Trap in the Flat Plate Configuration

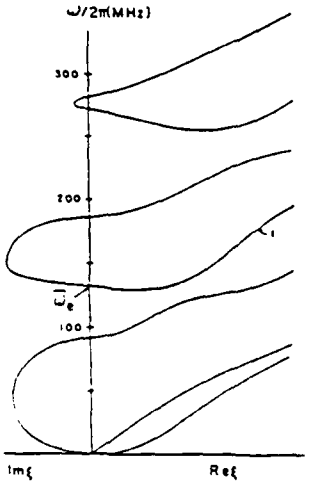

Figure 4 Dispersion Curves for the Composite Region Consisting of an Aluminum-Nitride Film on a Gallium-Arsenide Layer with ξ the Propagation Wavenumber

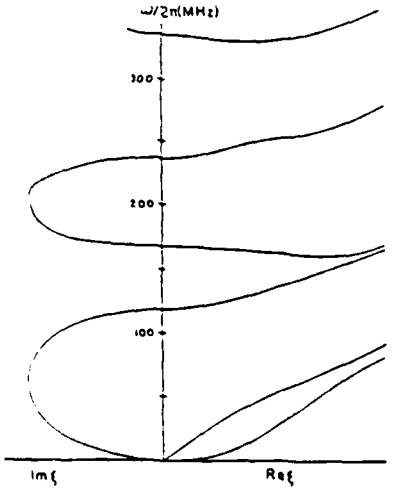

Figure 5 Dispersion Curves for the Gallium-Arsenide Layer without the Thin Film

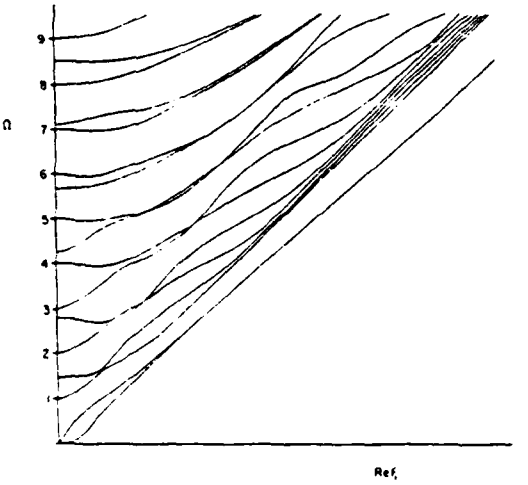

Figure 6 Dispersion Curves for the Gallium-Arsenide Wafer with Ω the Dimensionless Frequency Normalized with Respect to the First Thickness-Shear Frequency.

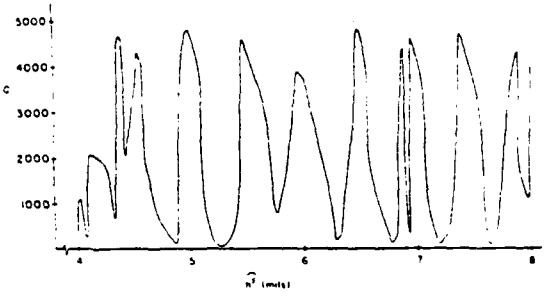

Figure 7 Quality Factor Versus Wafer Thickness when Trapping is not Present for the Composite Resonator Configuration Shown in Figure 1

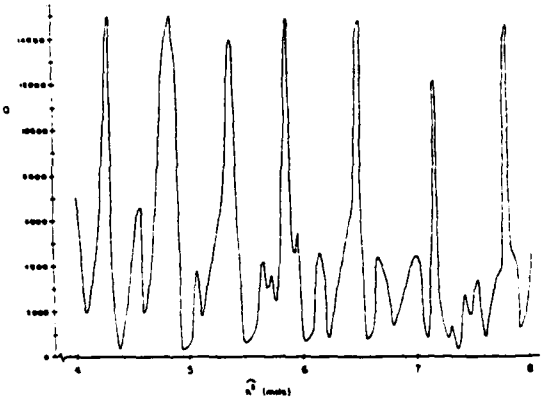

Figure 8 Quality Factor Versus Wafer Thickness when Trapping is not Present for the Composite Resonator Configuration Shown in Figure 2

Quality factor of the piezoelectric thin film on semiconductor composite resonator resulting from radiation into the semiconductor wafer

D. V. Shick, D. S. Stevens,[a] and H. F. Tiersten

Department of Mechanical Engineering, Aeronautical Engineering and Mechanics, Rensselaer Polytechnic Institute, Troy, New York 12180-3590

(Received 3 March 1986; accepted for publication 7 May 1986)

The composite resonator consists of a uniform thin layer etched in a small well-defined region of a semiconductor wafer to form a diaphragm, upon which is deposited a thin piezoelectric film along with the electrodes to form a resonant region directly on the wafer. Although the composite resonator, which operates in an essentially thickness-extensional mode, can be constructed to employ energy trapping, almost all existing experimental work in the literature is for the case when trapping is not present. All previous analytical work expressly ignores radiation into the bulk semiconductor except one treatment, which unrealistically ignores the junction between the etched diaphragm and the bulk semiconductor. In this work an analysis of the composite resonator driven into essentially thickness-extensional vibrations by the application of a voltage to strip electrodes is performed. The analysis includes all radiating plate waves in the thick portion of the semiconductor. The solution consists of a sum of terms satisfying all differential equations and boundary conditions on major surfaces exactly and uses the appropriate variational principle of linear piezoelectricity to satisfy the remaining conditions approximately. For the case of the aluminum–nitride film on gallium arsenide the Q is calculated for both the configuration in which the film ends at the edges of the electrodes and in which it continues to the edges of the etched diaphragm when trapping is not present and for the latter configuration when trapping is present. The calculations show that when trapping is not present the Q is a very rapidly varying function of the ratio of the composite resonator thickness to the wafer thickness and that the range of variation is very large, i.e., between one and two orders of magnitude. The calculations also reveal that when trapping is present the Q is always much larger and its range of variation much smaller than when trapping is not present.

I. INTRODUCTION

The composite resonator consists of a uniform thin layer etched in a small well-defined region of a semiconducting wafer to form a diaphragm, upon which is deposited a thin piezoelectric film along with the electrodes to form a resonant region directly on the wafer. In this work an analysis of the vibrations of a composite resonator is presented including the very important transverse behavior of the essentially thickness-extensional modes and the attendant radiation into the bulk semiconductor both for cases in which energy trapping is and is not present. The calculations are performed for the particular case of an aluminum–nitride film on gallium–arsenide.

Before proceeding with a discussion of this work, it is essential for clarity that we briefly explain the meaning of the words "energy trapping." Since the pure thickness-extensional resonant frequencies are cutoff frequencies, there is usually a nearby frequency range in which the transverse mode shape is evanescent. There is also a nearby frequency range in which the transverse mode shape is trigonometric. Consequently, by the selection of the appropriate thickness-extensional overtone (or fundamental) and/or the appropriate adjustment of the geometry in the electroded and unelectroded regions, the transverse modal behavior can be made to decay with distance away from the electrodes in the unelectroded region. The resulting vibration is called a trapped energy mode, which radiates a controllably small amount of energy into the adjacent thick portion of the semiconducting wafer and, hence, results in the highest possible Q, albeit with many nearby spurious modes with high Q. Alternatively, the overtone and/or geometry can be selected so that the mode does not decay with distance away from the electrode in the unelectroded region and the resulting vibration is not a trapped energy mode. In this case much more energy is radiated into the adjacent thick portion of the semiconducting wafer and much lower Q's result. Although there are still many nearby spurious modes, they are less troublesome because the Q's are lower. Almost all experimental work on the composite resonantor reported to date has been for this latter case.[1–6] On the other hand, a detailed analytical treatment of the composite resonator for the case when trapping is present appears in the literature[7] along with a detailed discussion of when trapping is and is not present.

Using the existing[8] constants of aluminum nitride, we have found that the fundamental essentially thickness-extensional mode will not trap for an aluminum-nitride film on a gallium–arsenide diaphragm in the flat-plate configuration.[9] However, the fundamental mode will trap if the gallium–arsenide diaphragm is appropriately notched a small amount in the electroded region, as shown in Fig. 9 of Ref. 7. In addition, we have found that the second essentially thickness-extensional mode will trap in the flat-plate configuration for the same film and substrate materials for appropriate film thickness to diaphragm thickness.

In this work an analysis of the vibrations of the composite

[a] Present address: AT&T Bell Laboratories, 1600 Osgood Street, North Andover, Massachusetts 01845

 0021-8979/86/192238-02$02.40

resonator, which is driven by the application of an ac voltage across strip electrodes on the major surfaces of the film, is performed. The analysis includes the pertinent waves in the active region of the composite resonator, as well as all radiating waves in the thick gallium–arsenide plate. All previous analytical work expressly ignores radiation into the bulk semiconductor except one treatment,[10] which unrealistically ignores the junction between the etched diaphragm and the bulk semiconductor. The solution is obtained by satisfying the differential equations for the piezoelectric film and semiconductor as well as all boundary conditions on the major surfaces of the film and semiconductor exactly and using the appropriate variational principle,[11] in which all conditions are natural conditions, to satisfy the remaining conditions along the minor interfaces and the inhomogeneous driving term that appears in a differential equation for the film in the electroded region approximately. The minor interfaces separate the electroded from the unelectroded regions of the resonator and the thin region of the gallium–arsenide from the thick region. Past experience shows that this type of approximation yields extremely accurate results if all the proper waves are included.[12,13] Both the configuration in which the film ends at the edges of the electrodes and in which it continues to the edges of the etched diaphragm have been considered when trapping is not present, along with the latter configuration when trapping is present. In each instance the quality factor (Q) at the resonance condition is calculated. The calculations show that when trapping is not present the Q is a very rapidly varying function of the ratio of the composite resonator thickness, i.e., the piezoelectric film plus the semiconductor layer, to the wafer thickness and that the range of variation of Q is very large, i.e., between one and two orders of magnitude. The calculations also reveal that when trapping is present the Q is always much larger and its range of variation with the thickness ratio much smaller than when trapping is not present.

II. BASIC EQUATIONS

The differential equations of motion and electrostatics and linear piezoelectric constitutive equations for aluminum nitride with x_3 the hexagonal axis may be written in the form[14]

$$c_{11}u_{1,11} + (c_{12} + c_{66})u_{2,12} + \quad _{,3} + c_{44}u_{1,33} + c_{66}u_{1,22} + c_{44}u_{3,13} + (e_{31} + e_{15})\varphi_{,13} \quad \rho\ddot{u}_1,$$

$$c_{11}u_{2,} \quad + (c_{66} + c_{12})u_{1,12} + c_{11}u_{2,} \quad + (c_{44} + c_{44})u_{2,33} + c_{44}u_{3,23} + (e_{31} + e_{15})\varphi_{,23} \quad \rho\ddot{u}_2,$$

$$c_{44}u_{3,11} + (c_{44} + c_{13})u_{1,13} + c_{44}u_{2,} \quad + (c_{44} + c_{13})u_{2,23} + c_{33}u_{3,33} + e_{15}\varphi_{,11} + e_{15}\varphi_{,22} + e_{33}\varphi_{,33} \quad \rho\ddot{u}_3, \tag{1}$$

$$e_{15}u_{3,11} + (e_{15} + e_{31})u_{1,13} + e_{15}u_{2,} \quad + (e_{15} + e_{31})u_{2,23} + e_{33}u_{3,33} \quad \epsilon_{11}\varphi_{,11} \quad \epsilon_{11}\varphi_{,22} \quad \epsilon_{33}\varphi_{,33} \quad 0, \tag{2}$$

$$T_1 \quad c_{11}u_{1,1} + c_{12}u_{2,2} + c_{13}u_{3,3} + e_{31}\varphi_{,3} \quad T_2 \quad c_{12}u_{1,1} + c_{11}u_{2,2} + c_{13}u_{3,3} + e_{31}\varphi_{,3},$$

$$T_3 \quad c_{13}u_{1,1} + c_{13}u_{2,2} + c_{33}u_{3,3} + e_{33}\varphi_{,3} \quad T_4 \quad c_{44}(u_{2,3} + u_{3,2}) + e_{15}\varphi_{,2},$$

$$T_5 \quad c_{44}(u_{3,1} + u_{1,3}) + e_{15}\varphi_{,1} \quad T_6 \quad c_{66}(u_{1,2} + u_{2,1}), \tag{3}$$

$$D_1 \quad e_{15}u_{1,3} + e_{15}u_{3,1} \quad \epsilon_{11}\varphi_{,1} \quad D_2 \quad e_{15}(u_{2,3} + u_{3,2}) \quad \epsilon_{11}\varphi_{,2} \quad D_3 \quad e_{31}u_{1,1} + e_{31}u_{2,2} + e_{33}u_{3,3} \quad \epsilon_{33}\varphi_{,3}, \tag{4}$$

where u_i, T_j, and D_i denote the components of the mechanical displacement, the stress tensor, and the electric displacement, respectively, and c_{ij}, e_{ij}, and ϵ_{ij} denote the elastic, piezoelectric, and dielectric constants, respectively, φ and ρ denote the electric potential and mass density, respectively, and we have employed the usual compressed matrix notation.[14] We employ Cartesian tensor notation, the summation convention for repeated tensor indices, the dot notation for partial differentiation with respect to time, and the convention that a comma followed by an index denotes partial differentiation with respect to a space coordinate. At this point we note that we have introduced a Cartesian coordinate system x_1, x_2, x_3 with the x_3 axis normal to the major surfaces of the aluminum nitride film. Similarly, the displacement equations of motion and linear elastic constitutive equations for the nonpiezoelectric gallium–arsenide semiconductor with x_3 along a cube axis take the form[14]

$$c_{11}u_{1,11} + (c_{12} + c_{44})u_{2,12} + (c_{13} + c_{44})u_{3,13} + c_{44}u_{1,33} + c_{44}u_{1,22} \quad \rho\ddot{u}_1,$$

$$c_{11}u_{2,} \quad + (c_{44} + c_{12})u_{1,12} + c_{11}u_{2,33} + (c_{13} + c_{44})u_{3,23} + c_{44}u_{2,11} \quad \rho\ddot{u}_2,$$

$$c_{44}u_{3,11} + (c_{44} + c_{13})u_{1,13} + c_{44}u_{2,} \quad + (c_{44} + c_{13})u_{2,23} + c_{33}u_{3,33} \quad \rho\ddot{u}_3, \tag{5}$$

$$T_1 \quad c_{11}u_{1,1} + c_{12}u_{2,2} + c_{13}u_{3,3} \quad T_2 \quad c_{12}u_{1,1} + c_{11}u_{2,2} + c_{13}u_{3,3} \quad T_3 \quad c_{13}u_{1,1} + c_{13}u_{2,2} + c_{33}u_{3,3},$$

$$T_4 \quad c_{44}(u_{2,3} + u_{3,2}), \quad T_5 \quad c_{44}(u_{3,1} + u_{1,3}), \quad T_6 \quad c_{44}(u_{1,2} + u_{2,1}) \tag{6}$$

We now note that in the essentially thickness-extensional modes in the region containing the film, which are the modes of interest in this work, the wave, or decay numbers along the plate are much smaller than the thickness wave numbers. As a consequence of these small wave and decay numbers along the plate and the small piezoelectric coupling of aluminum nitride, we can ignore the x_1 and x_2 dependence of all electrical variables as in Ref. 7, and in place of Eqs. (2) and (4), we have

$$e_{15}u_{3,} \quad \epsilon_{11}\varphi_{,} \quad 0, \tag{7}$$

$$D \quad e_{33}u \quad \epsilon_{33}\varphi_{,} \tag{8}$$

Figure 1 shows a schematic diagram of a cross section of a thin aluminum nitride film on a thin gallium–arsenide layer composite trapped-energy resonator for the configuration in which the film ends at the edge of the diaphragm. In the unelectroded regions the boundary conditions on the major surfaces are

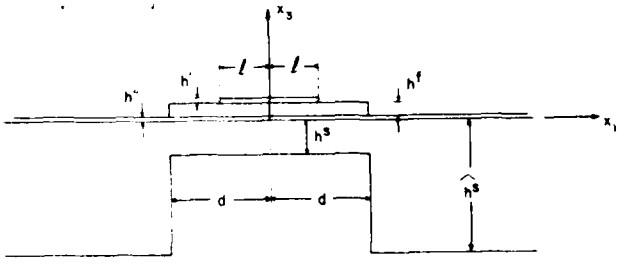

FIG. 1. Cross section of a composite resonator consisting of a thin piezoelectric film on a gallium arsenide layer with the film covering the entire layer.

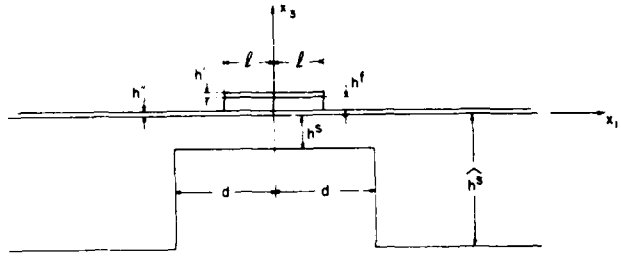

FIG. 2. Cross section of a composite resonator with the piezoelectric film ending at the edge of the electrodes.

$$T^f_{ij} = 0, \quad D^f_i = 0 \text{ at } x_3 = h^f, \tag{9}$$

$$T^f_{ij} - T^s_{ij} = h''\rho'' u'', \quad u^f = u^s_i, \quad D^f_i = 0 \text{ at } x_3 = 0, \tag{10}$$

$$T^s_{ij} = 0 \text{ at } x_3 = -h^s, \tag{11}$$

where the superscripts f and s stand for the thin-film and semiconductor layer, respectively, and ρ'' is the mass density of the ground electrode. The electrical condition in $(9)_2$ is a consequence of the fact that the x_1 and x_2 dependence of all electrical variables has been left out of account and the electric field in space vanishes at $x_3 = \infty$. Since the electrodes are much thinner than either the thin film or the layer, we have employed approximate thin-plate equations[17] for the electrode plating in $(10)_1$, and we have made use of the fact that the mechanical stiffness of the very thin electrode plating is negligible for small wavenumbers along the plate. Similarly, on the major surfaces of the composite plate in the electroded region the boundary conditions are

$$I^f_i = \rho' h' \ddot{u}'_i, \quad \varphi^f = V e^{i\omega t} \text{ at } x_3 = h^f, \tag{12}$$

$$\varphi^f = 0 \text{ at } x_3 = 0, \tag{13}$$

along with $(10)_2$ and $(11)_1$, which remain unchanged. The quantity ρ' is the mass density of the upper electrode.

Figure 2 shows a schematic diagram of a cross section for the configuration in which the film ends at the edges of the electrodes. The boundary conditions on the major surfaces of the composite plate in the electroded region, which still contains the film, are exactly the same as in the previous case. However, the boundary conditions on the major surfaces of the unelectroded plate, which no longer contains the film, are much simpler than in the previous case and in place of (9)–(11) we have

$$T^s_{ij} = 0 \text{ at } x_3 = 0 \text{ and } x_3 = -h^s. \tag{14}$$

For either configuration the corresponding boundary conditions on the major surfaces in the region of the bulk semiconductor are

$$T^s_{ij} = 0 \text{ at } x_3 = 0 \text{ and } x_3 = -\hat{h}^s. \tag{15}$$

Since we have replaced (2) and (4) by (7) and (8), respectively, no electrical conditions need be satisfied at a minor interface. Then the conditions that should be satisfied at each minor interface are the continuity of u_i, u_3, T_{i3}, and T_{33} and at each free edge are $T_{33} = T_{i3} = 0$. However, since in the approximation technique we employ the solution is written as a sum of eigensolutions, each of which satisfies the homogeneous differential equations and boundary conditions on the major surfaces for one of the three regions, i.e., the electroded composite, the unelectroded composite, and the bulk semiconductor, exactly, we cannot satisfy the continuity conditions across the interfaces between the regions exactly. Nevertheless, the remaining continuity conditions across the interfaces may be satisfied approximately by satisfying the proper form of the appropriate variational principle[11] of linear piezoelectricity, in which all conditions are natural conditions and all that remains is an integral over an inhomogeneous forcing term that arises in the solution plus integrals over the interfaces, because all other terms in that form of the variational principle vanish on account of the equations and conditions satisfied by the solution functions employed. The form of the variational principle of interest here is given in Eq. (6.44) of Ref. 11, which we reproduce here for the configuration shown in Fig. 3 in the form[18]

$$\begin{aligned}
\sum_m \Bigg(& \int_{V^{(m)}} \left[(\tau^{(m)}_{kl,k} - \rho^{(m)} \ddot{u}^{(m)}_l) \delta u^{(m)}_l + D^{(m)}_{k,k} \delta \varphi^{(m)} \right] dV \\
& + \int_{S_\sigma^{(m)}} \left[(\bar{t}^{(m)}_l - n^{(m)}_k \tau^{(m)}_{kl}) \delta u^{(m)}_l - (\bar{\sigma}^{(m)} + n^{(m)}_k D^{(m)}_k) \delta \varphi^{(m)} \right] dS \\
& + \int_{S_u^{(m)}} n^{(m)}_k \left[(u^{(m)}_l - \bar{u}^{(m)}_l) \delta \tau^{(m)}_{kl} + (\varphi^{(m)} - \bar{\varphi}^{(m)}) \delta D^{(m)}_k \right] dS \Bigg) \\
& + \int_{S_{12}} n^{(1)}_k \tfrac{1}{2} \left[(\tau^{(2)}_{kl} - \tau^{(1)}_{kl}) (\delta u^{(1)}_l + \delta u^{(2)}_l) + (u^{(1)}_l - u^{(2)}_l) (\delta \tau^{(1)}_{lk} + \delta \tau^{(2)}_{lk}) \right. \\
& \left. + (D^{(2)}_k - D^{(1)}_k) (\delta \varphi^{(1)} + \delta \varphi^{(2)}) - (\varphi^{(2)} - \varphi^{(1)}) (\delta D^{(1)}_k + \delta D^{(2)}_k) \right] dS = 0,
\end{aligned} \tag{16}$$

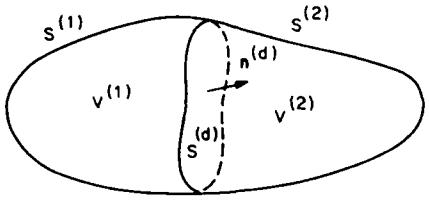

FIG. 3. Diagram of a bounded region containing an internal surface of discontinuity.

where $S^{(d)}$ denotes the surface of discontinuity separating region 1 from region 2, and $S_N^{(m)}$ and $S_C^{(m)}$ denote the portions of the mth surface on which natural- and constraint-type conditions,[19] respectively, are prescribed. We note that $S_N^{(m)}$ and $S_C^{(m)}$ refer to different portions of the surface for different terms in the boundary sums depending on each actual condition at a point. In (16) $n_k^{(m)}$ denotes the outwardly directed unit normal to the mth surface, $n_k^{(d)}$ denotes the unit normal to the surface of discontinuity directed from region 1 to region 2, $\bar{t}_l^{(m)}$, $\bar{\sigma}^{(m)}$, $\bar{u}_l^{(m)}$, and $\bar{\varphi}^{(m)}$ denote the prescribed tractions, charge, mechanical displacement, and electric potential, respectively, for the mth surface, and the meaning of the remaining quantities in (16) is obvious from earlier discussion. The variational condition in (16) for the simplest configuration, which is shown in Fig. 3, makes clear how to apply the variational condition to more complicated configurations such as shown in Figs. 1 and 2. Consequently, it is not worthwhile writing the general variational equivalent of (16) for each configuration because it becomes too cumbersome and the actual useful condition can be obtained from (16) for any configuration. Furthermore, in any given application what is taken as a surface of discontinuity for application of the variational principle (16) is not clear from the figure itself, but depends on what conditions the approximating functions satisfy.

III. PURE THICKNESS-EXTENSIONAL VIBRATIONS

Since in all the cases the composite resonator will be operated at a frequency in the vicinity of one of the pure thickness-extensional resonances of the composite plate, the pure thickness-extensional resonant frequencies of the composite are of particular importance in this work. It is shown in Sec. III of Ref. 7 that for the composite plate without a driving electrode but with a ground electrode, the pure thickness-extensional resonant frequencies are given by

$$\omega_c = (\bar{c}_{33}^{f}/\rho^{f})^{1/2}\eta_f^0(1 - R''/G^0), \tag{17}$$

where η_f^0 is the appropriate root of

$$\tan \eta_f^0 h^f + c^f \mu \tan \mu\sigma \eta_f^0 h^f = 0, \tag{18}$$

and

$$R'' = \frac{\rho'' h''}{\rho^f h^f}, \quad G^0 = \frac{1}{\cos^2 \eta_f^0 h^f} + \frac{c^f \mu^2 \sigma}{\cos^2 \mu\sigma \eta_f^0 h^f}, \tag{19}$$

with

$$c_{33}'' = c_{33}^{E} + [(e_{33}'')^2/\epsilon_{33}''], \quad c^f = c_{33}''/\bar{c}_{33}^{f},$$
$$\mu = (\bar{c}_{33}^{f}\rho^f/c_{33}''\rho'')^{1/2}, \quad \sigma = h''/h^f. \tag{20}$$

Similarly, for the completely electroded composite plate driven by a voltage it has also been shown in Sec. III of Ref. 7 that the pure thickness-extensional resonant frequencies are given by

$$\bar{\omega}_c = (\bar{c}_{33}^{f}/\rho^f)^{1/2}\eta_f^0(1 + P^0/G^0), \tag{21}$$

where

$$P^0 = \frac{k^2}{(\eta_f^0 h^f)^2} \times\left(\frac{2}{\cos \eta_f^0 h^f} - 2 + c^f \mu \tan \mu\sigma \eta_f^0 h^f \tan \eta_f^0 h^f\right) - R'' - R'(1 - c^f \mu \tan \eta_f^0 h^f \tan \mu\sigma \eta_f^0 h^f), \tag{22}$$

and

$$k^2 = (e_{33}^{f})^2/\bar{c}_{33}^{f}\epsilon_{33}^{f}, \quad R' = \rho' h'/\rho^f h^f. \tag{23}$$

The difference between the resonant frequencies of pure thickness-extensional vibrations of the composite plate with and without a driving electrode, i.e., $\omega_c - \bar{\omega}_c$ for the same η_f^0, is very important when trapping is present.

For later use in this work we now note from Eqs. (3.13) and (3.14) of Ref. 7 that when there is no driving electrode the solution for pure thickness vibrations takes the form

$$u_3^f = (A^f \cos \eta_f x_3 + B^f \sin \eta_f x_3)e^{i\omega t}, \tag{24}$$

$$u_3' = (A' \cos \eta_c x_3 + B' \sin \eta_c x_3)e^{i\omega t}, \tag{25}$$

where from Eq. (3.8) of Ref. 7 we have

$$\varphi^f = (e_{33}^{f}/\epsilon_{33}^{f})[u_3^f - u_3^f(0,t)], \tag{26}$$

which resulted in Eq. (17) of this work. Similarly, when there is a driving electrode and the composite plate is driven by a voltage $Ve^{i\omega t}$, from Eqs. (3.26) of Ref. 7 the solution takes the form

$$\bar{u}_3^f = u_3^f - (e_{33}^{f} V x_3/c_{33}^{f} h^f)e^{i\omega t},$$
$$\varphi^f = (e_{33}^{f}/\epsilon_{33}^{f})u_3^f + [Cx_3 + K + (Vx_3/h^f)]e^{i\omega t}, \tag{27}$$

where u_3^f is given in (24) and u_3' is still given by (25). This solution resulted in Eq. (21) of this work.

IV. STRAIGHT-CRESTED DISPERSION RELATIONS

In this section we obtain the straight-crested dispersion relations for the composite plate, the thin diaphragm without the film, and the bulk semiconductor because these determine the solution functions that are used in the variational condition (16). Since in this work we are considering strip electrodes as shown in Figs. 1 and 2, we are interested in the straight-crested eigensolutions varying with x_1 in each region. In the composite region we specifically treat propagating waves when the ground electrode is and the driving electrode is not present because these are somewhat simpler (less cumbersome) to treat than propagating waves between shorted electrodes, and on account of the small piezoelectric coupling and the small wavenumbers of interest in the composite region of the resonator, the dispersion relations and the associated solution for the case of shorted electrodes can readily be obtained from those for the case considered here

simply by employing the appropriate relations in Sec. III for the pure thickness solution in both cases exactly as in Ref. 7.

From the differential equations and boundary conditions presented in Sec. II we see that for the straight-crested waves varying along x_1, which are of interest in this work, we may take $u_2 = 0$ and from Eqs. (1), (7), and (5) we have the nontrivial differential equations

$$c^f_{11}u^f_{1,11} + (c^f_{13} + c^f_{44})u^f_{3,13} + c^f_{44}u^f_{1,33} = \rho^f\ddot{u}^f_1, \tag{28}$$

$$c^f_{44}u^f_{3,11} + (c^f_{13} + c^f_{44})u^f_{1,13} + c^f_{33}u^f_{3,33} + e^f_{33}\varphi^f_{,33} = \rho^f\ddot{u}^f_3, \tag{29}$$

$$e^f_{33}u^f_{3,33} - \epsilon^f_{33}\varphi^f_{,33} = 0, \tag{30}$$

$$c^s_{11}u^s_{1,11} + (c^s_{13} + c^s_{44})u^s_{3,13} + c^s_{44}u^s_{1,33} = \rho^s\ddot{u}^s_1, \tag{31}$$

$$c^s_{44}u^s_{3,11} + (c^s_{13} + c^s_{44})u^s_{1,13} + c^s_{33}u^s_{3,33} = \rho^s\ddot{u}^s_3, \tag{32}$$

and from Eqs. (9)–(11), (3), (6), and (8), we see that the boundary conditions for the unelectroded plate with a ground electrode take the form

$$c^f_{13}u^f_{1,1} + c^f_{33}u^f_{3,3} + e^f_{33}\varphi^f_{,3} = 0 \text{ at } x_3 = h', \tag{33}$$

$$u^f_{1,3} + u^f_{3,1} = 0, \quad e^f_{31}u^f_{1,3} - \epsilon^f_{33}\varphi^f_{,3} = 0 \text{ at } x_3 = h', \tag{34}$$

$$c^f_{13}u^f_{1,1} + c^f_{33}u^f_{3,3} + e^f_{33}\varphi^f_{,3} - c^s_{13}u^s_{1,1} - c^s_{33}u^s_{3,3} = h''\rho''\ddot{u}^s_3,$$

$$u^f_i = u^s_i \text{ at } x_3 = 0, \tag{35}$$

$$c^f_{44}(u^f_{1,3} + u^f_{3,1}) - c^s_{44}(u^s_{1,3} + u^s_{3,1}) = h''\rho''\ddot{u}^s_1,$$

$$u^f_1 = u^s_1, \quad e^f_{31}u^f_{3,3} - \epsilon^f_{33}\varphi^f_{,3} = 0 \text{ at } x_3 = 0, \tag{36}$$

$$c^s_{13}u^s_{1,1} + c^s_{33}u^s_{3,3} = 0,$$

$$u^s_{1,3} + u^s_{3,1} = 0 \text{ at } x_3 = -h^s. \tag{37}$$

As in the case of pure thickness vibrations, in order to satisfy Eqs. (30), $(34)_2$, and $(36)_1$, we first take φ^f in the form given in Eq. (26), which we note also satisfies the condition $\varphi^f = 0$ at $x_3 = 0$, and substitute into Eqs. (29), (33), and $(35)_1$ to obtain

$$c^f_{44}u^f_{3,11} + (c^f_{13} + c^f_{44})u^f_{1,13} + \bar{c}^f_{33}u^f_{3,33} = \rho^f\ddot{u}^f_3, \tag{38}$$

$$c^f_{13}u^f_{1,1} + \bar{c}^f_{33}u^f_{3,3} = 0 \text{ at } x_3 = h', \tag{39}$$

$$c^f_{13}u^f_{1,1} + \bar{c}^f_{33}u^f_{3,3} - c^s_{13}u^s_{1,1} - c^s_{33}u^s_{3,3} = h''\rho''\ddot{u}^s_3 \text{ at } x_3 = 0. \tag{40}$$

As a solution of Eqs. (28), (38), (31), and (32), we take

$$u^f_a = (A^f_a e^{\eta^f_a x_3} + B^f_a e^{-\eta^f_a x_3})e^{i\xi x_1}e^{i\omega t}, \tag{41}$$

$$u^s_a = (A^s_a e^{\eta^s_a x_3} + B^s_a e^{-\eta^s_a x_3})e^{i\xi x_1}e^{i\omega t}, \tag{42}$$

in which the subscripts a,b take the values 1 and 3 but skip 2. The solution functions in (41) satisfy Eqs. (28) and (38) provided

$$\sigma^f_{11}A^f_1 + \sigma^f_{13}A^f_3 = 0, \quad \sigma^f_{13}A^f_1 + \sigma^f_{33}A^f_3 = 0, \tag{43}$$

$$\sigma^f_{11}B^f_1 - \sigma^f_{13}B^f_3 = 0, \quad -\sigma^f_{13}B^f_1 + \sigma^f_{33}B^f_3 = 0, \tag{44}$$

where

$$\sigma^f_{11} = -c^f_{11}\xi^2 - c^f_{44}\eta^{f2} + \rho^f\omega^2,$$
$$\sigma^f_{13} = -(c^f_{13} + c^f_{44})\xi\eta_f,$$
$$\sigma^f_{33} = -c^f_{44}\xi^2 - \bar{c}^f_{33}\eta^{f2} + \rho^f\omega^2, \tag{45}$$

and the solution functions in (42) satisfy Eqs. (31) and (32) provided

$$\sigma^s_{11}A^s_1 + \sigma^s_{13}A^s_3 = 0, \quad \sigma^s_{13}A^s_1 + \sigma^s_{33}A^s_3 = 0, \tag{46}$$

$$\sigma^s_{11}B^s_1 - \sigma^s_{13}B^s_3 = 0, \quad -\sigma^s_{13}B^s_1 + \sigma^s_{33}B^s_3 = 0, \tag{47}$$

where

$$\sigma^s_{11} = -c^s_{11}\xi^2 - c^s_{44}\eta^{s2} + \rho^s\omega^2,$$
$$\sigma^s_{13} = -(c^s_{13} + c^s_{44})\xi\eta_s,$$
$$\sigma^s_{33} = -c^s_{44}\xi^2 - c^s_{33}\eta^{s2} + \rho^s\omega^2. \tag{48}$$

Each of these four systems, Eqs. (43), (44), (46), and (47), of two linear, homogeneous algebraic equations in two amplitudes yields nontrivial solutions when the determinant of the coefficients of the amplitudes vanishes. Both determinants for the film are identical, as are both determinants for the layer. Each of the two independent determinants is quadratic in ξ^2, η^2, and ω^2. Hence, for a given ξ and ω, each determinant yields two independent $\eta(\eta^{f(1)}_f, \eta^{f(2)}_f$ and $\eta^{s(1)}_s$, $\eta^{s(2)}_s)$ and each $\eta^{(i)}$ yields independent amplitude ratios from either of the two equations leading to each of the four determinants. Let us denote the eight sets of amplitude ratios by

$$A^{fi}_1 = \mu^{fi}A^{fi}_3, \quad B^{fi}_1 = \nu^{fi}B^{fi}_3, \quad A^{si}_1 = \mu^{si}A^{si}_3,$$
$$B^{si}_1 = \nu^{si}B^{si}_3, \quad i = 1,2. \tag{49}$$

As a solution of the boundary conditions $(34)_1$, (39), (40), $(35)_2$, $(36)_{1,2}$, and (37), we take

$$u^f_1 = \sum_{m=1}^{2}(A^{fm}_1 e^{\eta^{fm}x_3} + B^{fm}_1 e^{-\eta^{fm}x_3})e^{i\xi x_1}e^{i\omega t},$$

$$u^f_3 = \sum_{m=1}^{2}(\mu^{fm}A^{fm}_1 e^{\eta^{fm}x_3} + \nu^{fm}B^{fm}_1 e^{-\eta^{fm}x_3})e^{i\xi x_1}e^{i\omega t},$$

$$u^s_1 = \sum_{m=1}^{2}(A^{sm}_1 e^{\eta^{sm}x_3} + B^{sm}_1 e^{-\eta^{sm}x_3})e^{i\xi x_1}e^{i\omega t},$$

$$u^s_3 = \sum_{m=1}^{2}(\mu^{sm}A^{sm}_1 e^{\eta^{sm}x_3} + \nu^{sm}B^{sm}_1 e^{-\eta^{sm}x_3})e^{i\xi x_1}e^{i\omega t}. \tag{50}$$

Substituting from Eqs. (50) into the boundary conditions $(34)_1$, (39), (40), $(35)_2$, $(36)_{1,2}$, and (37) and employing Eqs. (49), for $h'' = 0$ we obtain

$$\sum_{n=1}^{2}\left[A_1^{(n)}(c_{11}^{(n)}\xi\mu_1^{(n)}+\bar{c}_{13}^{(n)}\eta_{1n})e^{i\eta_{1n}h^{(n)}}+B_1^{(n)}(c_{11}^{(n)}\xi\nu_1^{(n)}-\bar{c}_{13}^{(n)}\eta_{1n})e^{-i\eta_{1n}h^{(n)}}\right]=0,$$

$$\sum_{n=1}^{2}\left[A_2^{(n)}(\eta_{1n}\mu_1^{(n)}-\xi)e^{i\eta_{1n}h^{(n)}}+B_2^{(n)}(-\eta_{1n}\nu_1^{(n)}+\xi)e^{-i\eta_{1n}h^{(n)}}\right]=0,$$

$$\sum_{n=1}^{2}\left[A_1^{(n)}(c_{11}^{(n)}\xi\mu_1^{(n)}+\bar{c}_{13}^{(n)}\eta_{1n})+B_1^{(n)}(c_{11}^{(n)}\xi\nu_1^{(n)}-\bar{c}_{13}^{(n)}\eta_{1n})-A_3^{(n)}(c_{11}^{(n)}\xi\mu_3^{(n)}+c_{13}^{(n)}\eta_{3n})-B_3^{(n)}(c_{11}^{(n)}\xi\nu_3^{(n)}-c_{13}^{(n)}\eta_{3n})\right]=0,$$

$$\sum_{n=1}^{2}(A_1^{(n)}+B_1^{(n)}-A_3^{(n)}-B_3^{(n)})=0,$$

$$\sum_{n=1}^{2}\left[A_1^{(n)}c_{44}^{(n)}(\eta_{1n}\mu_1^{(n)}+\xi)+B_1^{(n)}c_{44}^{(n)}(-\eta_{1n}\nu_1^{(n)}+\xi)-A_3^{(n)}c_{44}^{(n)}(\eta_{3n}\mu_3^{(n)}+\xi)-B_3^{(n)}c_{44}^{(n)}(-\eta_{3n}\nu_3^{(n)}+\xi)\right]=0,$$

$$\sum_{n=1}^{2}(\mu_1^{(n)}A_1^{(n)}+\nu_1^{(n)}B_1^{(n)}-\mu_3^{(n)}A_3^{(n)}-\nu_3^{(n)}B_3^{(n)})=0,$$

$$\sum_{n=1}^{2}\left[A_3^{(n)}(c_{11}^{(n)}\xi\mu_3^{(n)}+c_{13}^{(n)}\eta_{3n})e^{-i\eta_{3n}h^{(n)}}+B_3^{(n)}(c_{11}^{(n)}\xi\nu_3^{(n)}-c_{13}^{(n)}\eta_{3n})e^{i\eta_{3n}h^{(n)}}\right]=0,$$

$$\sum_{n=1}^{2}\left[A_4^{(n)}(\eta_{3n}\mu_3^{(n)}+\xi)e^{-i\eta_{3n}h^{(n)}}+B_4^{(n)}(-\eta_{3n}\nu_3^{(n)}+\xi)e^{i\eta_{3n}h^{(n)}}\right]=0. \tag{51}$$

Equations (51) constitute a system of eight linear homogeneous algebraic equations in $A_1^{(n)}$, $B_1^{(n)}$, $A_3^{(n)}$, and $B_3^{(n)}$, which yield nontrivial solutions when the determinant of the coefficients vanishes. For a given geometry and ω the resulting equation yields an infinite number of roots ξ, each of which determines a point on the dispersion spectrum and yields amplitude ratios from any seven of the eight equations in Eqs. (51). Calculations are performed by first selecting values of ω and ξ, which enable the determination of the η_{1n} and η_{3n} from the two independent 2×2 determinants obtained from Eqs. (43) or (44) and Eqs. (46) or (47), respectively. These values of η_{1n} and η_{3n} enable the determination of the amplitude ratios $\mu_1^{(n)}$, $\nu_1^{(n)}$, $\mu_3^{(n)}$, and $\nu_3^{(n)}$ from either of the equations in Eqs. (43), (44), (46), and (47), respectively. Then all quantities in the determinant obtained from Eqs. (51) are known and the resulting determinantal equation either is or is not satisfied. If it is satisfied the values of ω and ξ selected are correct and constitute a point on the dispersion curves. If not, change either ω or ξ and repeat the calculation until the boundary condition determinantal equation is satisfied.

The pertinent dispersion curves for the aluminum–nitride film on the gallium–arsenide layer composite plate have been calculated and are shown in Fig. 4. We do not distinguish between the electroded film with shorted electrodes and the unelectroded film in the figure. This is done in great detail in Ref. 7. Furthermore, when required, the difference between the two can be calculated from $(\omega^e-\bar{\omega}^e)$ given in Sec. III. The dispersion curves are for a film thickness of 7 μm and a diaphragm thickness of 14 μm.

In the region of the bulk semiconductor the solution is considerably simpler than in the composite region of the resonator because there is only one section with traction-free upper and lower surfaces. However, although this problem can be simplified even further by placing the coordinate system in the center of the plate, it is not convenient for us to do this in this work because the solutions in each region are put together in the variational equation (16) when the solution to the forced vibration problem is obtained in the next section. In the region of the bulk semiconductor the differential equations are identical with those given in (31) and (32), but with carets over the variables, and which for clarity we write here in the form

$$\hat{c}_{11}^{(3)}\hat{u}_{1,11}^{(3)}+(\hat{c}_{13}^{(3)}+\hat{c}_{44}^{(3)})\hat{u}_{3,13}^{(3)}+\hat{c}_{44}^{(3)}\hat{u}_{1,33}^{(3)}=\rho^{(3)}\ddot{\hat{u}}_1^{(3)},$$

$$\hat{c}_{44}^{(3)}\hat{u}_{3,11}^{(3)}+(\hat{c}_{13}^{(3)}+\hat{c}_{44}^{(3)})\hat{u}_{1,13}^{(3)}+\hat{c}_{33}^{(3)}\hat{u}_{3,33}^{(3)}=\rho^{(3)}\ddot{\hat{u}}_3^{(3)}. \tag{52}$$

From (6) and (15) with $\hat{u}_2=0$ the boundary conditions take the form

$$\hat{c}_{13}^{(3)}\hat{u}_{1,1}^{(3)}+\hat{c}_{33}^{(3)}\hat{u}_{3,3}^{(3)}=0 \quad \text{at } x_3=0 \text{ and } x_3=-\hat{h}^{(3)}, \tag{53}$$

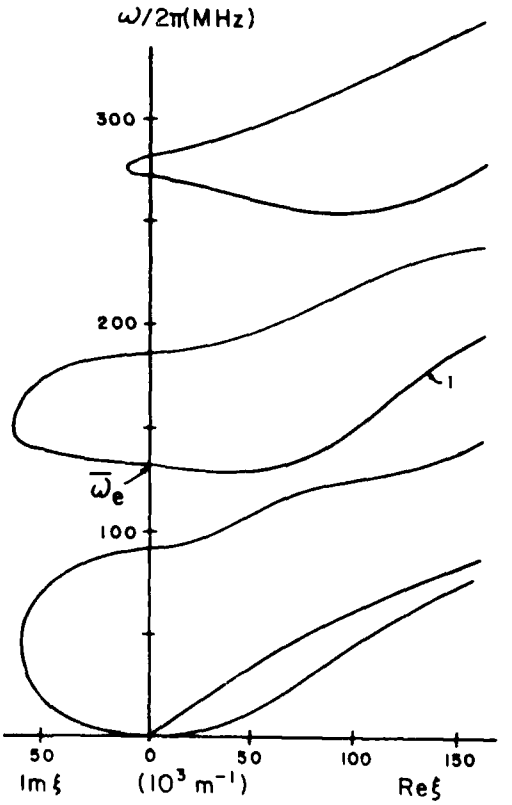

FIG. 4. Dispersion curves for the composite region consisting of an aluminum–nitride film on a gallium–arsenide layer.

$$c'_{44}(\hat{u}'_{1,3} + \hat{u}'_{3,1}) = 0 \text{ at } x_3 = 0 \text{ and } x_3 = -\hat{h}'. \tag{54}$$

As a solution of (52) consider

$$\hat{u}'_a = (\hat{A}'_a e^{i\hat{\eta}'_n x_3} + \hat{B}'_a e^{-i\hat{\eta}'_n x_3}) e^{i\hat{\xi}x_1} e^{i\omega t}, \tag{55}$$

which satisfies (52) provided

$$\sigma'_{11}\hat{A}'_1 + \sigma'_{13}\hat{A}'_3 = 0, \quad \sigma'_{13}\hat{A}'_1 + \sigma'_{33}\hat{A}'_3 = 0, \tag{56}$$

$$\sigma'_{11}\hat{B}'_1 - \sigma'_{13}\hat{B}'_3 = 0, \quad -\sigma'_{13}\hat{B}'_1 + \sigma'_{33}\hat{B}'_3 = 0, \tag{57}$$

where σ'_{11}, σ'_{13}, and σ'_{33} are given in (48). Each of the two systems of linear homogeneous algebraic equations in two amplitudes yields nontrivial solutions when the determinant of the coefficients of the amplitudes vanishes. Both determinants are identical and, in fact, are the same as the earlier determinants for the layer. Thus, for a given $\hat{\xi}$ and ω each determinant yields two independent $\hat{\eta}'_n$ ($\hat{\eta}'^{(1)}_n, \hat{\eta}'^{(2)}_n$) and each $\hat{\eta}'^{(m)}_n$ yields amplitude ratios from each system of linear algebraic equations, i.e., (56) and (57). Hence, there are four amplitude ratios, which we denote by

$$\hat{A}'^m_1 = \mu'^m \hat{A}'^m_3, \quad \hat{B}'^m_1 = \nu'^m \hat{B}'^m_3, \tag{58}$$

in which the μ'^m and ν'^m are the same as in (49).

As a solution of the boundary conditions (53) and (54), we take

$$\hat{u}'_1 = \sum_{m=1}^{2} (\hat{A}'^m_1 e^{i\hat{\eta}'^m_n x_3} + \hat{B}'^m_1 e^{-i\hat{\eta}'^m_n x_3}) e^{i\hat{\xi}x_1} e^{i\omega t},$$

$$\hat{u}'_3 = \sum_{m=1}^{2} (\mu'^m \hat{A}'^m_3 e^{i\hat{\eta}'^m_n x_3} + \nu'^m \hat{B}'^m_3 e^{-i\hat{\eta}'^m_n x_3}) e^{i\hat{\xi}x_1} e^{i\omega t}. \tag{59}$$

Substituting from (59) into the boundary conditions (53) and (54), we obtain

$$\sum_{m=1}^{2} [\hat{A}'^m_3 (c'_{13}\hat{\xi}\mu'^m + c'_{33}\hat{\eta}'^m_n) + \hat{B}'^m_3 (c'_{13}\hat{\xi}\nu'^m - c'_{33}\hat{\eta}'^m_n)] = 0,$$

$$\sum_{m=1}^{2} [\hat{A}'^m_3 (\hat{\eta}'^m_n \mu'^m + \hat{\xi}) + \hat{B}'^m_3 (-\hat{\eta}'^m_n \nu'^m + \hat{\xi})] = 0,$$

$$\sum_{m=1}^{2} [\hat{A}'^m_3 (c'_{13}\hat{\xi}\mu'^m + c'_{33}\hat{\eta}'^m_n) e^{-i\hat{\eta}'^m_n \hat{h}'} + \hat{B}'^m_3 (c'_{13}\hat{\xi}\nu'^m - c'_{33}\hat{\eta}'^m_n) e^{i\hat{\eta}'^m_n \hat{h}'}] = 0,$$

$$\sum_{m=1}^{2} [\hat{A}'^m_3 (\hat{\eta}'^m_n \mu'^m + \hat{\xi}) e^{-i\hat{\eta}'^m_n \hat{h}'} + \hat{B}'^m_3 (-\hat{\eta}'^m_n \nu'^m + \hat{\xi}) e^{i\hat{\eta}'^m_n \hat{h}'}] = 0. \tag{60}$$

Equations (60) constitute a system of four linear homogeneous algebraic equations in $\hat{A}'^m_3$ and $\hat{B}'^m_3$, which yields nontrivial solutions when the determinant of the coefficients vanishes. At this point it should be noted that if $\hat{A}'^m_3$ and $\hat{B}'^m_3$ are written as complex conjugates, the system can be simplified into solutions respectively symmetric and antisymmetric about the centerline of the plate, which may be treated separately. However, this is not particularly convenient for us because we need both the symmetric and antisymmetric solutions and we have already treated the composite plate, which programs are readily modified for this case. Clearly, this solution holds for the region of the thin diaphragm without the film provided only that $\hat{h}'$ is replaced by h'. Calculations are performed as in the case of the composite region with the given attendant reduction resulting from the elimination of the film.

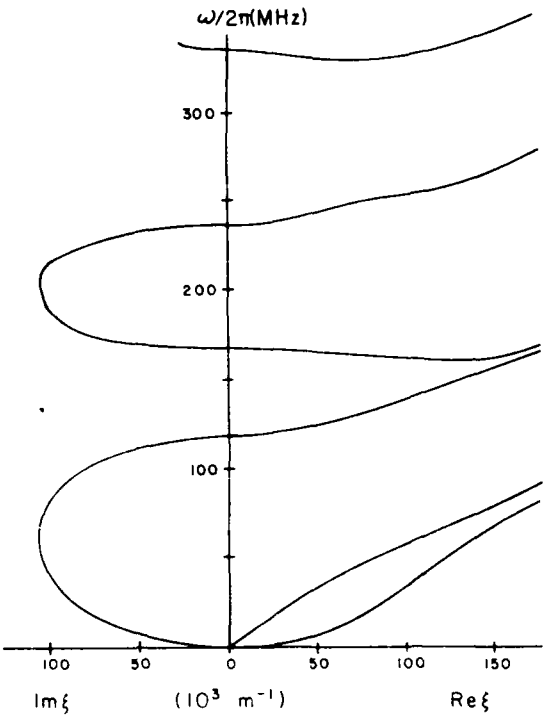

FIG. 5. Dispersion curves for the gallium-arsenide layer without the thin film

The pertinent dispersion curves for a 14-μm-thick gallium-arsenide diaphragm have been calculated and are shown in Fig. 5. The lowest 17 real dispersion curves for the bulk gallium-arsenide plate have been calculated and are shown in dimensionless form in Fig. 6. For the fundamental

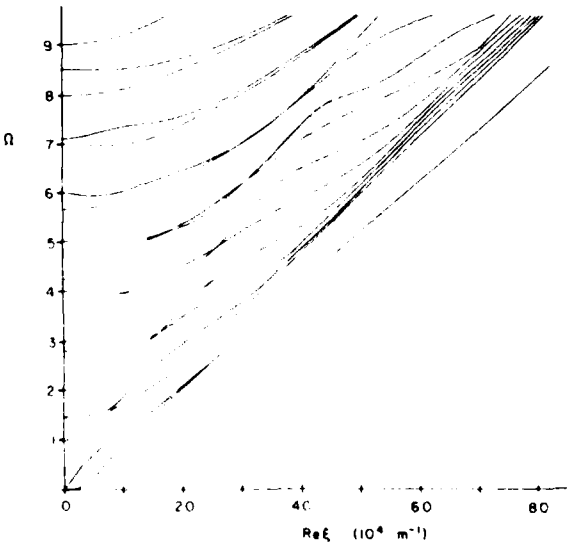

FIG. 6. Dispersion curves for the gallium arsenide wafer with Ω the dimensionless frequency normalized with respect to the first thickness-shear frequency

essentially thickness-extensional resonance for the composite dimensions mentioned (around 132 MHz), this number of dispersion curves is for a gallium–arsenide wafer thickness of about 5 mils. In this work we perform calculations for wafer thicknesses up to 8 mils for which there are 30 real dispersion curves for a frequency of 132 MHz. However, we do not bother to show the figure for more than 17 in this work.

V. FORCED VIBRATIONS OF COMPOSITE RESONATOR

In this section we determine the essentially thickness-extensional vibrations driven by the application of a steady-state driving voltage to the strip electrodes on the surfaces of the piezoelectric film of the composite resonator shown in Figs. 1 and 2. Since we include radiation into the bulk semiconductor, we can use the solution to calculate the Q at resonance of the mode resulting from radiation into the bulk semiconductor.

In accordance with the earlier discussion we take the approximate solution in the form

$$\bar{u}_a^f = \sum_{\beta=1}^{\bar{n}} \bar{K}^{(\beta)} \bar{u}_a^{f(\beta)} - \frac{e_{33}^f V x_3 e^{i\omega t}}{c_{33}^f h^f} \delta_{a3}, \quad \bar{u}_a^s = \sum_{\beta=1}^{\bar{n}} \bar{K}^{(\beta)} \bar{u}_a^{s(\beta)},$$

$$u_a^f = \sum_{\alpha=1}^{n} K^{(\alpha)} u_a^{f(\alpha)}, \quad u_a^s = \sum_{\alpha=1}^{n} K^{(\alpha)} u_a^{s(\alpha)}, \quad \hat{u}_a^s = \sum_{\gamma=1}^{\hat{n}} \hat{K}^{(\gamma)} \hat{u}_a^{s(\gamma)}, \tag{61}$$

where $\bar{n}$, n, and $\hat{n}$ denote the number of branches of the dispersion curves included in the electroded composite, unelectroded composite or diaphragm and bulk semiconductor, respectively, which are given in Figs. 4–6. The eigensolution functions $\bar{u}_a^{f(\beta)}$, $\bar{u}_a^{s(\beta)}$, $u_a^{f(\alpha)}$, $u_a^{s(\alpha)}$, $\hat{u}_a^{s(\gamma)}$ denote the solution functions that satisfy the homogeneous differential equations and the boundary conditions on the major surfaces for each of the respective regions and which were presented in Sec. IV and yield the dispersion curves shown in Figs. 4–6. At this point we note that since the driving voltage V is applied over the region $-l < x_1 < l$, the eigensolution functions in the electroded region of the composite resonator will be symmetric about $x_1 = 0$ and, consequently, the factor $e^{i\xi x_1}$ in (50) will be replaced by $(e^{i\xi x_1} + e^{-i\xi x_1})/2$ in the expressions for u_3^f and u_3^s and $(e^{i\xi x_1} - e^{-i\xi x_1})/2i$ in the expressions for u_1^f and u_1^s, respectively, in $(61)_{1,2}$. Since the solution functions $\bar{u}_a^{f(\beta)}$, $\bar{u}_a^{s(\beta)}$, $u_a^{f(\alpha)}$, $u_a^{s(\alpha)}$, and $\hat{u}_a^{s(\gamma)}$ satisfy the homogeneous differential equations and boundary conditions on the major surfaces for each of the respective regions and the solution is symmetric about $x_1 = 0$, when (61) will be substituted in (16) all that will remain may be written in the appropriate form

$$\begin{aligned}
&-\int_0^l \int_0^{h^f} \rho^f \omega^2 \frac{e_{33}^f V x_3}{c_{33}^f h^f} e^{i\omega t} \delta\bar{u}_1^f \, dx_3 \, dx_1 - \int_0^{h^f} (\bar{T}_{13}^f \, \delta\bar{u}_3^f + \bar{T}_{11}^f \, \delta\bar{u}_1^f)\Big|_{x_1=d} dx_3 \\
&+ \int_{\bar{h}^s}^{h^s} (\hat{T}_{11}^s \, \delta\hat{u}_1^s + \hat{T}_{13}^s \, \delta\hat{u}_3^s)\Big|_{x_1=d} dx_3 + \frac{1}{2}\int_{h^s}^{0} [(T_{11}^s - \bar{T}_{11}^s)(\delta\bar{u}_1^s + \delta u_1^s) \\
&+ (T_{13}^s - \bar{T}_{13}^s)(\delta\bar{u}_3^s + \delta u_3^s) + (\bar{u}_1^s - u_1^s)(\delta\bar{T}_{11}^s + \delta T_{11}^s) + (\bar{u}_3^s - u_3^s)(\delta\bar{T}_{13}^s + \delta T_{13}^s)]_{x_1=d} \, dx_3 \\
&+ \frac{1}{2}\int_0^{h^f} [(T_{11}^f - \bar{T}_{11}^f)(\delta\bar{u}_1^f + \delta u_1^f) + (T_{13}^f - \bar{T}_{13}^f)(\delta\bar{u}_3^f + \delta u_3^f) \\
&+ (\bar{u}_1^f - u_1^f)(\delta\bar{T}_{11}^f + \delta T_{11}^f) + (\bar{u}_3^f - u_3^f)(\delta\bar{T}_{13}^f + \delta T_{13}^f)]_{x_1=d} \, dx_3 \\
&+ \frac{1}{2}\int_{h^s}^{0} [(T_{11}^s - T_{11}^s)(\delta u_1^s + \delta\hat{u}_1^s) + (\hat{T}_{13}^s - T_{13}^s)(\delta u_3^s + \delta\hat{u}_3^s) \\
&+ (u_1^s - \hat{u}_1^s)(\delta T_{11}^s + \delta\hat{T}_{11}^s) + (u_3^s - \hat{u}_3^s)(\delta T_{13}^s + \delta\hat{T}_{13}^s)]_{x_1=d} \, dx_3 = 0,
\end{aligned} \tag{62}$$

for the case when trapping is not present and the film extends over the entire diaphragm, as shown in Fig. 1. When the film ends at the edges of the electrodes, as shown in Fig. 2, the fifth integral in (62) is not present and the second integral is replaced by

$$-\int_0^{h^f} (\bar{T}_{13}^f \, \delta\bar{u}_3^f + \bar{T}_{11}^f \, \delta\bar{u}_1^f)\Big|_{x_1=l} dx_3. \tag{63}$$

When trapping is present with a notch under the electroded region, as shown in Fig. 7, the fourth integral is taken from $-\bar{h}^s$ to 0 (instead of $-h^s$ to 0) and there is an additional term,

$$+\int_{\bar{h}^s}^{h^s} (T_{11}^s \, \delta u_1^s + T_{13}^s \, \delta u_3^s)\Big|_{x_1=l} dx_3, \tag{64}$$

in Eq. (62).

Since the solution functions in (61) are fixed, only the $\bar{K}^{(\beta)}$, $K^{(\alpha)}$, and $\hat{K}^{(\gamma)}$ are varied when (61) is substituted into (62). Accordingly, substituting from (61) into (62), employing (3), (6), and (50) with the appropriate aforementioned replacement in $(61)_{1,2}$ and (59), and performing the integrations, we obtain an equation of the form

$$\sum_{\beta=1}^{\bar{n}} \delta\bar{K}^{(\beta)} V \dot{\bar{c}}^{(\beta)} + \sum_{\beta=1}^{\bar{n}} \sum_{\delta=1}^{\bar{n}} \delta\bar{K}^{(\beta)} \bar{K}^{(\delta)} \bar{a}_{\beta\delta} + \sum_{\alpha=1}^{n} \sum_{\epsilon=1}^{n} \delta K^{(\alpha)} K^{(\epsilon)} a_{\alpha\epsilon} + \sum_{\gamma=1}^{\hat{n}} \sum_{\zeta=1}^{\hat{n}} \delta\hat{K}^{(\gamma)} \hat{K}^{(\zeta)} \hat{a}_{\gamma\zeta}$$
$$+ \sum_{\beta=1}^{\bar{n}} \sum_{\alpha=1}^{n} (\delta\bar{K}^{(\beta)} K^{(\alpha)} \bar{b}_{\beta\alpha} + \delta K^{(\alpha)} \bar{K}^{(\beta)} \bar{b}_{\beta\alpha}) + \sum_{\alpha=1}^{n} \sum_{\gamma=1}^{\hat{n}} (\delta K^{(\alpha)} \hat{K}^{(\gamma)} \hat{b}_{\alpha\gamma} + \delta\hat{K}^{(\gamma)} K^{(\alpha)} \hat{b}_{\alpha\gamma}) = 0, \tag{65}$$

where the expressions for $\bar{a}_{\beta\delta}$, $a_{\alpha\epsilon}$, $\hat{a}_{\gamma\zeta}$, $\bar{b}_{\beta\alpha}$, $\hat{b}_{\alpha\gamma}$, and $\bar{c}^{(\beta)}$ are given by

$$\bar{a}_{\beta\alpha} = \frac{1}{2} \sum_{m=1}^{2} \sum_{n=1}^{2} \big[g(\bar{\eta}^{\alpha}_{fm} + \bar{\eta}^{\beta}_{fn})^{h'}_{0} h^{\bar{\alpha}\bar{\beta}}_{fmn,1} + g(\bar{\eta}^{\alpha}_{fm} - \bar{\eta}^{\beta}_{fn})^{h'}_{0} h^{\bar{\alpha}\bar{\beta}}_{fmn,2} + g(\bar{\eta}^{\beta}_{fn} - \bar{\eta}^{\alpha}_{fm})^{h'}_{0} h^{\bar{\alpha}\bar{\beta}}_{fmn,3}$$
$$+ g(-\bar{\eta}^{\alpha}_{fm} - \bar{\eta}^{\beta}_{fn})^{h'}_{0} h^{\bar{\alpha}\bar{\beta}}_{fmn,4} + g(\bar{\eta}^{\alpha}_{sm} + \bar{\eta}^{\beta}_{sn})^{0}_{h} h^{\bar{\alpha}\bar{\beta}}_{smn,1} + g(\bar{\eta}^{\alpha}_{sm} - \bar{\eta}^{\beta}_{sn})^{0}_{h} h^{\bar{\alpha}\bar{\beta}}_{smn,2}$$
$$+ g(\bar{\eta}^{\beta}_{sn} - \bar{\eta}^{\alpha}_{sm})^{0}_{h} h^{\bar{\alpha}\bar{\beta}}_{smn,3} + g(-\bar{\eta}^{\alpha}_{sm} - \bar{\eta}^{\beta}_{sn})^{0}_{h} h^{\bar{\alpha}\bar{\beta}}_{smn,4} \big] e^{i(\bar{\xi}_{\alpha} + \bar{\xi}_{\beta})l},$$

$$\bar{b}_{\beta\alpha} = \frac{1}{2} \sum_{m=1}^{2} \sum_{n=1}^{2} \big[g(\bar{\eta}^{\alpha}_{fm} + \eta^{\beta}_{fn})^{h'}_{0} h^{\bar{\alpha}\beta}_{fmn,1} + g(\bar{\eta}^{\alpha}_{fm} - \eta^{\beta}_{fn})^{h'}_{0} h^{\bar{\alpha}\beta}_{fmn,2} + g(\eta^{\beta}_{fn} - \bar{\eta}^{\alpha}_{fm})^{h'}_{0} h^{\bar{\alpha}\beta}_{fmn,3}$$
$$+ g(-\bar{\eta}^{\alpha}_{fm} - \eta^{\beta}_{fn})^{h'}_{0} h^{\bar{\alpha}\beta}_{fmn,4} + g(\bar{\eta}^{\alpha}_{sm} + \eta^{\beta}_{sn})^{0}_{h} h^{\bar{\alpha}\beta}_{smn,1} + g(\bar{\eta}^{\alpha}_{sm} - \eta^{\beta}_{sn})^{0}_{h} h^{\bar{\alpha}\beta}_{smn,2}$$
$$+ g(\eta^{\beta}_{sn} - \bar{\eta}^{\alpha}_{sm})^{0}_{h} h^{\bar{\alpha}\beta}_{smn,3} + g(-\bar{\eta}^{\alpha}_{sm} - \eta^{\beta}_{sn})^{0}_{h} h^{\bar{\alpha}\beta}_{smn,4} \big] e^{i(\bar{\xi}_{\alpha} + \xi_{\beta})l},$$

$$a_{\beta\alpha} = \frac{1}{2} \sum_{m=1}^{2} \sum_{n=1}^{2} \{ \big[g(\eta^{\alpha}_{fm} + \eta^{\beta}_{fn})^{h'}_{0} h^{\alpha\beta}_{fmn,1} + g(\eta^{\alpha}_{fm} - \eta^{\beta}_{fn})^{h'}_{0} h^{\alpha\beta}_{fmn,2} + g(\eta^{\beta}_{fn} - \eta^{\alpha}_{fm})^{h'}_{0} h^{\alpha\beta}_{fmn,3}$$
$$+ g(-\eta^{\alpha}_{fm} - \eta^{\beta}_{fn})^{h'}_{0} h^{\alpha\beta}_{fmn,4} \big] e^{i(\xi_{\alpha} + \xi_{\beta})l}$$
$$+ \big[g(\eta^{\alpha}_{sm} + \eta^{\beta}_{sn})^{0}_{h} h^{\alpha\beta}_{smn,1} + g(\eta^{\alpha}_{sm} - \eta^{\beta}_{sn})^{0}_{h} h^{\alpha\beta}_{smn,2} + g(\eta^{\beta}_{sn} - \eta^{\alpha}_{sm})^{0}_{h} h^{\alpha\beta}_{smn,3}$$
$$+ g(-\eta^{\alpha}_{sm} - \eta^{\beta}_{sn})^{0}_{h} h^{\alpha\beta}_{smn,4} \big] (e^{i(\xi_{\alpha} + \xi_{\beta})l} + e^{i(\xi_{\alpha} + \xi_{\beta})d})$$
$$- 2\big[g(\eta^{\alpha}_{fm} + \eta^{\beta}_{fn})^{h'}_{0} (\tau^{fm}_{5\alpha} A^{fn}_{3\beta} + \tau^{fm}_{1\alpha} A^{fn}_{1\beta}) + g(\eta^{\alpha}_{fm} - \eta^{\beta}_{fn})^{h'}_{0} (\tau^{fm}_{5\alpha} B^{fn}_{3\beta} + \tau^{fm}_{1\alpha} B^{fn}_{1\beta})$$
$$+ g(\eta^{\beta}_{fn} - \eta^{\alpha}_{fm})^{h'}_{0} (\sigma^{fm}_{5\alpha} A^{fn}_{3\beta} + \sigma^{fm}_{1\alpha} A^{fn}_{1\beta}) + g(-\eta^{\alpha}_{fm} - \eta^{\beta}_{fn})^{h'}_{0} (\sigma^{fm}_{5\alpha} B^{fn}_{3\beta} + \sigma^{fm}_{1\alpha} B^{fn}_{1\beta}) \big] e^{i(\xi_{\alpha} + \xi_{\beta})d} \},$$

$$h_{\beta\alpha} = \frac{1}{2} \sum_{m=1}^{2} \sum_{n=1}^{2} \big[g(\eta^{\alpha}_{sm} + \hat{\eta}^{\beta}_{sn})^{0}_{h} h^{\alpha\beta}_{smn,1} + g(\eta^{\alpha}_{sm} - \hat{\eta}^{\beta}_{sn})^{0}_{h} h^{\alpha\beta}_{smn,2}$$
$$+ g(\hat{\eta}^{\beta}_{sn} - \eta^{\alpha}_{sm})^{0}_{h} h^{\alpha\beta}_{smn,3} + g(-\eta^{\alpha}_{sm} - \hat{\eta}^{\beta}_{sn})^{0}_{h} h^{\alpha\beta}_{smn,4} \big] e^{i\xi_{\alpha} d},$$

$$\hat{h}_{\beta\alpha} = \frac{1}{2} \sum_{m=1}^{2} \sum_{n=1}^{2} \{ \big[g(\hat{\eta}^{\alpha}_{sm} + \hat{\eta}^{\beta}_{sn})^{0}_{h} h^{\hat{\alpha}\hat{\beta}}_{smn,1} + g(\hat{\eta}^{\alpha}_{sm} - \hat{\eta}^{\beta}_{sn})^{0}_{h} h^{\hat{\alpha}\hat{\beta}}_{smn,2} + g(\hat{\eta}^{\beta}_{sn} - \hat{\eta}^{\alpha}_{sm})^{0}_{h} h^{\hat{\alpha}\hat{\beta}}_{smn,2}$$
$$+ g(-\hat{\eta}^{\alpha}_{sm} - \hat{\eta}^{\beta}_{sn})^{0}_{h} h^{\hat{\alpha}\hat{\beta}}_{smn,4} \big] + 2\big[g(\hat{\eta}^{\alpha}_{sm} + \hat{\eta}^{\beta}_{sn})^{h'}_{h} (\hat{\tau}^{sm}_{5\alpha} \hat{A}^{sn}_{3\beta} + \hat{\tau}^{sm}_{1\alpha} \hat{A}^{sn}_{1\beta})$$
$$+ g(\hat{\eta}^{\alpha}_{sm} - \hat{\eta}^{\beta}_{sn})^{h'}_{h} (\hat{\tau}^{sm}_{5\alpha} \hat{B}^{sn}_{3\beta} + \hat{\tau}^{sm}_{1\alpha} \hat{B}^{sn}_{1\beta}) + g(\hat{\eta}^{\beta}_{sn} - \hat{\eta}^{\alpha}_{sm})^{h'}_{h} (\hat{\sigma}^{sm}_{5\alpha} \hat{A}^{sn}_{3\beta} + \hat{\sigma}^{sm}_{1\alpha} \hat{A}^{sn}_{1\beta})$$
$$+ g(-\hat{\eta}^{\alpha}_{sm} - \hat{\eta}^{\beta}_{sn})^{h'}_{h} (\hat{\sigma}^{sm}_{5\alpha} \hat{B}^{sn}_{3\beta} + \hat{\sigma}^{sm}_{1\alpha} \hat{B}^{sn}_{1\beta}) \big] \}, \tag{66}$$

$$\bar{c}^{(\beta)} = -\frac{1}{2} \rho' \omega^2 \frac{e^{f}_{31}}{c^{f}_{33} h'} \frac{1}{\bar{\xi}_{\beta} l} \sum_{n=1}^{2} \big[\bar{A}^{fn}_{3\beta} f(\bar{\eta}^{\beta}_{fn}) + \bar{B}^{fn}_{3\beta} f(-\bar{\eta}^{\beta}_{fn}) \big]. \tag{67}$$

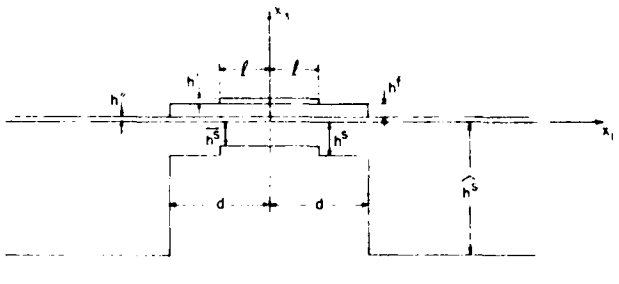

FIG. 7. Cross section of a composite resonator with the layer notched under the electrodes to cause trapping in the fundamental mode when it does not trap in the flat-plate configuration.

In (66) and (67) we have employed the definitions

$$g(\theta)^{h^p}_{h^q} = \int_{h^q}^{h^p} e^{i\theta x_3} dx_3 = \frac{1}{i\theta} (e^{i\theta h^p} - e^{i\theta h^q}) \quad (\theta \neq 0)$$
$$= h^p - h^q \quad (\theta = 0), \tag{68}$$

$$f(\eta) = (1/\eta^2)\big[e^{i\eta h'} (1 - i\eta h') - 1 \big], \tag{69}$$

$$\bar{\tau}^{fm}_{5\alpha} = c^{f}_{44} (i\bar{\eta}^{\alpha}_{fm} \bar{A}^{fm}_{3\alpha} + i\bar{\xi}_{\alpha} \bar{A}^{fm}_{1\alpha}),$$
$$\bar{\tau}^{fm}_{1\alpha} = i(c^{f}_{13} \bar{\xi}_{\alpha} \bar{A}^{fm}_{3\alpha} + c^{f}_{13} \bar{\eta}^{\alpha}_{fm} \bar{A}^{fm}_{1\alpha}),$$
$$\bar{\sigma}^{fm}_{5\alpha} = c^{f}_{14} (-i\bar{\eta}^{\alpha}_{fm} \bar{B}^{fm}_{3\alpha} + i\bar{\xi}_{\alpha} \bar{B}^{fm}_{1\alpha}),$$
$$\bar{\sigma}^{fm}_{1\alpha} = i(c^{f}_{13} \bar{\xi}_{\alpha} \bar{B}^{fm}_{3\alpha} - c^{f}_{13} \bar{\eta}^{\alpha}_{fm} \bar{B}^{fm}_{1\alpha}). \tag{70}$$

and $\bar{\tau}_{5\alpha}^{vm}$, $\bar{\tau}_{1\alpha}^{vm}$, $\bar{\sigma}_{5\alpha}^{vm}$, $\bar{\sigma}_{1\alpha}^{vm}$ are obtained by replacing f with s in (70). The expressions for the unelectroded composite or diaphragm and bulk semiconductor regions, respectively, i.e., $\tau_{5\alpha}^{fm}$, $\tau_{1\alpha}^{fm}$, $\sigma_{5\alpha}^{fm}$, $\sigma_{1\alpha}^{fm}$, $\tau_{5\alpha}^{vm}$, $\tau_{1\alpha}^{vm}$, $\sigma_{5\alpha}^{vm}$, $\sigma_{1\alpha}^{vm}$ and $\hat{\tau}_{5\alpha}^{vm}$, $\hat{\tau}_{1\alpha}^{vm}$, $\hat{\sigma}_{5\alpha}^{vm}$, $\hat{\sigma}_{1\alpha}^{vm}$ are obtained by replacing the quantities with the bars in (70) by the associated quantities without bars for the unelectroded composite or diaphragm or with carets for the bulk semiconductor. Furthermore, in (66) we have employed the additional definitions

$$
\begin{aligned}
h_{fmn,1}^{\alpha\beta} &= -\bar{\tau}_{5\alpha}^{fm} A_{5\beta}^{fn} + \tau_{5\beta}^{fn} \overline{A}_{5\alpha}^{fm} - \bar{\tau}_{1\alpha}^{fm} A_{1\beta}^{fn} + \tau_{1\beta}^{fn} \overline{A}_{1\alpha}^{fm}, \\
h_{fmn,2}^{\alpha\beta} &= -\bar{\tau}_{5\alpha}^{fm} B_{5\beta}^{fn} + \sigma_{5\beta}^{fn} \overline{A}_{5\alpha}^{fm} - \bar{\tau}_{1\alpha}^{fm} B_{1\beta}^{fn} + \sigma_{1\beta}^{fn} \overline{A}_{1\alpha}^{fm}, \\
h_{fmn,3}^{\alpha\beta} &= -\bar{\sigma}_{5\alpha}^{fm} A_{5\beta}^{fn} + \tau_{5\beta}^{fn} \overline{B}_{5\alpha}^{fm} - \bar{\sigma}_{1\alpha}^{fm} A_{1\beta}^{fn} + \tau_{1\beta}^{fn} \overline{B}_{1\alpha}^{fm}, \\
h_{fmn,4}^{\alpha\beta} &= -\bar{\sigma}_{5\alpha}^{fm} B_{5\beta}^{fn} + \sigma_{5\beta}^{fn} \overline{B}_{5\alpha}^{fm} - \bar{\sigma}_{1\alpha}^{fm} B_{1\beta}^{fn} + \sigma_{1\beta}^{fn} \overline{B}_{1\alpha}^{fm},
\end{aligned}
\tag{71}
$$

and the h's for the other regions are obtained by replacing the quantities in (71) by the appropriate quantities associated with each region. Since the variations in (65) are arbitrary, we obtain the inhomogeneous linear algebraic equations for the $\overline{K}^{(\alpha\beta)}$, $K^{(\alpha\gamma)}$, and $\hat{K}^{(\alpha\gamma)}$ in the form

$$
\begin{aligned}
&\sum_{\beta=1}^{\bar{n}} \overline{K}^{(\alpha\beta)} \bar{a}_{\beta\gamma} + \sum_{\gamma=1}^{n} K^{(\alpha\gamma)} \bar{b}_{\gamma\alpha} = -\bar{v}^{(\alpha\beta)}, \quad \beta = 1,\ldots,\bar{n}, \\
&\sum_{\gamma=1}^{n} K^{(\alpha\gamma)} a_{\gamma\alpha} + \sum_{\beta=1}^{\bar{n}} \overline{K}^{(\beta\alpha)} \bar{b}_{\beta\alpha} + \sum_{\gamma=1}^{\hat{n}} \hat{K}^{(\alpha\gamma)} \hat{b}_{\alpha\gamma} = 0, \\
&\qquad \alpha = 1,\ldots,n, \\
&\sum_{\alpha=1}^{n} \hat{K}^{(\gamma\alpha)} \hat{a}_{\alpha\gamma} + \sum_{\alpha=1}^{n} K^{(\alpha\gamma)} \hat{b}_{\alpha\gamma} = 0, \quad \gamma = 1,\ldots,\hat{n},
\end{aligned}
\tag{72}
$$

which constitute $\bar{n} + n + \hat{n}$ inhomogeneous linear algebraic equations for $\bar{n}\overline{K}^{(\alpha\beta)}$, $nK^{(\alpha\gamma)}$, and $\hat{n}\hat{K}^{(\gamma\alpha)}$.

VI. QUALITY FACTOR RESULTING FROM RADIATION

In this section we calculate the quality factor due to radiation into the bulk semiconductor for each of the three cases from the analysis presented in Sec. V. Although the solution may be obtained from the analysis in Sec. V at any driving frequency for which all the pertinent dispersion curves are available, in this work we are interested in the solution only at the fundamental essentially thickness-extensional resonance for each of the three configurations. It is clear from experience[12,14] that under these circumstances we need consider only the essentially thickness-extensional branch in the composite region (either electroded or not) of the resonator, which is the curve labeled 1 in Fig. 4. However, in the thin region of the semiconductor without the film and the bulk semiconductor all pertinent dispersion curves shown in the respective Figs. 5 and 6 must be included to obtain accuracy. The use of only one branch for the composite region means that we always have $\bar{n} = 1$ and $n = 1$ for the configuration shown in Figs. 1 and 7 but not for the configuration shown in Fig. 2, for which all curves shown in Fig. 5 must be included.

As usual, the quality factor Q is defined by

$$
Q = (K + U)/E^{inc}, \tag{73}
$$

where

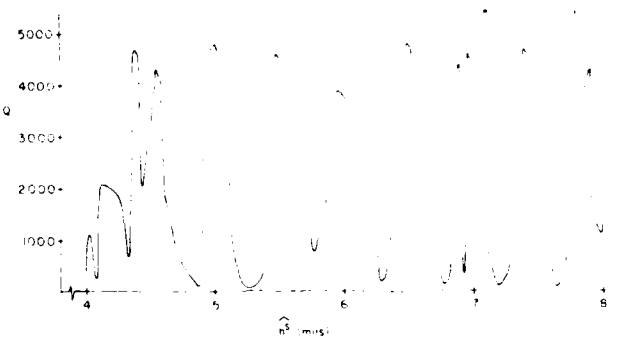

FIG. 8. Quality factor vs wafer thickness when trapping is not present for the composite resonator configuration shown in Fig. 1.

$$
\begin{aligned}
K &= \frac{1}{T}\int_0^T dt\, \frac{1}{2}\,\mathrm{Re}\int_d^{d} dx_1 \int_{h'}^{h} \frac{1}{2}\, p\dot{u}_\alpha \dot{u}_\alpha^* \, dx_3, \\
U &= \frac{1}{T}\int_0^T dt\, \frac{1}{2}\,\mathrm{Re}\left(\int_d^{d} dx_1 \int_{h'}^{h} \frac{1}{2}\,[c_{11}u_{1,1}u_{1,1}^* \right. \\
&\quad + c_{33}u_{3,3}u_{3,3}^* + 2c_{13}u_{1,1}u_{3,3}^* \\
&\quad \left. + c_{44}(u_{1,3}+u_{3,1})(u_{1,3}+u_{3,1})^*]\,dx_3\right), \\
E^{inc} &= -2\int_0^T dt\, \frac{1}{2}\,\mathrm{Re}\int_{h'}^{0} (-\hat{T}_{1\alpha}\dot{\hat{u}}_\alpha^*)_{x_3=d}\, dx_3,
\end{aligned}
\tag{74}
$$

in which T is the period of the vibration and we have taken the liberty of writing the integrals in $(74)_{1,2}$ over discontinuous functions to achieve brevity. For a given geometry and mode, resonance is determined by obtaining Q over a (narrow) range of frequencies and finding the frequency for which Q is a maximum.

In performing the calculations we have found that it is imperative that all radiating plate waves in the thick region of the gallium–arsenide be included in order to achieve accuracy. Since at a given frequency the number of radiating waves in a plate goes up significantly with thickness, we have considered gallium–arsenide wafers no thicker than 8 mils at a frequency around 132 MHz, for which there are 30 radiating plate waves. Results are presented for wafer thicknesses

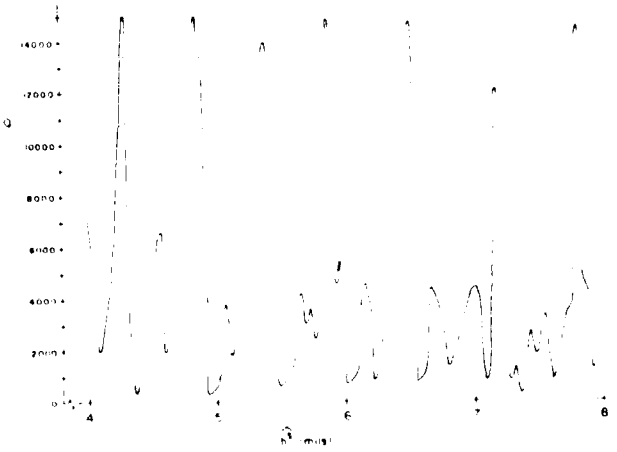

FIG. 9. Quality factor vs wafer thickness when trapping is not present for the composite resonator configuration shown in Fig. 2.

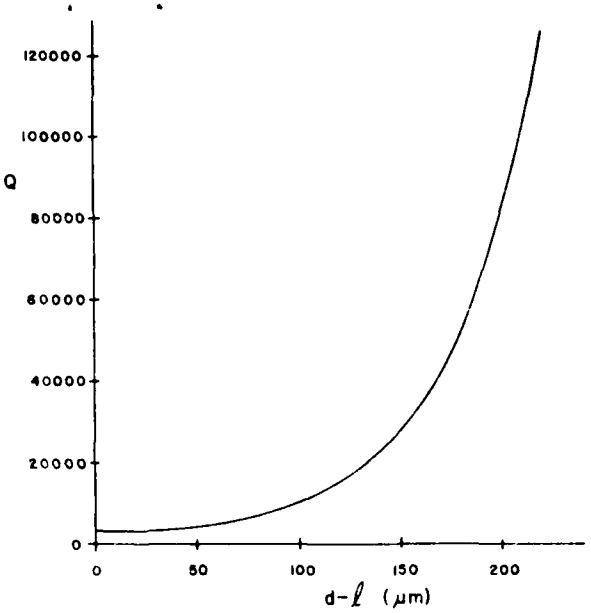

FIG. 10. Quality factor vs distance from edge of electrode to edge of diaphragm when trapping is present for the composite resonator configuration shown in Fig. 7. The width of the electrodes $2l$ varies from 580 to 420 μm.

ranging from 4 to 8 mils because this is considered to be within the practical range. All the results presented are for a film thickness of 7 μm and a diaphragm thickness of 14 μm and the lateral dimensions of each configuration were adjusted slightly to maintain the same resonant frequency for computational convenience. Since the calculated Q is a very rapidly varying function of the wafer thickness, calculations had to be performed for very small increments in thickness, i.e., 1 μm, in order to get all the peaks and valleys in the interval.

In the absence of trapping, for the case shown in Fig. 1 the results are plotted in Fig. 8, which shows the aforementioned sharp variation in Q with wafer thickness. It can be seen from the figure that the highest Q obtained is about 4750 and the lowest is about 10, and there are about 10 peaks for thicknesses between 4 and 8 mils. The highest valleys have Q's of about 700 and 2000, respectively. For the case shown in Fig. 2, the results are plotted in Fig. 9, which shows variations in Q with wafer thickness similar to Fig. 8, but in this case the Q's are considerably higher. It can be seen from the figure that the highest Q obtained is about 15 000 and the lowest Q is about 200. Calculations were performed when

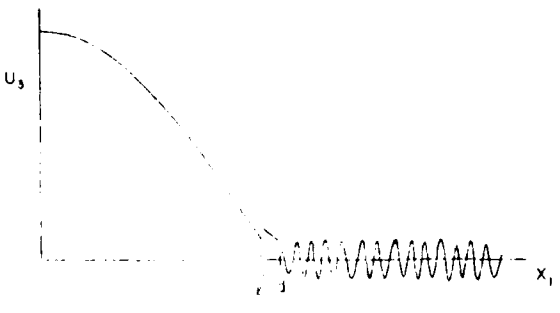

FIG. 11. Typical thickness displacement along the surface of the composite resonator for the configuration shown in Fig. 1.

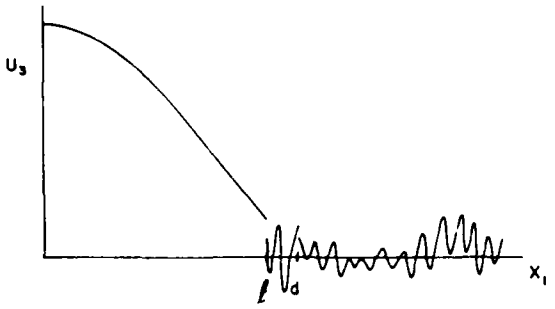

FIG. 12. Typical thickness displacement along the surface of the composite resonator for the configuration shown in Fig. 2.

trapping was induced in the fundamental mode by notching the diaphragm under the electrode as shown in Fig. 7. As expected, the Q due to radiation can be made as high as we wish simply by extending the lateral dimensions of the film and diaphragm. Figure 10 gives Q as a function of $(d - l)$, i.e., the distance from the edge of the electrode to the edge of the diaphragm. It can be seen from the figure that Q increases very rapidly with $(d - l)$ and at $d = 2l$, $Q = 70\,000$ for this geometry. For these calculations the wafer thickness was 6 mils. Even when trapping is present the Q is a varying function of wafer thickness, but the range of the variation is less than 1/10 of that when trapping is not present, which is not of interest since the Q with trapping is so much higher than the Q without trapping. In interpreting the foregoing information it should be remembered that the high Q's calculated should be higher than the actual Q's because the material Q and the Q due to radiation into the air are not included. The results discussed above mean that in order to obtain reasonably high Q when trapping is not present, for a given wafer thickness the thicknesses of the film and diaphragm must be very precisely selected.

Since all conditions are natural conditions in the variational condition in (62), the approximate solution does not expressly match the mode shape at the interfaces unless it is exact. Consequently, the extent to which the calculated mode shape matches at the interfaces gives an indication of the accuracy of the approximate solution obtained. Typical plots of the u_3-displacement field, which is the large one for the essentially thickness-extensional modes considered here, for the configurations shown in Figs. 1 and 2 are shown in Figs. 11 and 12, respectively. It can be seen from the figures that the u_3-displacement field matches quite well at the interfaces. Consequently, we can conclude that the approximate solution obtained is quite accurate.

ACKNOWLEDGMENTS

We wish to thank Dr. K. M. Lakin of Iowa State University for referring us to Ref. 8 and acquainting us with the difficulty mentioned in Ref. 9. This work was supported in part by the Air Force Office of Scientific Research under Grant No. AFOSR-84-0351.

[1] W. Grudkowski, J. F. Black, T. M. Reeder, D. E. Cullen, and R. A. Wagner, Appl. Phys. Lett. 37, 993 (1980).
[2] K. M. Lakin and J. S. Wang, Appl. Phys. Lett. 38, 125 (1981).

[8] K. H. Nakamura, H. Sasaki, and H. Shimizu, Electron. Lett. **17**, 507 (1981).
[9] T. W. Grudkowski, J. F. Black, G. W. Drake, and D. E. Callen, in *Proceedings of the 36th Annual Symposium on Frequency Control* (U.S. Army Electronics Research and Development Command, Fort Monmouth, NJ, 1982), p. 539.
[10] J. S. Wang and K. M. Lakin, Appl. Phys. Lett. **40**, 308 (1982).
[11] K. M. Lakin, J. S. Wang and A. R. Landin, *Proceedings of the 36th Annual Symposium on Frequency Control* (U.S. Army Electronics Research and Development Command, Fort Monmouth, NJ, 1982), p. 517.
[12] H. F. Tiersten and D. S. Stevens, J. Appl. Phys. **54**, 5893 (1983).
[13] K. Tsubouchi, K. Sugai, and N. Mikoshiba, *1981 Ultrasonics Symposium Proceedings*, IEEE Cat. No. 81 CH 1689-5 (Institute of Electrical and Electronics Engineers, New York, 1981), p. 375.
[14] The accuracy of the values of the material constants of aluminum nitride in the literature is open to some question because the published value of c_{33} yields resonant frequencies that differ significantly from measured resonant frequencies reported in the literature.
[15] R. F. Milsom, J. F. Curran, S. L. Murray, S. Ferry-Wood, and M. Redwood, *1983 Ultrasonics Symposium Proceedings*, IEEE Cat. No. 83 CH 1947-1 (Institute of Electrical and Electronics Engineers, New York, 1983), p. 498. Some experimental work when trapping is present is reported in this reference.
[16] H. F. Tiersten, *Linear Piezoelectric Plate Vibrations* (Plenum, New York, 1969), Chap. 6, Sec. 4.
[17] H. F. Tiersten and B. K. Sinha, *1978 Ultrasonics Symposium Proceedings*, IEEE Cat. No. 78 CH 1482-9 (Institute of Electrical and Electronics Engineers, New York, 1978), p. 167.
[18] D. V. Shick, H. F. Tiersten, and B. K. Sinha, *1981 Ultrasonics Symposium Proceedings*, IEEE Cat. No. 81 CH 1689-9 (Institute of Electrical and Electronics Engineers, New York, 1981), p. 452.
[19] H. F. Tiersten, *Linear Piezoelectric Plate Vibrations* (Plenum, New York, 1969), Eqs. (7.28) and (7.29).
[20] H. F. Tiersten, *Linear Piezoelectric Plate Vibrations* (Plenum, New York, 1969), Chap. 7, Sec. 1.
[21] B. A. Auld, *Acoustic Fields and Waves in Solids* (Wiley, New York, 1973), Vol. I, p. 210.
[22] H. F. Tiersten, *Linear Piezoelectric Plate Vibrations* (Plenum, New York, 1969), Chap. 14, Sec. 4.
[23] There is an error in sign before the last term in Eq. (6.44) of Ref. 11 and an incorrect subscript on a variable, both of which have been corrected in (16). The symbol τ is used in (16) in place of T because it is used in Eq. (6.44) of Ref. 11.
[24] Since constraint-type conditions arise in (16) as natural conditions because of the use of Lagrange multipliers, the approximating functions need not satisfy them when (16) is employed.

A PERTURBATION CALCULATION OF THE QUALITY FACTOR OF THE PIEZOELECTRIC THIN FILM ON SEMICONDUCTOR COMPOSITE RESONATOR DUE TO RADIATION INTO THE WAFER

D.V. Shick and H.F. Tiersten

Rensselaer Polytechnic Institute
Troy, New York 12180-3590

1. Introduction

In a recent analysis[1,2] of the piezoelectric thin film on semiconductor composite resonator vibrating in an essentially thickness-extensional mode it was shown that the quality factor (Q) due to radiation into the bulk semiconductor is a very sharply varying function of the ratio of the thickness of the resonator to that of the film if trapping is not present, but not if trapping is present. The treatment employs a very accurate but extremely cumbersome variational approximation technique and is restricted to the case of strip electrodes and diaphragms.

In this work a perturbation analysis of the Q due to radiation into the semiconductor wafer is presented, which is considerably less cumbersome to use than the earlier variational treatment and is not restricted to the case of strip electrodes and diaphragms. In the treatment the resonant mode of interest is determined from the equation for transversely varying essentially thickness-extensional modes in composite resonators[3] and simple approximate but very accurate conditions at the edges of the diaphragm. This resonant mode is then used to determine the near field radiation into the semiconductor wafer by means of a variational approximation procedure[4]. Of course, as in the earlier work[1,2], all radiating plate waves in the wafer are included in order to achieve accuracy. Finally, the mode in the composite resonator and the radiation field in the wafer are employed in a perturbation integral[5] to calculate the Q. Calculations are performed for the cases of rectangular electrodes and diaphragms and strip electrodes and diaphragms both when trapping is and is not present. For the case of strip electrodes and diaphragms the calculated results are shown to be in good agreement with the earlier more cumbersome direct calculations[1,2].

2. Perturbation Procedure

Since the coupling is small in the piezoelectric thin film, we need consider only the elastic portion of the equation for the first perturbation of the eigenfrequency, which may be written in the form[5]

$$\Delta_\mu = H_\mu/2\omega_\mu\,, \quad \omega = \omega_\mu - \Delta_\mu\,, \tag{1}$$

where ω_μ and ω are the unperturbed and perturbed eigenfrequencies, respectively, and

$$H_\mu = \int_S n_i (T_{ij} g_j^\nu - u_j T_{ij}^\nu)\, dS\,, \tag{2}$$

where n_i denotes the outwardly directed unit normal to the surface S of the resonator and the normalized displacement field g_j^ν is defined by

$$g_j^\nu = u_j^\mu / N_\mu\,, \quad N_\mu^2 = \int_V \rho u_j^\mu u_j^\nu\, dV\,, \tag{3}$$

in which u_j^ν denotes the purely real mechanical displacement field associated with the mode of interest in the composite resonator and T_{ij}^ν denotes the associated stress tensor. A cross-section of the composite resonator attached to the semiconductor wafer is shown in Fig.1. A schematic plan view of the assumed composite resonator is shown in Fig.2 along with the assumed approximate edge condition ($u_3 = 0$). Thus, for the problem at hand the surface S in (2) denotes the surface along which the semiconductor portion of the composite resonator abuts the wafer. The calculated mode in the composite resonator shown in Fig.2 results in tractions $\bar{t}_\ell$ and displacements $\bar{u}_\ell$ that are applied to the wafer along the surface at which it abuts the resonator as shown in Fig.3. These tractions t_ℓ and displacements $\bar{u}_\ell$ then cause radiation fields in the wafer, which are calculated by means of a very accurate variational approximation procedure[6]. These radiation fields in the wafer produce a reaction back on the composite resonator along S. The stresses T_{ij} and displacements u_j in (2) denote this back reaction field.

Since the radiating fields in the wafer are chosen to satisfy the differential equations in and boundary conditions on the major surfaces of the wafer exactly, all that remains of the appropriate variational principle in which all conditions are natural conditions is given by[4]

$$\int_{S_N} (\bar{t}_\ell - n_k \hat{T}_{k\ell}) \delta\hat{u}_\ell\, ds + \int_{S_C} n_k (\hat{u}_\ell - \bar{u}_\ell) \delta\hat{T}_{k\ell}\, dS = 0\,. \tag{4}$$

0090-5607/86/0000-00377 $1.00 © 1986 IEEE

In (4) $\bar{t}_\ell$ and $\bar{u}_\ell$ are known from the resonant eigensolution $T^{\mu}_{\ell k}$, u^{μ}_{ℓ} and $\hat{u}_\ell$ and $\hat{T}_{k\ell}$ are found from the expressions for the solution field radiating into the wafer. At this point we note that the reaction $\hat{u}_\ell$, $T_{k\ell}$ from the radiating field is complex, the real part of which yields a small change in frequency when substituted in (2), which is negligible and not of interest here, and the imaginary part of which yields the attenuation due to radiation into the wafer from (2) which is sought here. From the well-known relation $\omega = \omega_\mu - i\omega_\mu/2Q$ and (1), we obtain

$$Q = -i\omega_\mu^2/H_\mu . \tag{5}$$

3. Transversely Varying Thickness-Extensional Modes

As noted in Sec.2, a plan view for the determination of the mode of interest in the composite resonator is shown in Fig.2, in which the - denotes the electroded region, the S, the side region, the T, the top (and bottom) region and the C, the corner regions. This notation is essential for the treatment of the trapped modes, but is not needed for the untrapped modes because in the untrapped case the edges of the electrodes are relatively unimportant. It has been shown in Sec.5 of Ref.3 that the homogeneous equation governing the essentially thickness-extensional modes may be written in the form

$$M_n\left(\frac{\partial^2 f^n}{\partial x_1^2} + \frac{\partial^2 f^n}{\partial x_2^2}\right) - \bar{c}^f_{33}\bar{\eta}^2_{fn} f^n + \omega^2 f^n = 0 , \tag{6}$$

where n denotes the order of the pure thickness mode in the composite resonator, both the superscript and subscript f denote the film and $\bar{\eta}_{fn} = \bar{\eta}_{fn}$ in an electroded region while $\bar{\eta}_{fn} = \hat{\eta}_{fn}$ in an unelectroded region. Furthermore, it has also been shown in Sec.V of Ref.3 that at an interface between electroded and unelectroded regions we have the continuity of f^n and df^n/dn, where d/dn denotes the normal derivative. Within the approximation made[5] in obtaining Eq.(6) it may readily be shown[6-8] that for either completely free or completely fixed conditions (here completely fixed) along the edges of the diaphragm shown in Fig.2, the appropriate condition is $f^n = 0$. The expression for the coefficient M_n, which is very important because its sign indicates whether trapping is or is not present in the flat composite plate configuration, is given in Eq.(4.44) along with (4.41), (4.42), (4.37), (4.38) and (4.33) of Ref.3 and clearly is much too cumbersome to present here[9].

It has been shown in Sec.V of Ref.3 that the dominant u_3-displacement field accompanying the mode is given by

$$u_3^{fn} = {}_o u_3^{fn} f^n(x_1,x_2,t),\ u_3^{sn} = {}_o u_3^{sn} f^n(x_1,x_2,t), \tag{7}$$

where the superscripts f and s denote the film and semiconductor diaphragm, respectively, and ${}_o u_3$ represents the thickness dependence only and is given by

$$\begin{aligned} {}_o u_3^{fn} &= A_3^{fln}\cos\bar{\eta}^o_{fn}x_3 + B_3^{fln}\sin\bar{\eta}^o_{fn}x_3 , \\ &\qquad 0 < x_3 < h^f , \\ {}_o u_3^{sn} &= A_3^{sln}\cos\bar{\eta}^o_{sn}x_3 + B_3^{sln}\sin\bar{\eta}^o_{sn}x_3 , \\ &\qquad 0 > x_3 > -h^s , \end{aligned} \tag{8}$$

and the amplitudes are given in Eqs.(5.20) of Ref.3. Since only the semiconductor diaphragm abuts the wafer as shown in Fig.1 only the variable in the semiconductor are relevant here. However, in order to calculate the tractions $\bar{t}_\ell$ and displacements $\bar{u}_\ell$ that the mode in the composite resonator exerts on the wafer as shown in Fig.3, we need the associated displacement fields u_1^s and u_2^s in the semiconductor diaphragm in addition to u_3^s. These functions differ for the different f^n and associated u_3^{sn}, which occur in the different regions for the trapped case but not for the untrapped case. Since the f^n has the same functional form over the entire composite resonator in the untrapped case as it has over the electroded region in the trapped case, we write u_1^s and u_2^s for this functional form for f^n only[8]. It has been shown in Sec.V of Ref.3 that for

$$f^n = \cos\bar{\xi}x_1 \cos\bar{\nu}x_2 e^{i\omega t} , \tag{9}$$

which is the above mentioned f^n,

$$\begin{aligned} u_1^s &= \frac{\bar{\xi}}{\bar{\zeta}^2}\tau^s(x_3)\sin\bar{\xi}x_1\cos\bar{\nu}x_2\, e^{i\omega t} , \\ u_2^s &= \frac{\bar{\nu}}{\bar{\zeta}^2}\tau^s(x_3)\cos\bar{\xi}x_1\sin\bar{\nu}x_2\, e^{i\omega t} , \end{aligned} \tag{10}$$

where

$$\begin{aligned} \tau^s &= A_1^{s1}\sin\bar{\eta}^o_s x_3 + A_1^{s2}\sin\kappa^s\bar{\eta}^o_s x_3 + B_1^{s1}\cos\bar{\eta}^o_s x_3 \\ &\quad + B_1^{s2}\sin\kappa^s\bar{\eta}^o_s x_3 , \quad \bar{\zeta}^2 = \bar{\xi}^2 + \bar{\nu}^2 , \end{aligned} \tag{11}$$

and κ^s and the amplitudes are given in (4.30) and (4.26), respectively, of Ref.3.

As already noted, in the untrapped case for the fundamental mode for any n, f^n is given by

$$f^n = \cos\bar{\xi}x_1 \cos\bar{\nu}x_2\, e^{i\omega t} , \tag{12}$$

where from the edge conditions[8] for the mode of interest

$$\bar{\xi} = \pi/2d , \quad \bar{\nu} = \pi/2w , \tag{13}$$

with which the unperturbed resonant frequency ω_μ may be obtained from[8]

$$\rho^f \omega_\mu^2 = \bar{c}^f_{33}\bar{\eta}_f^2 + M_n(\bar{\xi}^2+\bar{\nu}^2) . \qquad (14)$$

In the trapped case the expressions for f^n in each of the respective regions shown in Fig.2 are given by[8]

$$\bar{f}^n = \bar{E}\cos\bar{\xi}x_1\cos\bar{\nu}x_2 , \quad f^{ns} = (E^s_- e^{-\xi(x_1-\ell)} + E^s_+ e^{\xi(x_1-\ell)})\cos\bar{\nu}x_2$$

$$f^{nT} = (E^T_- e^{-\nu(x_2-b)} + E^T_+ e^{\nu(x_2-b)})\cos\bar{\xi}x_1 ,$$

$$f^{nC} = E^C_1 e^{-\xi(x_1-\ell)-\nu(x_2-b)} + E^C_2 e^{-\xi(x_1-\ell)+\nu(x_2-b)} + E^C_3 e^{\xi(x_1-\ell)-\nu(x_2-b)} + E^C_4 e^{\xi(x_1-\ell)+\nu(x_2-b)} \qquad (15)$$

where $\bar{\xi}$ and $\bar{\nu}$ are determined from the lowest roots of the transcendental equations

$$\bar{\xi}\tan\bar{\xi}\ell = \xi\frac{(1+e^{-2\xi(d-\ell)})}{1-e^{-2\xi(d-\ell)}} ,$$

$$\bar{\nu}\tan\bar{\nu}\ell = \nu\frac{(1+e^{-2\nu(w-b)})}{1-e^{-2\nu(w-b)}} , \qquad (16)$$

with the aid of (6.7) of Ref.3. All amplitude coefficients in (15) are known in terms of $\bar{E}$ from the relations[8]

$$E^S_- = \frac{\bar{E}\cos\bar{\xi}\ell}{1-e^{-2\xi(d-\ell)}} , \quad E^T_- = \frac{\bar{E}\cos\bar{\nu}b}{1-e^{-2\nu(w-b)}} ,$$

$$E^C_1 = \frac{\bar{E}\cos\bar{\xi}\ell\cos\bar{\nu}b}{(1-e^{-2\xi(d-\ell)})(1-e^{-2\nu(w-b)})} ,$$

$$E^C_2 = -e^{-2\nu(w-b)}E^C_1, \quad E^C_3 = -e^{-2\xi(d-\ell)}E^C_1 ,$$

$$E^C_4 = e^{-2\xi(d-\ell)-2\nu(w-b)}E^C_1 . \qquad (17)$$

As already noted, u^s_1 and u^s_2 are known from $\bar{f}^n$ in the electroded region from the relations (10) and (11) and for the other regions equivalent relations which are not shown here are employed[8].

4. Variable-Crested Waves in Wafer

In this section we obtain the solution functions for the near field waves with slowly varying crests and the associated dispersion relations. The stress equations of motion and the linear elastic constitutive equations for the semiconductor wafer may be written in the tensor form[8,10,11]

$$\hat{T}^s_{ij,i} = \rho^s\ddot{\hat{u}}^s_j , \quad \hat{T}^s_{ij} = c^s_{ijk\ell}\hat{u}^s_{k,\ell} , \qquad (18)$$

where the notation is conventional, and we note that the equations are too cumbersome to write out in detail. From either Figs.1 or 3 we see that the boundary conditions on the major surfaces of the semiconducting plate may be written in the form

$$\hat{T}^s_{3j} = 0 \quad \text{at } x_3 = 0 \text{ and } x_3 = -\hat{h}^s . \qquad (19)$$

In considering waves radiating in the $+x_1$-direction, we first note that since $\bar{\nu}$ is small[8], $\hat{T}^s_{12}$ is an order of magnitude smaller than $\hat{T}^s_{13}$ and $\hat{u}^s_1$, and $\hat{u}^s_2$ is an order of magnitude smaller than $\hat{u}^s_1$ and $\hat{u}^s_3$. Hence, $\hat{u}^s_2$, the x_2-differential equation and $\hat{T}^s_{32}$ are negligible for radiation in the x_1-direction. Of course, equivalent statements hold for radiation in the x_2-direction since $\bar{\xi}$ is small. Accordingly, for waves with slowly varying crests and propagating in the $+x_1$-direction in the near field, we write

$$\hat{u}^s_a = \cos\bar{\nu}x_2\sum_{m=1}^{2}\hat{C}^{(m)}(\hat{\beta}^{+(m)}_a e^{i\hat{\eta}^{(m)}x_3} + \hat{\beta}^{-(m)}_a e^{-i\hat{\eta}^{(m)}x_3})e^{-i\hat{\xi}(x_1-d)}e^{i\omega t} , \quad a = 1,3, \qquad (20)$$

for either the untrapped case or the electroded region for the trapped case and we do not bother to write the solution for any other regions for the trapped case. The $\hat{\eta}^{(m)}$, $\hat{\beta}^{+(m)}_a$, $\hat{\beta}^{-(m)}_a$ and $\hat{C}^{(m)}$ are determined by satisfying (18) and (19) in the usual way[8,2,3]. From this solution the lowest 17 real dispersion curves for the bulk gallium-arsenide plate have been calculated and are shown in dimensionless form in Fig.4. For the fundamental essentially thickness-extensional resonance of the composite resonator consisting of a 7 μm thick aluminum-nitride film on a 14 μm thick gallium-arsenide diaphragm, which is around 132 MHz, this number of dispersion curves is for a gallium-arsenide wafer thickness of about 5 mils. In this work we perform calculations for wafer thicknesses up to 8 mils for which there are 30 real dispersion curves for a frequency of 132 MHz. However, we do not bother to show the figure for more than 17.

Similarly, for waves with slowly varying crests in the x_1-direction and propagating in the $+x_2$-direction in the near field, we have

$$\hat{u}^s_b = \cos\bar{\xi}x_1\sum_{m=1}^{2}\hat{C}^{(m)}(\hat{\beta}^{+(m)}_b e^{i\hat{\eta}^{(m)}x_3} + \hat{\beta}^{-(m)}_b e^{-i\hat{\eta}^{(m)}x_3})e^{-i\hat{\xi}(x_2-w)}e^{i\omega t} , \quad b = 2,3, \qquad (21)$$

for the same types of regions as in the previous case. From this solution we obtain the propagating dispersion curves for near field radiating waves in the x_2-direction. The dispersion curves are just like those in Fig.4.

5. Variational Analysis of Radiation into Wafer

In this section we determine the waves radiating

into the semiconductor wafer due to the tractions and displacements resulting from the mode in the composite resonator by means of a variational approximation procedure, as indicated in Sec.2. Since the near radiation fields emanate from the edges of the diaphragm, which are normal to x_1 and x_2, respectively, we may determine the near fields radiating in the x_1- and x_2-directions separately. Accordingly, for radiation in the x_1-direction, from (4), we obtain[8]

$$\int_{-w}^{w} dx_2 \Big[\int_{-\hat{h}^s}^{-h^s} (\hat{T}_{11}^s \delta\hat{u}_1^s + \hat{T}_{13}^s \delta\hat{u}_3^s)\big|_{x_1=d}\, dx_3 + \int_{-h^s}^{0} [\hat{T}_{11}^s \delta\hat{u}_1 + (-T_{13}^s + \hat{T}_{13}^s)\delta\hat{u}_3^s]\big|_{x_1=d}\, dx_3 + \int_{-h^s}^{0} [-(\hat{u}_1^s - g_1^s)\delta\hat{T}_{11}^s - \hat{u}_3^s \delta\hat{T}_{13}^s]\big|_{x_1=d}\, dx_3 \Big] = 0 , \quad (22)$$

where, as already indicated, the forcing terms resulting from the mode in the composite resonator are T_{13}^s and g_1^s. For radiation in the x_2-direction we simply interchange subscripts 1 and 2 and replace w by d.

For radiation in the x_1-direction we now expand the solution in the wafer as a sum of waves with slowly varying crests in the x_2-direction and propagating in the x_1-direction, which were discussed in Sec.4 and are given in (20). Thus

$$\hat{u}_a^s = \sum_{\alpha=1}^{\hat{N}} \hat{K}_S^{(\alpha)} \hat{u}_a^{s(\alpha)} , \quad (23)$$

where each of the $\hat{u}_a^{s(\alpha)}$ are of the form given in (20), $\hat{N}$ denotes the number of branches of the dispersion curves required[8] for the N propagating plate waves. Since the $\hat{u}_a^{s(\alpha)}$ are fixed, only the $\hat{K}_s^{(\alpha)}$ are varied when (23) is substituted into (22). Accordingly, substituting from (23) into (22), employing $(18)_2$ and performing the integrations, we obtain[8] an equation of the form

$$\sum_{\beta=1}^{\hat{N}} \Big[\sum_{\alpha=1}^{\hat{N}} \hat{K}_S^{(\alpha)} A_{\alpha\beta}^S + C_\beta^S \Big] \delta\hat{K}_S^{(\beta)} = 0 , \quad (24)$$

where the expressions for $A_{\alpha\beta}^S$ and C_β^S are too lengthy to present here. Since the variations in (24) are arbitrary, we obtain[8] the inhomogeneous linear algebraic equations for the $\hat{K}_s^{(\alpha)}$ in the form

$$\sum_{\alpha=1}^{\hat{N}} \hat{K}_S^{(\alpha)} A_{\alpha\beta}^S = -C_\beta^S , \quad \beta = 1, \ldots \hat{N} . \quad (25)$$

In a similar way for radiation in the x_2-direction, we obtain[8]

$$\sum_{\gamma=1}^{\hat{N}} \hat{K}_T^{(\gamma)} A_{\gamma\delta}^T = -C_\delta^T , \quad \delta = 1, \ldots \hat{N} . \quad (26)$$

Equations (25) and (26) each constitute $\hat{N}$ inhomogeneous linear algebraic equations for the $\hat{N}$ unknowns $\hat{K}_S^{(\alpha)}$ from (25) and the $\hat{N}$ unknowns $\hat{K}_T^{(\gamma)}$ from (26), respectively. When the $\hat{K}_S^{(\alpha)}$ and the $\hat{K}_T^{(\gamma)}$ have been determined, the near field radiating solution is known[8].

6. Quality Factor Resulting from Radiation

In this section we calculate the Q due to radiation into the semiconductor wafer from the analyses presented in the previous sections. Accordingly, from Secs.3-5 we see that the perturbation integral takes the form[8]

$$H_{\omega} = -\int_{-w}^{w} dx_2 \Big[\int_{-h^s}^{0} [-\hat{u}_3^{S*s}\hat{T}_{13}^s + \hat{T}_{11}^S g_1^s)_{x_1=d} + (\hat{u}_3^{S*s}\hat{T}_{13}^s - \hat{T}_{11}^S g_1^s)_{x_1=-d}]dx_3 \Big] + \int_{-d}^{d} dx_1 \Big[\int_{-h^s}^{0} [-\hat{u}_3^{T*s}\hat{T}_{23}^s + \hat{T}_{22}^T g_2^s)_{x_2=w} + (\hat{u}_3^{T*s}\hat{T}_{23}^s - \hat{T}_{22}^T g_2^s)_{x_2=-w}]dx_3 \Big] . \quad (27)$$

Substituting the imaginary parts of the solutions determined in Sec.5 into (27), we obtain[8]

$$H_{\omega} = 2i\Big[\int_{-w}^{w} dx_2 \int_{-h^s}^{0} \sum_{\alpha=1}^{\hat{N}} \Big[\mathrm{Im}(-\hat{K}_S^{(\alpha)}\hat{u}_3^{S(\alpha)})T_{13}^s + \mathrm{Im}(-\hat{K}_S^{(\alpha)}\hat{u}_1^{S(\alpha)})T_{11}^s \Big]_{x_1=d} dx_3 + \int_{-d}^{d} dx_1 \int_{-h^s}^{0} \sum_{\gamma=1}^{\hat{N}} \Big[\mathrm{Im}(-\hat{K}_T^{(\gamma)}\hat{u}_3^{T(\gamma)})T_{23}^s + \mathrm{Im}(-\hat{K}_T^{(\gamma)}\hat{u}_2^{T(\gamma)})T_{22}^s \Big]_{x_2=w} dx_3 \Big] , \quad (28)$$

which may now be used to calculate the Q from (5). Of course, as in the earlier work[1,2] all radiating plate waves in the thick region of the gallium-arsenide are included to achieve accuracy. Since at a given frequency the number of radiating waves in a plate goes up significantly with thickness, when trapping is not present we have considered gallium-arsenide wafers no thicker than 8 mils at a frequency around 132 MHz, for which there are 30 radiating plate waves. Results are presented for wafer thicknesses ranging from 4 mils to 8 mils because this is considered to be within the

practical range. For the untrapped case the results presented are for a film thickness of 7 microns and a diaphragm thickness of 14 microns. Both strip diaphragms 600 microns wide and square diaphragms with lateral dimensions of 600 microns × 600 microns were considered. The strips are treated for comparison with the earlier work[1,2]. For the trapped case the results presented are for a film thickness of 12 microns and a diaphragm thickness of 14 microns because the trapping is considerably better for this combination of thicknesses than the other at the second thickness mode[8]. For this combination of thicknesses the second thickness mode is around 250 MHz. In the trapped case both strip electrodes 500 microns wide and square electrodes with lateral dimensions of 500 microns × 500 microns were considered. The lateral dimensions of both the strip and square diaphragms was varied and the wafer thickness is 6 mils.

In the absence of trapping for the strip case the values of Q calculated from Eq.(5) of this work are plotted as the solid curve in Fig.5, in which the dotted curve from Fig.8 of Ref.2 is also plotted for purposes of comparison. It can be seen from the figure that the agreement is quite good. However, although the highest Q's calculated in this work are very nearly the same as those obtained in the earlier more cumbersome direct calculation[1,2], the lowest Q's calculated by means of the perturbation procedure tend to be nearly an order of magnitude higher than those calculated by the earlier direct procedure[1,2]. We are not absolutely sure of the reason for this discrepancy, but there are two possibilities. The perturbation procedure might be tending to lose its accuracy for low Q because of the increased radiation or the resonant frequency might not have been sufficiently precisely determined by means of the earlier direct procedure[1,2] for the accurate determination of the lowest Q values. However, Fig.5 reveals that the highest Q's calculated by the perturbation procedure are consistently slightly higher than those calculated using the earlier direct procedure, which tends to support the second possibility. The figure also shows that the location of the peaks and valleys of Q with wafer thickness determined by means of the perturbation procedure is in quite good agreement with those obtained from the earlier direct calculation[1,2]. Also in the absence of trapping the Q's calculated from Eq.(5) for the square diaphragm are plotted in Fig.6. It can be seen from the figure that the peaks and valleys are in essentially the same positions as in the strip case, but that the Q's are considerably lower, roughly between 1/2 to 2/3 of the values in the strip case. This is as expected because of the radiation in two orthogonal directions for rectangular diaphragms. When trapping is present the Q's calculated from Eq.(5) for both the strip and square case are plotted in Fig.7 as a function of $(d - \ell)$, i.e., the distance from the edge of the electrode to the edge of the diaphragm. It can be seen from the figure that, as expected, Q increases very rapidly with $(d - \ell)$ and for the same value of $(d - \ell)$ the Q is about twice as large in the strip case as in the rectangular case. If a film thickness of, say, 8 microns had been employed, the required $(d - \ell)$ for good Q would be much larger[8].

Acknowledgements

This work was supported in part by the Air Force Office of Scientific Research under Grant No. AFOSR-84-0351.

References

1. D.S. Stevens, H.F. Tiersten and D.V. Shick, "On the Reduction in Quality Factor of the Piezoelectric Thin Film on Semiconductor Composite Resonator Due to Radiation into the Bulk Semiconductor," 1985 Ultrasonics Symposium Proceedings, IEEE Cat. No.85CH2209-5, Institute of Electrical and Electronic Engineers, New York, 311 (1985).
2. D.V. Shick, D.S. Stevens and H.F. Tiersten, "Quality Factor of the Piezoelectric Thin Film on Semiconductor Composite Resonator Resulting from Radiation into the Semiconductor Wafer," J. Appl. Phys., 60, 2238 (1986).
3. H.F. Tiersten and D.S. Stevens, "An Analysis of Thickness-Extensional Trapped Energy Resonant Device Structures with Rectangular Electrodes in the Piezoelectric Thin Film on Silicon Configuration," J. Appl. Phys., 54, 5893 (1983).
4. H.F. Tiersten, Linear Piezoelectric Plate Vibrations (Plenum, New York, 1969), Chap.t, Sec.4.
5. H.F. Tiersten and B.K. Sinha, "A Perturbation Analysis of the Attenuation and Dispersion of Surface Waves," J. Appl. Phys., 49, 87 (1978).
6. Ref.4, Chap.15, Sec.5.
7. H.F. Tiersten and R.C. Smythe, "Coupled Thickness-Shear and Thickness-Twist Vibrations of Unelectroded AT-Cut Quartz Plates," J. Acoust. Soc. Am., 78, 1684 (1985).
8. For more detail see D.V. Shick and H.F. Tiersten, "A Perturbation Calculation of the Quality Factor of the Piezoelectric Thin Film on Semiconductor Composite Resonator Resulting from Radiation into the Semiconductor Wafer," to be issued as a technical report, Rensselaer Polytechnic Institute, Troy, New York 12180-3590.
9. In Eq.(4.37) of Ref.3 the expression $n_{14} = (C_{33}^f r^f - C_{13}^f)\cos \eta_{f2} h_f$ was inadvertently omitted.
10. B.A. Auld, Acoustic Fields and Waves in Solids (Wiley, New York, 1973), Vol.I, p.210.
11. Ref.3, Eqs.(2.5) and (2.6), Ref.2, Eqs.(5) and (6).

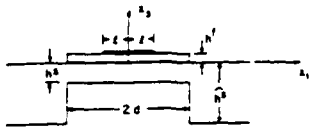

Figure 1. Cross-Section of a Composite Resonator

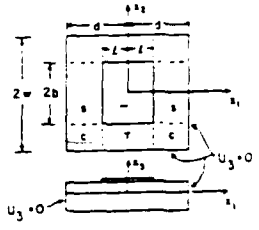

Figure 2. Plan View of Model for Analyses of Composite Resonator Mode Shapes

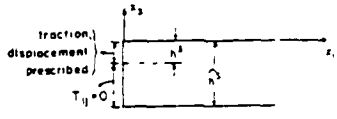

Figure 3. Cross-Section for Variational Analysis of Radiation into Wafer

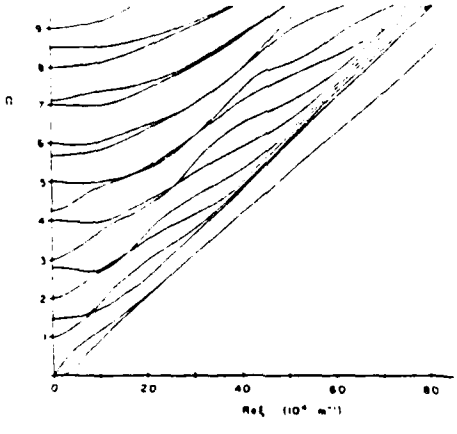

Figure 4. Dispersion Curves for the Gallium-Arsenide Wafer with $\hat{\Omega}$ the Dimensionless Frequency Normalized with Respect to the First Thickness-Shear Frequency

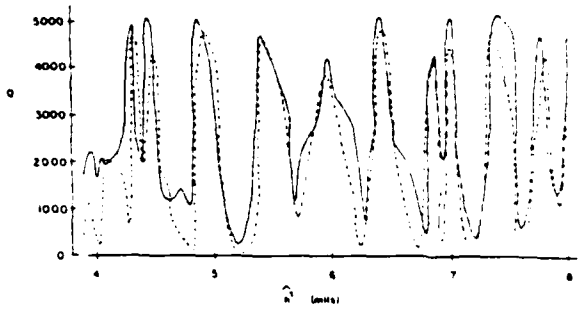

Figure 5. Quality Factor Versus Wafer Thickness When Trapping Is Not Present for the Strip Composite Resonator

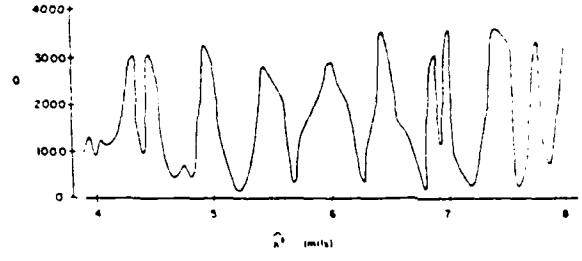

Figure 6. Quality Factor Versus Wafer Thickness When Trapping Is Not Present for the Rectangular Composite Resonator

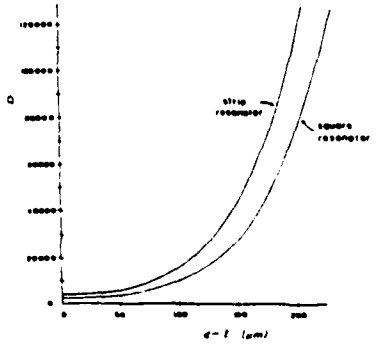

Figure 7. Quality Factor Versus Distance from Edge of Electrode to Edge of Diaphragm When Trapping Is Present

A PERTURBATION CALCULATION OF THE QUALITY FACTOR OF THE PIEZOELECTRIC THIN FILM ON SEMICONDUCTOR COMPOSITE RESONATOR RESULTING FROM RADIATION INTO THE WAFER

D.V. Shick and H.F. Tiersten
Department of Mechanical Engineering,
Aeronautical Engineering & Mechanics
Rensselaer Polytechnic Institute
Troy, New York 12180-3590

ABSTRACT

In a variational analysis of the vibrations of the piezoelectric thin film on semiconductor composite resonator it was shown that the quality factor (Q) due to radiation into the semiconductor wafer is a sharply varying function of the ratio of the thickness of the resonator to that of the film if trapping is not present, but not if trapping is present. The treatment is very cumbersome to use and is restricted to the case of strip electrodes and diaphragms. In this work a perturbation procedure for the calculation of the Q due to radiation into the wafer is presented, which is considerably less cumbersome to use than the earlier treatment and is not restricted to the case of strip electrodes and diaphragms. The resonant mode of interest is determined from an equation for transversely varying thickness modes in composite resonators and simple approximate but accurate conditions at the edges of the diaphragm, from which the radiation into the wafer is obtained using a variational approximation procedure. The resonant mode and resulting radiation field are employed in a perturbation integral to calculate the Q. For the case of strip electrodes and diaphragms the calculated results are shown to be in good agreement with the earlier more cumbersome calculations. In addition the perturbation calculations are performed for the case of rectangular electrodes and diaphragms.

1. Introduction

The composite resonator consists of a uniform thin layer etched in a small well-defined region of a semiconductor wafer to form a diaphragm, upon which is deposited a thin piezoelectric film along with the electrodes to form a resonant region directly on the wafer. In a recent analysis[1] of the composite resonator vibrating in an essentially thickness-extensional mode it was shown that the quality factor (Q) due to radiation into the bulk semiconductor is a very sharply varying function of the ratio of the thickness of the diaphragm to that of the film if trapping is not present, but not if trapping is present. A brief explanation of the meaning of the words "energy trapping" is given in the Introduction of Ref.1. The treatment employs a very accurate but extremely cumbersome variational approximation technique and is restricted to the case of strip electrodes and diaphragms.

In this work a perturbation procedure for the calculation of the Q due to radiation into the semiconductor wafer is presented, which is considerably less cumbersome to use than the earlier variational treatment and is not restricted to the case of strip electrodes and diaphragms. In the treatment the resonant mode of interest is determined from the equation for transversely varying essentially thickness-extensional modes in composite resonators[2] and simple approximate but very accurate conditions at the edges of the diaphragm. This resonant mode is then used to determine the near field radiation into the semi-conductor wafer by means of a variational approximation procedure[3]. Of course, as in the earlier work[1], all radiating plate waves in the wafer are included in order to achieve accuracy. Finally, the mode in the composite

resonator and the radiation field in the wafer are employed in a perturbation integral[4] to calculate the Q. Calculations are performed for the cases of rectangular electrodes and diaphragms and strip electrodes and diaphragms both when trapping is and is not present. For the case of strip electrodes and diaphragms the calculated results are shown to be in good agreement with the earlier more cumbersome direct calculations[1]. As in the earlier work[1], all calculations are performed for the particular case of an aluminum-nitride film on gallium-arsenide. Since the fundamental essentially thickness-extensional mode will not trap for an aluminum-nitride film on a gallium-arsenide diaphragm in the flat plate configuration and the second thickness-extensional mode will trap for a sufficiently thick aluminum-nitride film[5], the Q is calculated for the second essentially thickness-extensional mode when trapping is present and for the fundamental, when trapping is not present.

2. Perturbation Procedure

Since the coupling is small in the piezoelectric thin film and the semiconductor is assumed to be nonpiezoelectric, we need consider only the elastic portion of the equation for the first perturbation of the eigenfrequency, which may be written in the form[4]

$$\Delta_\mu = H_\mu / 2\omega_\mu , \quad \omega = \omega_\mu - \Delta_\mu , \tag{2.1}$$

where ω_μ and ω are the unperturbed and perturbed eigenfrequencies, respectively, and

$$H_\mu = \int_S n_i (T_{ij} g_j^\mu - u_j T_{ij}^\mu) \, dS , \tag{2.2}$$

where n_i denotes the outwardly directed unit normal to the surface S of the resonator. Since, as already noted, any piezoelectric coupling is ignored, the constitutive equation for the stress tensor T_{ij} is given by

$$T_{ij} = c_{ijk\ell} u_{k,\ell}, \tag{2.3}$$

where the $c_{ijk\ell}$ denote the elastic constants and u_k is the mechanical displacement vector. Standard Cartesian tensor notation is employed along with the summation convention for repeated tensor indices and the comma convention for partial differentiation with respect to a space coordinate, as in Ref.4. The normalized displacement field g_j^μ is defined by

$$g_j^\mu = u_j^\mu / N_\mu, \quad N_\mu^2 = \int_V \rho u_j^\mu u_j^\mu \, dV, \tag{2.4}$$

in which u_j^μ denotes the purely real mechanical displacement field associated with the mode of interest in the composite resonator and T_{ij}^μ denotes the associated stress tensor. A cross-section of the composite resonator attached to the semiconductor wafer is shown in Figure 1. A schematic plan view of the assumed composite resonator is shown in Figure 2 along with the assumed approximate edge condition ($u_3 = 0$) for the transverely varying thickness-extensional mode, in accordance with the explanation in the next section. Thus, for the problem at hand the surface S in (2.2) denotes the surface along which the semiconductor portion of the composite resonator abuts the wafer. The calculated mode in the composite resonator shown in Figure 2 results in tractions $\bar{t}_\ell$ and displacements $\bar{u}_\ell$ that are applied to the wafer along the surface at which it abuts the resonator as shown in

Figure 3. These tractions $\bar{t}_\ell$ and displacements $\bar{u}_\ell$ then cause radiation fields in the wafer, which are calculated by means of a very accurate variational approximation procedure in Sec.5. These radiation fields in the wafer produce a reaction back on the composite resonator along S. The stresses T_{ij} and displacements u_j in (2.2) denote this back reaction field.

Since the radiating fields in the wafer are chosen to satisfy the differential equations in and boundary conditions on the major surfaces of the wafer exactly, in the purely elastic case all that remains of the appropriate variational principle in which all conditions are natural conditions is given by[3,6]

$$\int_{S_N} (\bar{t}_\ell - n_k \hat{T}_{k\ell}) \delta\hat{u}_\ell \, dS + \int_{S_C} n_k (\hat{u}_\ell - \bar{u}_\ell) \delta\hat{T}_{k\ell} \, dS = 0 , \tag{2.5}$$

where S_N and S_C denote the portions of the surface along the left end of the wafer shown in Figure 3 on which natural- and constraint-type conditions[7], respectively, are prescribed. We note that S_N and S_C refer to different portions of the surface for different terms in the boundary integrals depending on each actual condition at a point. In (2.5) n_k denotes the outwardly directed unit normal to the wafer and we note that for surfaces along which the diaphragm abuts the wafer the n_ℓ in (2.2) and (2.5) are equal in magnitude and opposite in sign. In (2.5) $\bar{t}_\ell$ and $\bar{u}_\ell$ are known from the resonant eigensolution $T^{\mu}_{\ell k}$, u^{μ}_{ℓ} and $\hat{u}_\ell$ and $\hat{T}_{k\ell}$ are found from the expressions for the solution field radiating into the wafer, which are obtained in Sec.5. At this point we note that the reaction $\hat{u}_\ell$, $\hat{T}_{k\ell}$ from the radiating field is complex,

the real part of which yields a small change in frequency when substituted in (2.2), which is negligible and not of interest here, and the imaginary part of which yields the attenuation due to radiation into the wafer from (2.2) which is sought here. From the well-known relation $\omega = \omega_\mu - i\omega_\mu/2Q$ and (2.1), we obtain

$$Q = - i\omega_\mu^2/H_\mu . \tag{2.6}$$

3. Transversely Varying Thickness-Extensional Modes

As noted in Sec.2, a plan view for the determination of the mode of interest in the composite resonator is shown in Figure 2, in which the - denotes the electroded region, the S, the side region, the T, the top (and bottom) region and the C, the corner regions. This notation is essential for the treatment of the trapped modes, but is not needed for the untrapped modes because in the untrapped case the edges of the electrodes are relatively unimportant. It has been shown in Sec.V of Ref.2 that the homogeneous equation governing the essentially thickness-extensional modes may be written in the form

$$M_n\left(\frac{\partial^2 f^n}{\partial x_1^2} + \frac{\partial^2 f^n}{\partial x_2^2}\right) - \bar{c}_{33}^f \tilde{\eta}_{fn}^2 f^n + \rho^f \ddot{f}^n = 0 , \tag{3.1}$$

where n denotes the order of the pure thickness mode in the composite resonator, both the superscript and subscript f denote the film and $\tilde{\eta}_{fn} = \bar{\eta}_{fn}$ in an electroded region while $\tilde{\eta}_{fn} = \hat{\eta}_{fn}$ in an unelectroded region, which are defined in Eqs.(4.48) and (4.46), respectively, of Ref.2 with the aid of the appropriate root of (3.22) of Ref.2, which gives η_{fn}^o and with (3.20) η_{sn}^o, and $\bar{c}_{33}^f$ is defined in Eq.(3.12) of Ref.2.

The expression for the coefficient M_n, which is very important because its sign indicates whether trapping is or is not present in the flat composite plate configuration, is given in Eq.(4.44) along with (4.41), (4.42), (4.37), (4.38) and (4.33) of Ref.2 and clearly is much too cumbersome to present here[8]. It has also been shown in Sec.V of Ref.2 that the dominant u_3-displacement field accompanying the mode is given by

$$u_3^{fn} = {}_ou_3^{fn} f^n(x_1,x_2,t),\ u_3^{sn} = {}_ou_3^{sn} f^n(x_1,x_2,t), \tag{3.2}$$

where the superscripts f and s denote the film and semiconductor diaphragm, respectively, and ${}_ou_3$ represents the thickness dependence only and is given by

$$\begin{aligned} {}_ou_3^{fn} &= A_3^{fln} \cos \eta_{fn}^o x_3 + B_3^{fln} \sin \eta_{fn}^o x_3, \quad 0 < x_3 < h^f, \\ {}_ou_3^{sn} &= A_3^{sln} \cos \eta_{sn}^o x_3 + B_3^{sln} \sin \eta_{sn}^o x_3, \quad 0 > x_3 > -h^s, \end{aligned} \tag{3.3}$$

and the amplitudes are given in Eqs.(5.20) of Ref.2. Furthermore, it has also been shown in Secs.IV and V of Ref.2 that at an interface between electroded and unelectroded regions we have the continuity of the two quantities

$$f^n,\ df^n/dn, \tag{3.4}$$

where d/dn denotes the normal derivative (here either d/dx_1 or d/dx_2). However, the boundary conditions along the edge of the assumed resonator shown in Fig.2 that are consistent with the approximation made in obtaining Eq.(3.1) must be explained.

It has been shown that to lowest order the pertinent constitutive equations for in-plane tractions take the form[2]

$$T_{11} = c_{13}u_{3,3}, \quad T_{22} = c_{13}u_{3,3}, \quad T_{13} = c_{44}(u_{3,1}+u_{1,3}),$$

$$T_{23} = c_{44}(u_{3,2}+u_{2,3}), \quad T_{12} = c_{66}(u_{1,2}+u_{2,1}) = 0, \tag{3.5}$$

for both the piezoelectric thin film and the diaphragm essentially because u_1 and u_2 are an order of magnitude smaller than u_3 for small wavenumbers along the plate and each differentiation with respect to x_1 or x_2 reduces the order of magnitude by one. On an edge normal to x_1 the uniqueness theorem[9] reveals that we must specify one term of each of the three products

$$T_{11}u_1, \quad T_{12}u_2, \quad T_{13}u_3. \tag{3.6}$$

However, by virtue of the aforementioned ordering $T_{12}u_2$ is two orders of magnitude smaller than each of the other two terms and, hence, may be neglected, as already indicated in $(3.5)_5$. Consequently, on a free edge normal to x_1 we should satisfy

$$T_{11} = 0, \quad T_{13} = 0 \tag{3.7}$$

and on a fixed edge normal to x_1 we should satisfy

$$u_1 = 0, \quad u_3 = 0. \tag{3.8}$$

Similar considerations for an edge normal to x_2 reveal that on a free edge we should satisfy

$$T_{22} = 0, \quad T_{23} = 0, \tag{3.9}$$

and on a fixed edge we should satisfy

$$u_2 = 0, \quad u_3 = 0. \tag{3.10}$$

Since in the approximation made in obtaining Eq.(3.1) governing the essentially thickness-extensional modes, we have eliminated all waves except the important one, we can satisfy only one of the two conditions in each of (3.7) - (3.10). However, since for small wavenumbers along the plate u_3 is large while u_1 and u_2 are small, from this fact and (3.5) it is clear that one of the two conditions in each of (3.7) - (3.10) is large and the other is small. Consequently, we take the small equation in each of (3.7) - (3.10) to be satisfied approximately and require the solution to satisfy the large equation in each of (3.7) - (3.10) only. Since in each instance the large term in each of (3.7) - (3.10) is either u_3 or $u_{3,3}$, we have shown that for either completely free or completely fixed conditions along the edges of the diaphragm shown in Fig.2, the appropriate condition is

$$f^n = 0 , \tag{3.11}$$

on account of (3.2) and (3.3). From Fig.1 it is clear that the edge of the film is free while the edge of the diaphragm is essentially fixed, and we have shown that in this approximation (3.11) is the appropriate condition for either case. This means that within this approximation both u_3 and either T_{11} or T_{22} vanish simultaneously along the edge of the resonator.

Since only the semiconductor diaphragm abuts the wafer as shown in Fig.1 only the variables in the semiconductor are relevant here. However, in order to calculate the tractions $\bar{t}_\ell$ and displacements $\bar{u}_\ell$ that the mode in the composite resonator exerts on the wafer as shown in Fig.3, we need the associated displacement fields u_1^s and u_2^s in the

semiconductor diaphragm in addition to u_3^s.

In the untrapped case for the fundamental mode for any n, f^n is given by

$$f^n = \cos \bar{\xi}x_1 \cos \bar{\nu}x_2 \, e^{i\omega t}, \tag{3.12}$$

the substitution of which in (3.1) yields

$$\rho^f \omega^2 = \bar{c}_{33}^f \bar{\eta}_f^2 + M_n(\bar{\xi}^2 + \bar{\nu}^2), \tag{3.13}$$

in which for convenience we have assumed that the upper electrode covers the entire film since the edges of the electrode are unimportant because they do not cause exponential decay in the unelectroded region in the untrapped case. Substituting from (3.12) into the edge conditions (3.11) for the mode of interest, we obtain

$$\bar{\xi} = \pi/2d, \quad \bar{\nu} = \pi/2w, \tag{3.14}$$

with which the unperturbed resonant frequency ω may be obtained from (3.13). It has been shown in Sec.V of Ref.2 that for (3.12), we have

$$u_1^s = \frac{\bar{\xi}}{\bar{\zeta}} \tau^s(x_3) \sin \bar{\xi}x_1 \cos \bar{\nu}x_2 \, e^{i\omega t},$$

$$u_2^s = \frac{\bar{\nu}}{\bar{\zeta}} \tau^s(x_3) \cos \bar{\xi}x_1 \sin \bar{\nu}x_2 \, e^{i\omega t}, \tag{3.15}$$

where

$$\tau^s = A_1^{s1} \sin \eta_s^o x_3 + A_1^{s2} \sin \kappa^s \eta_s^o x_3 + B_1^{s1} \cos \eta_s^o x_3$$
$$+ B_1^{s2} \sin \kappa^s \eta^o x_3, \quad \bar{\zeta}^2 = \bar{\xi}^2 + \bar{\nu}^2, \tag{3.16}$$

and κ^s and the amplitudes are given in (4.30) and (4.26), respectively, of Ref.2.

In the trapped case we have Eq.(3.1) with $\tilde{\bar{\eta}}_{fn} = \bar{\eta}_{fn}$ in the electroded region denoted — and $\tilde{\bar{\eta}}_{fn} = \hat{\bar{\eta}}_{fn}$ in the unelectroded regions denoted S and T in Fig.2 and as usual ignoring (3.1) in the relatively unimportant corner regions denoted C. In addition the solution must satisfy the continuity conditions in (3.4) between the — and S and T regions and between the S and C and T and C regions and the conditions (3.11) along the edge of the diaphragm, i.e., at $x_1 = \pm d$ and $x_2 = \pm w$. Clearly then for the symmetric modes in x_1 and x_2 the expressions for f^n in each of the respective regions shown in Fig.2 are given by

$$\bar{f}^n = \bar{E}\cos\bar{\xi}x_1\cos\bar{\nu}x_2\,,\quad f^{ns} = (E_-^S e^{-\xi(x_1-\ell)} + E_+^S e^{\xi(x_1-\ell)})\cos\bar{\nu}x_2\,,$$

$$f^{nT} = (E_-^T e^{-\nu(x_2-b)} + E_+^T e^{\nu(x_2-b)})\cos\bar{\xi}x_1\,,$$

$$f^{nC} = E_1^C e^{-\xi(x_1-\ell)-\nu(x_2-b)} + E_2^C e^{-\xi(x_1-\ell)+\nu(x_2-b)}\,,$$

$$+ E_3^C e^{\xi(x_1-\ell)-\nu(x_2-b)} + E_4^C e^{\xi(x_1-\ell)+\nu(x_2-b)}\,, \qquad (3.17)$$

the substitution of which in (3.1) yields (3.13) along with

$$\rho^f\omega^2 = \bar{c}_{33}^f\hat{\bar{\eta}}_{fn}^2 - M_n(\xi^2 - \bar{\nu}^2),$$

$$\rho^f\omega^2 = \bar{c}_{33}^f\hat{\bar{\eta}}_{fn}^2 - M_n(\nu^2 - \bar{\xi}^2)\,. \qquad (3.18)$$

Substituting from (3.17) into (3.4) at $x_1 = \ell$ and $x_2 = b$ and into (3.11) at $x_1 = d$ and $x_2 = w$, we obtain

$$\bar{\xi} \tan \bar{\xi}\ell = \xi \frac{(1+e^{-2\xi(d-\ell)})}{1-e^{-2\xi(d-\ell)}},$$

$$\bar{\nu} \tan \bar{\nu}\ell = \nu \frac{(1+e^{-2\nu(w-b)})}{1-e^{-2\nu(w-b)}}, \tag{3.19}$$

where

$$E_{\pm}^{S} = \frac{\bar{E}\cos \bar{\xi}\ell}{1-e^{\pm 2\xi(d-\ell)}}, \quad E_{\pm}^{T} = \frac{\bar{E}\cos \bar{\nu}b}{1-e^{\pm 2\nu(w-b)}},$$

$$E_1^C = \frac{\bar{E}\cos \bar{\xi}\ell \cos \bar{\nu}b}{(1-e^{-2\xi(d-\ell)})(1-e^{-2\nu(w-b)})},$$

$$E_2^C = -e^{-2\nu(w-b)}E_1^C, \quad E_3^C = -e^{-2\xi(d-\ell)}E_1^C,$$

$$E_4^C = e^{-2\xi(d-\ell)-2\nu(w-b)}E_1^C. \tag{3.20}$$

Now, as in Ref.2, from (3.13), (3.18) and Eqs.(3.21), (3.23), (3.31) and (3.32) of *Ref.2, we obtain*

$$\xi = \left[\frac{2\bar{c}_{33}^{f}}{M_n}(\eta_f^o)^2 \hat{\Delta}^n - \bar{\xi}^2\right]^{1/2}, \quad \nu = \left[\frac{2\bar{c}_{33}^{f}}{M_n}(\eta_f^o)^2 \hat{\Delta}^n - \bar{\nu}^2\right]^{1/2}, \tag{3.21}$$

where

$$\hat{\Delta}^n = -(P^{on}+R'')/G^{on}, \tag{3.22}$$

and R'', G^{on} and P^{on} are defined in Eqs.(3.19), (3.24) and (3.33), respectively, of Ref.2. Equations (3.19), with (3.21) and (3.22) constitute two independent transcendental equations for ξ and ν for a given ℓ, b, d and w, which may readily be solved for the fundamental mode of interest. The eigenfrequencies for that mode may then be determined from (3.13).

In the trapped case since we have growing and decaying solutions in the S and T regions, from Secs.III and V of Ref.2 it is clear that

$$u_1^{sS} = \frac{\xi}{\zeta^S}\tau^s(x_3)\left[E_-^S e^{-\xi(x_1-\ell)} - E_+^S e^{\xi(x_1-\ell)}\right]\cos\bar{\nu}x_2,$$

$$u_2^{sT} = \frac{\xi}{\zeta^T}\tau^s(x_3)\left[E_-^T e^{-\nu(x_2-b)} - E_+^T e^{\nu(x_2-b)}\right]\cos\bar{\xi}x_1, \qquad (3.23)$$

where

$$(\zeta^S)^2 = \bar{\nu}^2 - \xi^2, \quad (\zeta^T)^2 = \bar{\xi}^2 - \nu^2, \qquad (3.24)$$

and u_1^{sS} is for the side region and u_2^{sT} is for the top region. We further observe that since all wavenumbers along the resonator are small, u_2^s in the S region and u_1^s in the T region are negligible for radiation in the x_1- and x_2-directions, respectively, in the wafer, as discussed more completely in Sec.4. Moreover, it is clear that for the corner regions u_1^{sC} and u_2^{sC} may be obtained from (3.23) simply by replacing the respective trigonometric functions in each term by the exponential function in brackets in the other term and ζ^C is given by

$$(\zeta^C)^2 = -(\xi^2 + \nu^2). \qquad (3.25)$$

4. Variable-Crested Waves in Wafer

In this section we obtain the solution functions for the near field waves with slowly varying crests and the associated dispersion relations. The displacement equations of motion and the linear elastic constitutive equations for the nonpiezoelectric gallium-arsenide semiconductor wafer with x_3 along a cube axis take the form[10]

$$c_{11}\hat{u}_{1,11} + (c_{13}+c_{44})\hat{u}_{2,12} + (c_{13}+c_{44})\hat{u}_{3,13} + c_{44}\hat{u}_{1,22} + c_{44}\hat{u}_{1,33} = \rho\ddot{\hat{u}}_1 ,$$

$$c_{44}\hat{u}_{2,11} + (c_{44}+c_{13})\hat{u}_{1,12} + c_{11}\hat{u}_{2,22} + (c_{13}+c_{44})\hat{u}_{3,23} + c_{44}\hat{u}_{2,33} = \rho\ddot{\hat{u}}_2 ,$$

$$c_{44}\hat{u}_{3,11} + (c_{44}+c_{13})\hat{u}_{1,31} + c_{44}\hat{u}_{3,22} + (c_{44}+c_{13})\hat{u}_{2,23} + c_{33}\hat{u}_{3,33} = \rho\ddot{\hat{u}}_3 , \tag{4.1}$$

$$\hat{T}_{11} = c_{11}\hat{u}_{1,1} + c_{13}\hat{u}_{2,2} + c_{13}\hat{u}_{3,3} , \quad \hat{T}_{22} = c_{13}\hat{u}_{1,1} + c_{11}\hat{u}_{2,2} + c_{13}\hat{u}_{3,3} ,$$

$$\hat{T}_{33} = c_{13}\hat{u}_{1,1} + c_{13}\hat{u}_{2,2} + c_{33}\hat{u}_{3,3} ,$$

$$\hat{T}_{23} = c_{44}(\hat{u}_{3,2} + \hat{u}_{2,3}) , \quad \hat{T}_{12} = c_{44}(\hat{u}_{1,2} + \hat{u}_{2,1}) , \quad \hat{T}_{31} = c_{44}(\hat{u}_{3,1} + \hat{u}_{1,3}) , \tag{4.2}$$

where the carets are used to denote the wafer as distinct from the diaphragm.

From either Figs.1 or 3 we see that the boundary conditions on the major surfaces of the semiconducting plate may be written in the form

$$\hat{T}^s_{3j} = 0 \text{ at } x_3 = 0 \text{ and } x_3 = -\hat{h}^s . \tag{4.3}$$

In considering waves radiating in the x_1-direction, we first note that since $\bar{\nu}$ and ν are small, from (4.1) and (4.2) it is clear that $\hat{T}^s_{12}$ is an order of magnitude smaller than $\hat{T}^s_{13}$ and $\hat{u}^s_1$, and $\hat{u}^s_2$ is an order of magnitude smaller than $\hat{u}^s_1$ and $\hat{u}^s_3$. Hence, $\hat{u}^s_2$, the x_2-differential equation and $\hat{T}^s_{32}$ are negligible for radiation in the x_1-direction.

Under these circumstances, from (4.1) we see that the differential equations that must be satisfied take the reduced form

$$c^s_{11}\hat{u}^s_{1,11} + (c^s_{13}+c^s_{44})\hat{u}^s_{3,13} + c^s_{44}\hat{u}^s_{1,33} = \rho^s\ddot{\hat{u}}^s_1 ,$$

$$c^s_{44}\hat{u}^s_{3,11} + (c^s_{13}+c^s_{44})\hat{u}^s_{1,13} + c^s_{33}\hat{u}^s_{3,33} = \rho^s\ddot{\hat{u}}^s_3 , \tag{4.4}$$

and from (4.2) and (4.3) the boundary conditions take the reduced form

$$c_{13}^s \hat{u}_{1,1}^s + c_{33}^s \hat{u}_{3,3}^s = 0 \quad \text{at } x_3 = 0 \text{ and } x_3 = -\hat{h}^s , \tag{4.5}$$

$$c_{44}^s (\hat{u}_{1,3}^s + \hat{u}_{3,1}^s) = 0 \quad \text{at } x_3 = 0 \text{ and } x_3 = -\hat{h}^s . \tag{4.6}$$

For waves with slowly varying crests in the x_2-direction and propagating in the $+x_1$-direction in the near field consider

$$\hat{u}_a^s = \cos \bar{\nu} x_2 (\hat{A}_a^s e^{i\hat{\eta}_s x_3} + \hat{B}_a^s e^{-i\hat{\eta}_s x_3}) , \; e^{i\hat{\xi}(x_1 - d)} e^{i\omega t} , \quad a = 1,3 , \tag{4.7}$$

which satisfies (4.4) provided

$$\sigma_{11}^s \hat{A}_1^s + \sigma_{13}^s \hat{A}_3^s = 0 , \quad \sigma_{13}^s \hat{A}_1^s + \sigma_{33}^s \hat{A}_3^s = 0 , \tag{4.8}$$

$$\sigma_{11}^s \hat{B}_1^s - \sigma_{13}^s \hat{B}_3^s = 0 , \quad -\sigma_{13}^s \hat{B}_1^s + \sigma_{33}^s \hat{B}_3^s = 0 , \tag{4.9}$$

where

$$\begin{aligned} \sigma_{11}^s &= -c_{11}^s \hat{\xi}^2 - c_{44}^s \hat{\eta}_s^2 + \rho^s \omega^2 , \\ \sigma_{13}^s &= -(c_{13}^s + c_{44}^s) \hat{\xi} \hat{\eta}_s , \\ \sigma_{33}^s &= -c_{44}^s \hat{\xi}^2 - c_{33}^s \hat{\eta}_s^2 + \rho^s \omega^2 . \end{aligned} \tag{4.10}$$

Each of the two systems of linear homogeneous algebraic equations in two amplitudes yields nontrivial solutions when the determinant of the coefficients of the amplitudes vanishes. Both determinants are identical and each is quadratic in $\hat{\xi}^2$, $\hat{\eta}_s^2$ and ω^2. Thus, for a given ξ and ω each determinant yields two independent $\hat{\eta}_s$ ($\hat{\eta}_s^{(1)}$, $\hat{\eta}_s^{(2)}$) and each $\hat{\eta}_s^{(i)}$ yields amplitude ratios from each system of linear algebraic equations, i.e., (4.8) and (4.9). Hence, there are four amplitude ratios, which we denote by

$$\hat{A}_1^{si} = \mu^{si} \hat{A}_3^{si} , \quad \hat{B}_1^{si} = \nu^{si} \hat{B}_3^{si} . \tag{4.11}$$

As a solution of the boundary conditions (4.5) and (4.6), we take

$$\hat{u}_3^s = \cos\bar{\nu}x_2 \sum_{m=1}^{2} (\hat{A}_3^{sm} e^{i\hat{\eta}_{sm}x_3} + \hat{B}_3^{sm} e^{-i\hat{\eta}_{sm}x_3}) e^{i\hat{\xi}(x_1-d)} e^{i\omega t},$$

$$\hat{u}_1^s = \cos\bar{\nu}x_2 \sum_{m=1}^{2} (\hat{\mu}^{sm}\hat{A}_3^{sm} e^{i\hat{\eta}_{sm}x_3} + \hat{\nu}^{sm}\hat{B}_3^{sm} e^{-i\hat{\eta}_{sm}x_3}) e^{i\hat{\xi}(x_1-d)} e^{i\omega t}. \tag{4.12}$$

Substituting from (4.12) into the boundary conditions (4.5) and (4.6) we obtain

$$\sum_{n=1}^{2} \left[\hat{A}_3^{sn}(c_{13}^s\hat{\xi}\hat{\mu}^{sn} + c_{33}^s\hat{\eta}_{sn}) + \hat{B}_3^{sn}(c_{13}^s\hat{\xi}\hat{\nu}^{sn} - c_{33}^s\hat{\eta}_{sn})\right] = 0,$$

$$\sum_{n=1}^{2} \left[\hat{A}_3^{sn}(\hat{\eta}_{sn}\hat{\mu}^{sn} + \hat{\xi}) + \hat{B}_3^{sn}(-\hat{\eta}_{sn}\hat{\nu}^{sn} + \hat{\xi})\right] = 0,$$

$$\sum_{n=1}^{2} \left[\hat{A}_3^{sn}(c_{13}^s\hat{\xi}\hat{\mu}^{sn} + c_{33}^s\hat{\eta}_{sn})e^{-i\hat{\eta}_{sn}\hat{h}^s} + \hat{B}_3^{sn}(c_{13}^s\hat{\xi}\hat{\nu}^{sn} - c_{33}^s\hat{\eta}_{sn})e^{i\hat{\eta}_{sn}\hat{h}^s}\right] = 0,$$

$$\sum_{n=1}^{2} \left[\hat{A}_3^{sn}(\hat{\eta}_{sn}\hat{\mu}^{sn} + \hat{\xi})e^{i\hat{\eta}_{sn}\hat{h}^s} + \hat{B}_3^{sn}(-\hat{\eta}_{sn}\hat{\nu}^{sn} + \hat{\xi})e^{i\hat{\eta}_{sn}\hat{h}^s}\right] = 0. \tag{4.13}$$

Equations (4.13) constitute a system of four linear homogeneous algebraic equations in $\hat{A}_3^{sn}$ and $\hat{B}_3^{sn}$, which yields nontrivial solutions when the determinant of the coefficients vanishes. Calculations are performed in the usual way[1,2] and yield the $\hat{\eta}_{sn}$, $\hat{\mu}^{sn}$, $\hat{\nu}^{sn}$, $\hat{A}^{sn}$ and $\hat{B}^{sn}$ along with the dispersion relation $\omega = \omega(\hat{\xi})$.

The functions in (4.12) are for either the untrapped case or the electroded region for the trapped case and since for slowly varying crests only the slowly varying terms, i.e., the $\cos\bar{\nu}x_2$ in (4.12), which have no influence on the radiating waves or the dispersion relation, change, it is not purposeful to write the solution for any other regions for the trapped case. From the solution the lowest 17 real dispersion curves for the bulk gallium-arsenide plate have been

calculated and are shown in dimensionless form in Fig.4, which is identical with Fig.6 of Ref.1 since for slowly varying crests, the crests do not influence the dispersion relation $\omega = \omega(\hat{\xi})$. For the fundamental essentially thickness-extensional resonance of the composite resonator consisting of a 7 μm thick aluminum-nitride film on a 14 μm thick gallium-arsenide diaphragm, which is around 132 MHz, this number of dispersion curves is for a gallium-arsenide wafer thickness of about 5 mils. In this work we perform calculations for wafer thicknesses up to 8 mils for which there are 30 real dispersion curves for a frequency of 132 MHz. However, we do not bother to show the figure for more than 17.

Similarly, since statements equivalent to the foregoing hold for waves with slowly varying crests in the x_1-direction and propagating in the x_2-direction in the near field, the differential equations and boundary conditions that must be satisfied may be obtained from (4.4) - (4.6) simply by replacing all indices 1 by 2 in (4.4) - (4.6). Under these circumstances the near field radiating solution takes the form

$$\hat{u}_3^s = \cos \bar{\xi} x_1 \sum_{m=1}^{2} (\hat{A}_3^{sm} e^{i\hat{\eta}_{sm} x_3} + \hat{B}_3^{sm} e^{-i\hat{\eta}_{sm} x_3}) e^{i\hat{\nu}(x_2 - w)} e^{i\omega t},$$

$$\hat{u}_2^s = \cos \bar{\xi} x_1 \sum_{m=1}^{2} (\hat{\mu}^{sm} \hat{A}_3^{sm} e^{i\hat{\eta}_{sm} x_3} + \hat{\nu}^{sm} \hat{B}_3^{sm} e^{-i\hat{\eta}_{sm} x_3}) e^{i\hat{\nu}(x_2 - w)} e^{i\omega t}, \tag{4.14}$$

in place of the form shown in (4.12). From this solution we obtain the propagating dispersion curves for near field radiating waves in the x_2-direction. The dispersion curves are identical with those in Fig.4.

5. Variational Analysis of Radiation into Wafer

In this section we determine the waves radiating into the semiconductor wafer due to the tractions and displacements resulting from the mode in the composite resonator by means of a variational approximation procedure, as indicated in Sec.2. Since the near radiation fields emanate from the edges of the diaphragm, which are normal to x_1 and x_2, respectively, we may determine the near fields radiating in the x_1- and x_2-directions separately. Accordingly, we first consider radiation in the x_1-direction. From Fig.3 we see that the edge of the wafer below the diaphragm is traction free, i.e., $T_{1j} = 0$. In Sec.3 we have shown that for the mode in the resonator T_{12} vanishes to the order of approximation throughout and u_3 and T_{11} both vanish simultaneously along the edge of the resonator[11], i.e., where the diaphragm abuts the wafer, while both T_{13} and u_1 exist along the same edge. Furthermore, in Sec.4 it is shown that since the transverse mode shape is slowly varying in the wafer, for radiating waves propagating in the x_1-direction in the wafer u_2 is negligible[11]. As a consequence of the foregoing, for propagation in the $\pm x_1$-direction in the untrapped case Eq.(2.5) takes the form

$$\int_{-w}^{w} dx_2\Big[\int_{-\hat{h}^s}^{-h^s} (\hat{T}^s_{11}\delta\hat{u}^s_1 + \hat{T}^s_{13}\delta\hat{u}^s_3)\Big|_{x_1=d} dx_3 + \int_{-h^s_o}^{o} [\hat{T}^s_{11}\delta\hat{u}_1$$

$$+ (-T^s_{13} + \hat{T}^s_{13})\delta\hat{u}^s_3]\Big|_{x_1=d} dx_3 + \int_{-h^s}^{o} [-(\hat{u}^s_1 - g^s_1)\delta\hat{T}^s_{11}$$

$$- \hat{u}^s_3\delta\hat{T}^s_{13}]\Big|_{x_1=d} dx_3\Big] = 0\,, \qquad (5.1)$$

where, as already indicated, the forcing terms resulting from the mode in the composite resonator are T^s_{13} and g^s_1. In the trapped case, the integral from -w to w is replaced by integrals over the S and C regions, respectively, i.e., from -w to -b and -b to b and b to w, in accordance with the solution in (3.17) and the expressions for u^S_1 and u^S_2 given and discussed at the end of Sec.3. For radiation in the x_2-direction we simply interchange subscripts 1 and 2 and replace w by d in (5.1) for the untrapped case and w by d and b by ℓ for the trapped case.

For radiation in the x_1-direction we now expand the solution in the wafer as a sum of waves with slowly varying crests in the x_2-direction, which were discussed in Sec.4 and are given in (4.12). Thus

$$\hat{u}^s_a = \sum_{\alpha=1}^{\hat{N}} \hat{K}^{(\alpha)}_S \hat{u}^{s(\alpha)}_a\,, \quad a = 1,3, \qquad (5.2)$$

where each of the $\hat{u}_a^{s(\alpha)}$ are of the form given in (4.12) and $\hat{N}$ denotes the number of branches of the dispersion curves required for the $\hat{N}$ propagating plate waves for a given wafer thickness. Since the $\hat{u}_a^{s(\alpha)}$ are fixed, only the $\hat{K}_S^{(\alpha)}$ are varied when (5.2) is substituted into (5.1). Accordingly, substituting from (5.2) into (5.1), employing (4.2) and performing the integrations, we obtain an equation of the form

$$\sum_{\beta=1}^{\hat{N}} \left[\sum_{\alpha=1}^{\hat{N}} K_S^{(\alpha)} A_{\alpha\beta} + C_\beta^S \right] \delta K_S^{(\beta)} = 0 , \tag{5.3}$$

where

$$\begin{aligned} A_{\alpha\beta} = \sum_{m=1}^{2} \sum_{n=1}^{2} \Big[& g(\hat{\eta}_{sm}^{\alpha} + \hat{\eta}_{sn}^{\beta})_{-\hat{h}^s}^{o} (\hat{\tau}_{1\alpha}^{sm}\hat{\mu}_{\beta}^{sm} + \hat{\tau}_{5\alpha}^{sm})\, \hat{A}_{3\beta}^{sn} \\ & - g(\hat{\eta}_{sm}^{\alpha} + \hat{\eta}_{sn}^{\beta})_{-h^s}^{o} (\hat{\mu}_{\alpha}^{sm}\hat{\tau}_{1\beta}^{sn} + \hat{\tau}_{5\beta}^{sn})\, \hat{A}_{3\alpha}^{sm} \\ & + g(\hat{\eta}_{sm}^{\alpha} - \hat{\eta}_{sn}^{\beta})_{-\hat{h}^s}^{o} (\hat{\tau}_{1\alpha}^{sm}\hat{\nu}_{\beta}^{sn} + \hat{\tau}_{5\alpha}^{sn})\hat{B}_{3\beta}^{sn} - g(\hat{\eta}_{sm}^{\alpha} - \hat{\eta})_{-h^s}^{o} (\hat{\mu}_{\alpha}^{sm}\hat{\sigma}_{1\beta}^{sn} + \hat{\sigma}_{5\beta}^{sn})\hat{A}_{3\alpha}^{sm} \\ & + g(-\hat{\eta}_{sm}^{\alpha} + \hat{\eta}_{sn}^{\beta})_{-\hat{h}^s}^{o} (\hat{\sigma}_{1\alpha}^{sm}\hat{\mu}_{\beta}^{sn} + \hat{\sigma}_{5\alpha}^{sm})\hat{A}_{3B}^{sn} - g(-\hat{\eta}_{sm}^{\alpha} + \hat{\eta}_{sn}^{\beta})_{-h^s}^{o} (\hat{\nu}_{\alpha}^{sm}\hat{\tau}_{1\beta}^{sn} + \hat{\tau}_{5\beta}^{sn})\hat{B}_{3\alpha}^{sm} \\ & + g(-\hat{\eta}_{sm}^{\alpha} - \hat{\eta}_{sn}^{\beta})_{-\hat{h}^s}^{o} (\hat{\sigma}_{1\alpha}^{sm}\hat{\nu}_{\beta}^{sn} + \hat{\sigma}_{5\alpha}^{sm})\hat{B}_{3\beta}^{sn} - g(-\hat{\eta}_{sm}^{\alpha} - \hat{\eta}_{sn}^{\beta})_{-h^s}^{o} (\hat{\nu}_{\alpha}^{sm}\hat{\sigma}_{1\beta}^{sn} + \hat{\sigma}_{5\beta}^{sn})\hat{B}_{3\alpha}^{sm} \Big] , \end{aligned} \tag{5.4}$$

$$\begin{aligned} C_\beta^S = \frac{1}{N_\mu}\, c_{44}\bar{\xi} \sin \bar{\xi} d \Bigg[& A_3^{s1} \sum_{m=1}^{2} \Big[\hat{A}_{3\beta}^{sm} g_c (\hat{\eta}_{sm}^{\beta}, \eta_s^o)_{-h^s} + \hat{B}_{3\beta}^{sm} g_c (-\hat{\eta}_{sm}^{\beta}, \eta_s^o)_{-h^s} \\ & + B_3^{s1} \sum_{m=1}^{2} \Big[\hat{A}_{3\beta}^{sm} g_s (\hat{\eta}_{sm}^{\beta}, \eta_s^o)_{-h^s} + \hat{B}_{3\beta}^{sm} g_s (-\hat{\eta}_{sm}^{\beta}, \eta_s^o)_{-h^s} \Big] \Bigg] \end{aligned}$$

$$+\frac{1}{N_\mu}\frac{\bar{\varepsilon}}{\bar{\zeta}}\sin\bar{\xi}d\Bigg[\sum_{m=1}^{2}\hat{\tau}_{5\beta}^{sm}\Big[A_1^{s1}g_s(\hat{\eta}_{sm}^{\beta},\eta_s^o)_{-h^s}+A_1^{s2}g_s(\hat{\eta}_{sm}^{\beta},\varkappa\eta_s^o)_{-h^s}$$

$$+B_1^{s1}g_c(\hat{\eta}_{sm}^{\beta},\eta_s^o)_{-h^s}+B_1^{s2}g_c(\hat{\eta}_{sm}^{\beta},\varkappa\eta_s^o)_{-h^s}$$

$$+\sum_{m=1}^{2}\hat{\sigma}_{5\beta}^{sm}\Big[A_1^{s1}g_s(-\hat{\eta}_{sm}^{\beta},\eta_s^o)_{-h^s}+A_1^{s2}g_s(-\hat{\eta}_{sm}^{\beta},\varkappa\eta_s^o)_{-h^s}$$

$$+B_1^{s1}g_c(-\hat{\eta}_{sm}^{\beta},\eta_s^o)_{-h^s}+B_1^{s2}g_c(-\hat{\eta}_{sm}^{\beta},\varkappa\eta_s^o)_{-h^s}\Big]\Bigg], \tag{5.5}$$

and N_μ is the normalization factor, which is defined in (2.4) and for the mode in the composite resonator is given by

$$N_\mu^2=dw\Big[\rho_f g_{sc}(A_3^{f1},B_3^{f1},\eta_f^o)_o^{hf}+\rho_s g_{sc}(A_3^{s1},B_3^{s1},\eta_s^o)_{-h}^{o}{}^{s}\Big], \tag{5.6}$$

where

$$g_{sc}(A,B,\eta)_{h_1}^{h_2}\equiv\int_{h_1}^{h_2}(A\cos\eta x+B\sin\eta x)^2\,dx$$

$$=\Big[\frac{(A^2-B^2)\sin(2\eta x)-4AB\cos^2(\eta x)+2(A^2+B^2)\eta x}{4\eta}\Big]_{x=h_1}^{x=h_2}. \tag{5.7}$$

In (5.4) and (5.5) we have employed the definitions

$$\hat{\tau}_{1\alpha}^{sm}=i\hat{A}_{3\alpha}^{sm}(-c_{11}\hat{\xi}_\alpha\hat{\mu}_\alpha^{sm}+c_{13}\hat{\eta}_{sm}^{\alpha}),$$

$$\hat{\tau}_{5\alpha}^{sm}=i\hat{A}_{3\alpha}^{sm}c_{44}(-\hat{\xi}_\alpha+\hat{\eta}_{sm}^{\alpha}\hat{\mu}_\alpha^{sm}),$$

$$\hat{\sigma}_{1\alpha}^{sm}=i\hat{B}_{3\alpha}^{sm}(-c_{11}\hat{\xi}_\alpha\hat{\nu}_\alpha^{sm}-c_{13}\hat{\eta}_{sm}^{\alpha}),$$

$$\hat{\sigma}_{5\alpha}^{sm}=i\hat{B}_{3\alpha}^{sm}c_{44}(-\hat{\xi}_\alpha-\hat{\eta}_{sm}^{\alpha}\hat{\nu}_\alpha^{sm}), \tag{5.8}$$

$$g(\theta)_{h_1}^{h_2} = \int_{h_1}^{h_2} e^{i\theta x}\,dx = \frac{1}{i\theta}\,(e^{i\theta h_2} - e^{i\theta h_1}), \quad \theta \neq 0$$

$$= h_2 - h_1 \quad , \quad \theta = 0 \qquad (5.9)$$

$$g_c(\theta,\varphi)_h = \int_h^o e^{i\theta x}\cos\varphi x\,dx = \frac{i\theta}{\varphi^2 - \theta^2}\left[1 - e^{i\theta h}(\cos\varphi h - i\,\frac{\varphi}{\theta}\sin\varphi h)\right], \quad \theta \neq \varphi$$

$$= \frac{i}{4\theta}\,(e^{2i\theta h} - 1) - \frac{h}{2}\,, \quad \theta = \varphi\,,$$

$$g_s(\theta,\varphi)_h = \int_h^o e^{i\theta x}\sin\varphi x\,dx = \frac{-\varphi}{\varphi^2 - \theta^2}\left[1 - e^{i\theta h}(\cos\varphi h - i\,\frac{\theta}{\varphi}\sin\varphi h)\right], \quad \theta \neq \varphi$$

$$= \frac{1}{4\theta}\,(e^{2i\theta h} - 1) - i\,\frac{h}{2}\,, \quad \theta = \varphi\,. \qquad (5.10)$$

The foregoing is for the untrapped case. For the trapped case $A_{\alpha\beta}$ is unchanged and C_β^S may be obtained from the expressions in (5.5) simply by replacing $\bar{\xi}\sin\bar{\xi}d$ by $\xi\cos\bar{\xi}\ell/\sinh\xi(d-\ell)$ and $\bar{\zeta}$ by ζ^S and N_μ takes the form

$$N_\mu^2 = \left[\left(\ell + \frac{\sin 2\bar{\xi}\ell}{2\bar{\xi}}\right) + 2\left(\frac{\cos\bar{\xi}\ell}{1 - e^{-2\xi(d-\ell)}}\right)^2 \frac{e^{-2\xi(d-\ell)}}{\xi}\,[\sinh 2\xi(d-\ell) - 2\xi(d-\ell)]\right]$$

$$\times\left[\left(b + \frac{\sin 2\bar{\nu}b}{2\bar{\nu}}\right) + 2\left(\frac{\cos\bar{\nu}b}{1 - e^{-2\nu(w-b)}}\right)^2 \frac{e^{-2\nu(w-b)}}{\nu}\,[\sinh 2\nu(w-b) - 2\nu(w-b)]\right]$$

$$\times\left[\rho^f g_{sc}(A_3^{f1}, B_3^{f1}, \eta_f^o)_o^{h^f} + \rho_s g_{sc}(A_3^{s1}, B_3^{s1}, \eta_f^o)_{-h^s}^{o}\right], \qquad (5.11)$$

in place of (5.6). Since the variations in (5.3) are arbitrary, we obtain the inhomogeneous linear algebraic equations for the $\hat{K}_s^{(\alpha)}$ in the form

$$\sum_{\alpha=1}^{\hat{N}} \hat{K}_S^{(\alpha)} A_{\alpha\beta} = -\,C_\beta^S, \quad \beta = 1, \ldots \hat{N}\,. \qquad (5.12)$$

In a similar way for radiation in the x_2-direction, we obtain

$$\sum_{\gamma=1}^{\hat{N}} \hat{K}_T^{(\gamma)} A_{\gamma\delta} = -C_\delta^T, \quad \delta = 1, \ldots . \hat{N}, \tag{5.13}$$

where $A_{\gamma\delta}$ is given in (5.4) and C_δ^T may be obtained from the expression in (5.5) for the untrapped case and the revised expression for the trapped case simply by replacing $\bar{\xi}$ by $\bar{\nu}$, d by w and ℓ by b. Equations (5.12) and (5.13) each constitute $\hat{N}$ inhomogeneous linear algebraic equations for the $\hat{N}$ unknowns $\hat{K}_S^{(\alpha)}$ from (5.12) and the $\hat{N}$ unknowns $\hat{K}_T^{(\gamma)}$ from (5.13), respectively. When the $\hat{K}_S^{(\alpha)}$ and the $\hat{K}_T^{(\gamma)}$ have been determined, the near field radiating solution is known.

6. Quality Factor Resulting from Radiation

In this section we calculate the Q due to radiation into the semiconductor wafer from the analyses presented in the previous sections. In accordance with Secs.3 - 5 it is clear that in the untrapped case the perturbation integral takes the form

$$H_\mu = \int_{-w}^{w} dx_2 \Big[\int_{-h^s}^{o} [-\hat{u}_3^S T_{13}^s + \hat{T}_{11}^s g_1^s)_{x_1=d} + (\hat{u}_3^S T_{13}^s - \hat{T}_{11}^S g_1^s)_{x_1=-d}] dx_3 \Big]$$

$$+ \int_{-d}^{d} dx_1 \Big[\int_{-h^s}^{o} [-\hat{u}_3^T T_{23}^s + \hat{T}_{22}^T g_2^s)_{x_2=w} + (\hat{u}_3^T T_{23}^s - \hat{T}_{22}^T g_2^s)_{x_2=-w}] dx_3 \Big] , \tag{6.1}$$

while in the trapped case the integral from -w to w is replaced by integrals from -w to -b and -b to b and b to w and the integral from -d to d is replaced by integrals from -d to $-\ell$ and $-\ell$ to ℓ and ℓ to d, in accordance with the solution in (3.17) and the expressions for u_1^s and u_2^s given and discussed at the end of Sec.3. Substituting the

imaginary parts of the solutions determined in Secs.3 and 5 into (6.1) for the untrapped case and into the equivalent integral for the trapped case and performing the integrations, we obtain

$$H_\mu = \frac{1}{N_\mu}\left[\bar{\xi}\sin\bar{\xi}d\left(w + \frac{\sin 2\bar{\nu}w}{\bar{\nu}}\right)\sum_{\alpha=1}^{\hat{N}}\hat{K}_S^{(\alpha)}\left(H_1^{(\alpha)} + \frac{H_2^{(\alpha)}}{\zeta^S}\right)\right]$$
$$+\bar{\nu}\sin\bar{\nu}w\left(d + \frac{\sin 2\bar{\xi}d}{\bar{\xi}}\right)\sum_{\alpha=1}^{\hat{N}}\hat{K}_T^{(\alpha)}\left(H_1^{(\alpha)} + \frac{H_2^{(\alpha)}}{\zeta^T}\right)\Bigg] \qquad (6.2)$$

in the untrapped case and

$$H_\mu = \frac{1}{N_\mu}\Bigg(\frac{\xi\cos\bar{\xi}\ell}{\sinh\xi(d-\ell)}\left[b + \frac{\sin\bar{\nu}b}{\bar{\nu}} + \frac{1}{2\nu}\left(\frac{\cos\bar{\nu}b}{\sinh\nu(w-b)}\right)^2\right.$$
$$\left.\times\left[\sinh 2\nu(w-b) - 2\nu(w-b)\right]\right]\sum_{\alpha=1}^{\hat{N}}\hat{K}_S^{(\alpha)}\left(H_1^{(\alpha)} + \frac{H_2^{(\alpha)}}{\zeta^S}\right)$$
$$+\frac{\nu\cos\bar{\nu}b}{\sinh\nu(w-b)}\left[\ell + \frac{\sin\bar{\xi}\ell}{\bar{\xi}} + \frac{1}{2\xi}\left(\frac{\cos\bar{\xi}\ell}{\sinh\xi(d-\ell)}\right)^2\right.$$
$$\left.\times\left[\sinh 2\xi(d-\ell) - 2\xi(d-\ell)\right]\right]\sum_{\alpha=1}^{\hat{N}}\hat{K}_T^{(\alpha)}\left(H_1^{(\alpha)} + \frac{H_2^{(\alpha)}}{\zeta^T}\right)\Bigg) \qquad (6.3)$$

in the trapped case, where

$$H_1^{(\alpha)} = c_{44}\Bigg[A_3^{s1}\sum_{m=1}^{2}\Big[\hat{A}_{3\alpha}^{sm}g_c(\hat{\eta}_{sm}^{\alpha},\eta_s^o)_{-h^s} - \hat{A}_{3\alpha}^{sm^*}g_c(-\hat{\eta}_{sm}^{\alpha^*},\eta_s^o)_{-h^s} + \hat{B}_{3\alpha}^{sm}g_c(-\hat{\eta}_{sm}^{\alpha},\eta_s^o)_{-h^s}$$
$$- \hat{B}_{3\alpha}^{sm^*}g_c(\hat{\eta}_{sm}^{\alpha^*},\eta_s^o)_{-h^s}\Big] + B_3^{s1}\sum_{m=1}^{2}\Big[\hat{A}_{3\alpha}^{sm}g_s(\hat{\eta}_{sm}^{\alpha},\eta_s^o)_{-h^s} - \hat{A}_{3\alpha}^{sm^*}g_s(-\hat{\eta}_{sm}^{\alpha^*},\eta_s^o)_{-h^s}$$
$$+ \hat{B}_{3\alpha}^{sm}g_s(-\hat{\eta}_{sm}^{\alpha},\eta_s^o)_{-h^s} - \hat{B}_{3\alpha}^{sm^*}g_s(\hat{\eta}_{sm}^{\alpha^*},\eta_s^o)_{-h^s}\Big]\Bigg],$$

$$H_2^{(\alpha)} = \Bigg[\sum_{m=1}^{2} \hat{\tau}_{5\alpha}^{sm} \Big[A_1^{s1} g_s(\hat{\eta}_{sm}^{\alpha}, \eta_s^o)_{-h^s} + A_1^{s2} g_s(\hat{\eta}_{sm}^{\alpha}, \varkappa\eta_s^o)_{-h^s} + B_1^{s1} g_c(\hat{\eta}_{sm}^{\alpha}, \eta_s^o)_{-h^s}$$

$$- B_1^{s2} g_c(\hat{\eta}_{sm}^{\alpha}, \varkappa\eta_s^o)_{-h^s} \Big] - \hat{\tau}_{5\alpha}^{sm*} \Big[A_1^{s1} g_s(-\hat{\eta}_{sm}^{\alpha*}, \eta_s^o)_{-h^s} + A_1^{s2} g_s(-\hat{\eta}_{sm}^{\alpha*}, \varkappa\eta_s^o)_{-h^s}$$

$$+ B_1^{s1} g_c(-\hat{\eta}_{sm}^{\alpha*}, \eta_s^o)_{-h^s} + B_1^{s2} g_c(-\hat{\eta}_{sm}^{\alpha*}, \varkappa\eta_s^o)_{-h^s} \Big] + \hat{\sigma}_{5\alpha}^{sm} \Big[A_1^{s1} g_s(-\hat{\eta}_{sm}^{\alpha}, \eta_s^o)_{-h^s}$$

$$+ A_1^{s2} g_s(-\hat{\eta}_{sm}^{\alpha}, \varkappa\eta_s^o)_{-h^s} + B_1^{s1} g_c(-\hat{\eta}_{sm}^{\alpha}, \eta_s^o)_{-h^s} + B_1^{s2} g_c(-\hat{\eta}_{sm}^{\alpha}, \varkappa\eta_s^o)_{-h^s} \Big]$$

$$- \hat{\sigma}_{5\alpha}^{sm*} \Big[A_1^{s1} g_s(\hat{\eta}_{sm}^{\alpha*}, \eta_s^o)_{-h^s} + A_1^{s2} g_s(\hat{\eta}_{sm}^{\alpha*}, \varkappa\eta_s^o)_{-h^s} + B_1^{s1} g_c(\hat{\eta}_{sm}^{\alpha*}, \eta_s^o)_{-h^s}$$

$$+ B_1^{s2} g_c(\hat{\eta}_{sm}^{\alpha*}, \varkappa\eta_s^o)_{-h^s} \Big] \Bigg] . \qquad (6.4)$$

Either Eq. (6.2) or (6.3) may now be used to calculate the Q from (2.6) Of course, as in the earlier work[1] all radiating plate waves in the thick region of the gallium-arsenide are included to achieve accuracy. Since at a given frequency the number of radiating waves in a plate goes up significantly with thickness, when trapping is not present we have considered gallium-arsenide wafers no thicker than 8 mils at a frequency around 132 MHz, for which there are 30 radiating plate waves. Results are presented for wafer thicknesses ranging from 4 mils to 8 mils because this is considered to be within the practical range. For the untrapped case the results presented are for a film thickness of 7 microns and a diaphragm thickness of 14 microns. Both strip diaphragms 600 microns wide and square diaphragms with lateral dimensions of 600 microns × 600 microns were considered. The strips are treated for comparison with the earlier work[1]. The results can readily be obtained for the strip case from the analysis for the

rectangular case simply by allowing w and b to get very large compared with ℓ and d, for which $\bar{\nu} \to 0$ and the C and T regions are eliminated as is radiation in the x_2-direction. For the trapped case the results presented are for a film thickness of 12 microns and a diaphragm thickness of 14 microns because the trapping is considerably better for this combination of thicknesses and trapping does not exist for the other at the second thickness mode[5]. For this combination of thicknesses the second thickness mode is around 250 MHz. In the trapped case both strip electrodes 500 microns wide and square electrodes with lateral dimensions of 500 microns × 500 microns were considered. The lateral dimensions of both the strip and square diaphragms was varied and the wafer thickness is 6 mils.

In the absence of trapping for the strip case the values of Q calculated from Eq.(2.6) of this work are plotted as the solid curve in Fig.5, in which the dotted curve from Fig.8 of Ref.1 is also plotted for purposes of comparison. It can be seen from the figure that the agreement is quite good. However, although the highest Q's calculated in this work are very nearly the same as those obtained in the earlier more cumbersome direct calculation[1], the lowest Q's calculated by means of the perturbation procedure tend to be nearly an order of magnitude higher than those calculated by the earlier direct procedure[1]. We are not absolutely sure of the reason for this discrepancy, but there are two possibilities. The perturbation procedure might be tending to lose its accuracy for low Q because of the increased radiation or the resonant frequency might not have been sufficiently precisely determined by means of the earlier direct procedure[1] for the accurate determination of the lowest Q values.

However, Fig.5 reveals that the highest Q's calculated by the perturbation procedure are consistently slightly higher than those calculated using the earlier direct procedure, which tends to support the second possibility. The figure also shows that the location of the peaks and valleys of Q with wafer thickness determined by means of the perturbation procedure is in quite good agreement with those obtained from the earlier direct calculation[1]. Also,in the absence of trapping the Q's calculated from Eq.(2.6) for the square diaphragm are plotted in Fig.6. It can be seen from the figure that the peaks and valleys are in essentially the same positions as in the strip case, but that the Q's are considerably lower, roughly between 1/2 to 2/3 of the values in the strip case. This is as expected because of the radiation in two orthogonal directions for rectangular diaphragms. When trapping is present the Q's calculated from Eq.(2.6) for both the strip and square case are plotted in Fig.7 as a function of $(d - \ell)$, i.e., the distance from the edge of the electrode to the edge of the diaphragm. It can be seen from the figure that, as expected, Q increases very rapidly with $(d - \ell)$ and for the same value of $(d - \ell)$ the Q is about twice as large in the strip case as in the rectangular case. If a film thickness of, say, 8 microns had been employed, the required $(d - \ell)$ for good Q would be much larger because although trapping is present for that ratio of thicknesses, the dispersion curve for the trapped mode, i.e., the value of M_n, indicates that the spatial decay rate at resonance is much slower than for the ratio of thicknesses considered here.

Acknowledgements

We wish to thank Y.S. Zhou for help with the calculations.

This work was supported in part by the Air Force Office of Scientific Research under Grant No. AFOSR-84-0351.

REFERENCES

1. D.V. Shick, D.S. Stevens and H.F. Tiersten, "Quality Factor of the Piezoelectric Thin Film on Semiconductor Composite Resonator Resulting from Radiation into the Semiconductor Wafer," J. Appl. Phys., 60, 2238 (1986).

2. H.F. Tiersten and D.S. Stevens, "An Analysis of Thickness-Extensional Trapped Energy Resonant Device Structures with Rectangular Electrodes in the Piezoelectric Thin Film on Silicon Configuration," J. Appl. Phys., 54, 5893 (1983).

3. H.F. Tiersten, Linear Piezoelectric Plate Vibrations (Plenum, New York, 1969), Chap.6, Sec.4

4. H.F. Tiersten and B.K. Sinha, "A Perturbation Analysis of the Attenuation and Dispersion of Surface Waves," J. Appl. Phys., 49, 87 (1978).

5. In Ref.1 it incorrectly states that the second thickness-extensional mode will trap for any ratio of film thickness to diaphragm thickness for aluminum-nitride on gallium-arsenide. It will trap for ratios of film thickness to diaphragm thickness larger than .69.

6. Ref.1, Eq.(16).

7. Since constraint-type conditions arise in (2.5) as natural conditions because of the use of Lagrange multipliers, the approximating functions need not satisfy them when (2.5) is employed.

8. In Eq.(4.37) of Ref.2 the expression $n_{14} = (c_{33}^f r^f - c_{13}^f)\cos \eta_{f2} h_f$ was inadvertently omitted.

9. Ref.3, Chap.5, Sec.4, Chap.15, Sec.5.

10. B.A. Auld, Acoustic Fields and Waves in Solids (Wiley, New York, 1973), Vol.I, p.210.

11. For radiation in the x_2-direction the subscripts 1 and 2 are interchanged throughout the explanation.

12. The sign of the wavenumber $\hat{\xi}$ for each wave is selected so as to correspond to radiation in the $+ x_1$-direction.

FIGURE CAPTIONS

Figure 1 Cross-Section of a Composite Resonator

Figure 2 Plan View of Model for Analyses of Composite Resonator Mode Shapes

Figure 3 Cross-Section for Variational Analysis of Radiation into Wafer

Figure 4 Dispersion Curves for the Gallium-Arsenide Wafer with Ω the Dimensionless Frequency Normalized with Respect to the First Thickness-Shear Frequency

Figure 5 Quality Factor Versus Wafer Thickness when Trapping is not Present for the Strip Composite Resonator. The dotted curves are from Fig.8 of Ref.1.

Figure 6 Quality Factor Versus Wafer Thickness when Trapping is not Present for the Rectangular Composite Resonator

Figure 7 Quality Factor Versus Distance from Edge of Electrode to Edge of Diaphragm when Trapping is Present

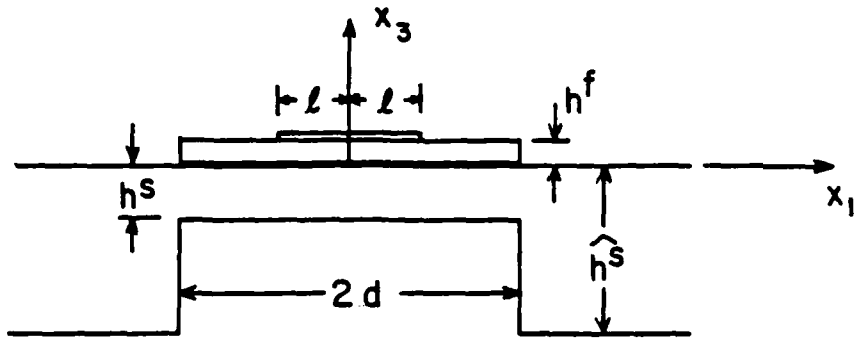

Figure 1

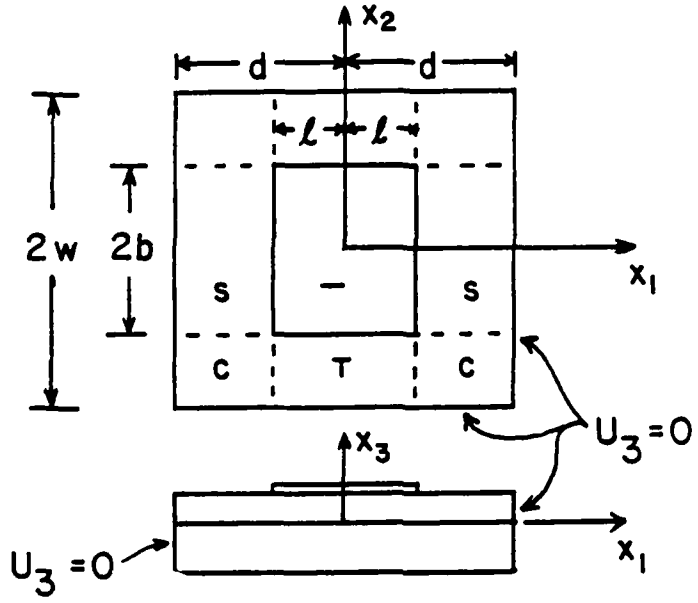

Figure 2

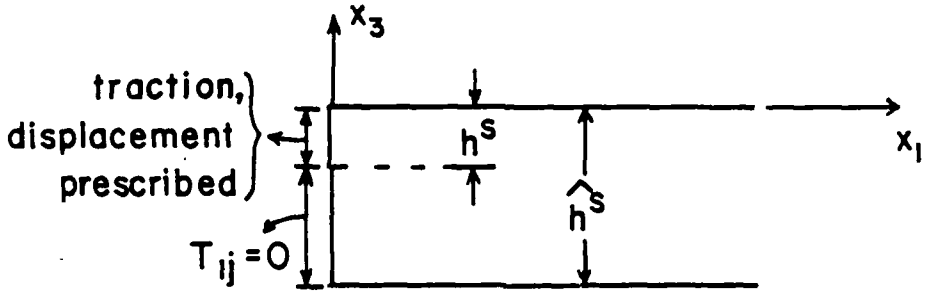

Figure 3

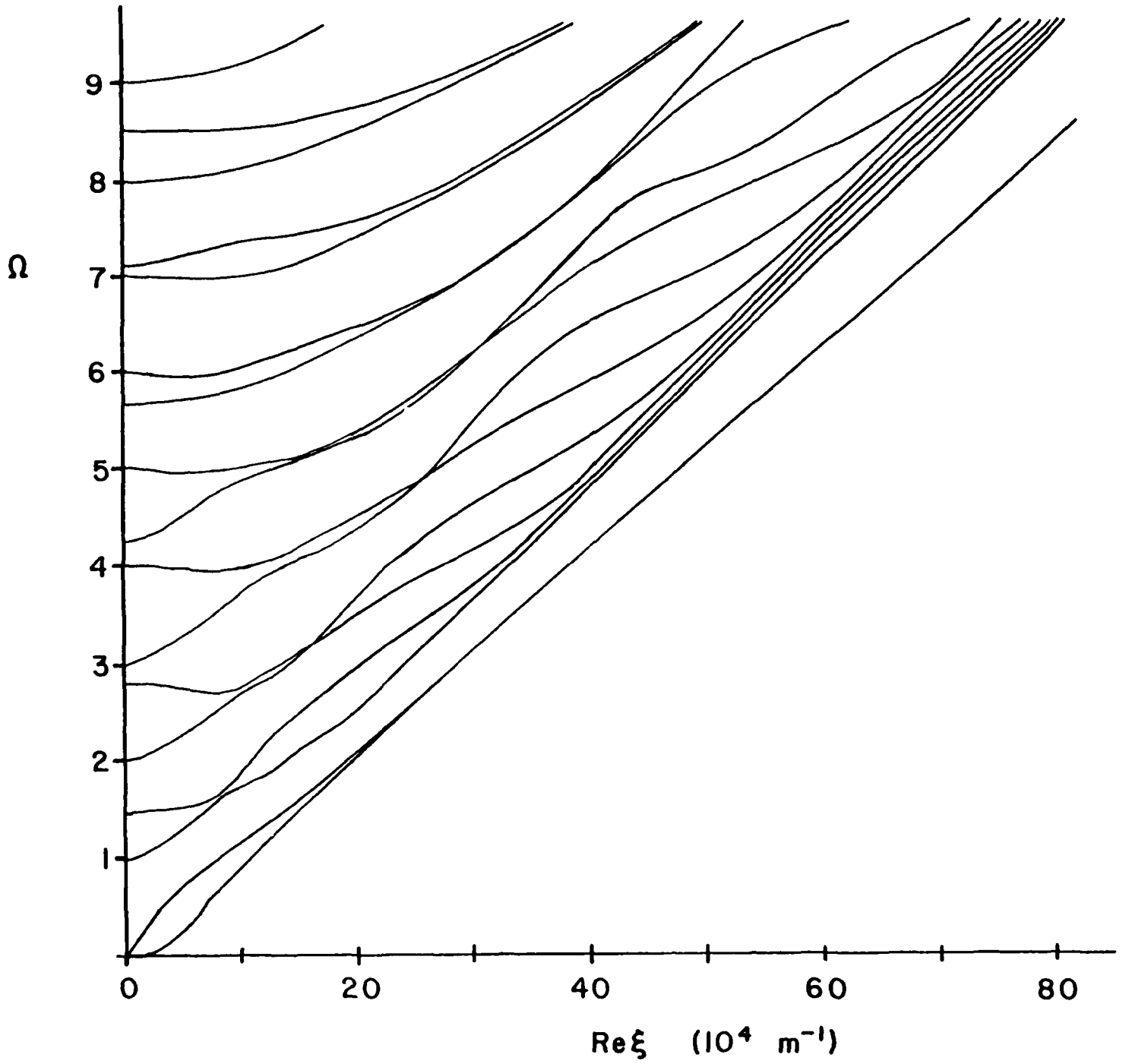

Figure 4

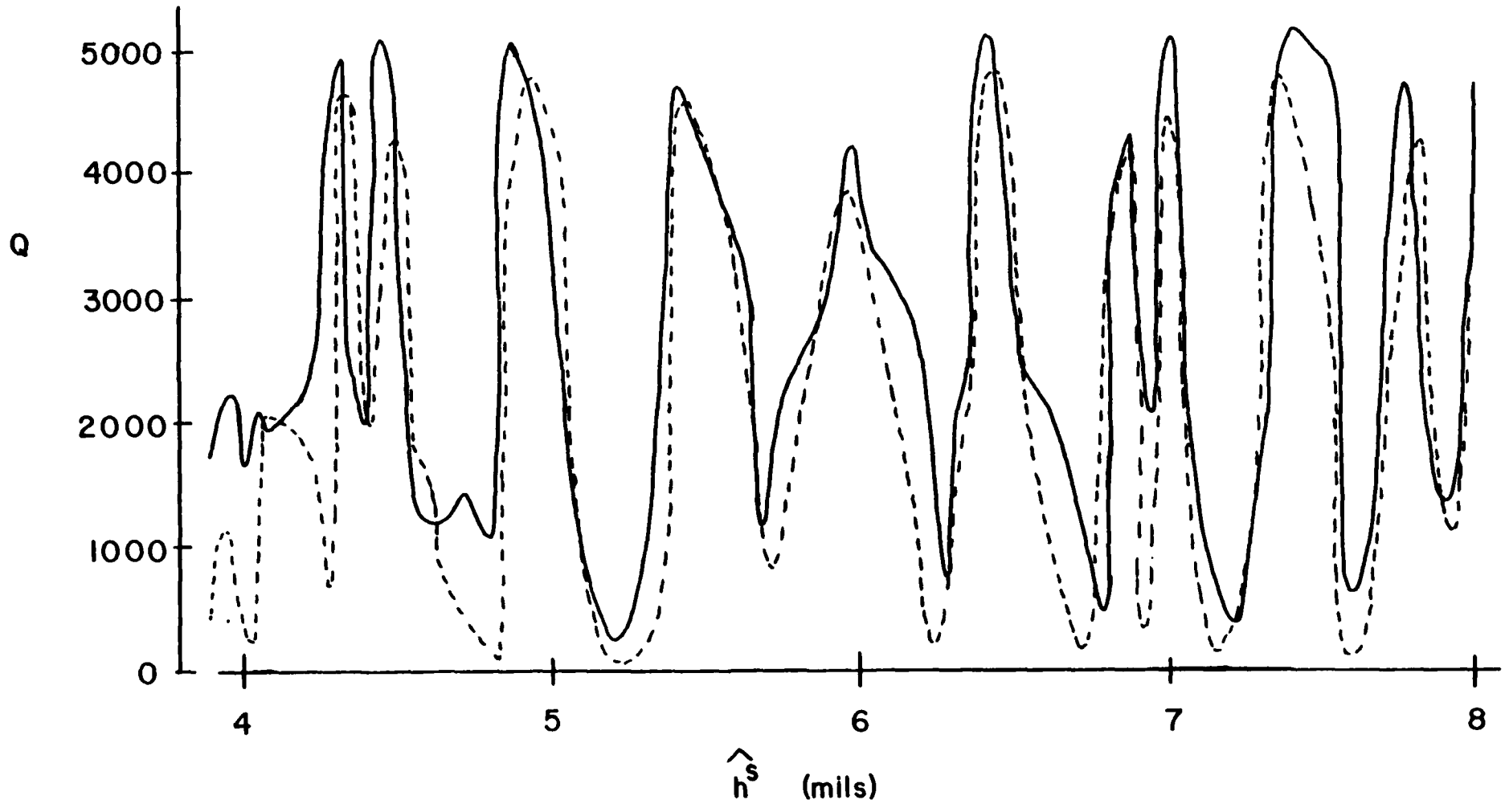

Figure 5

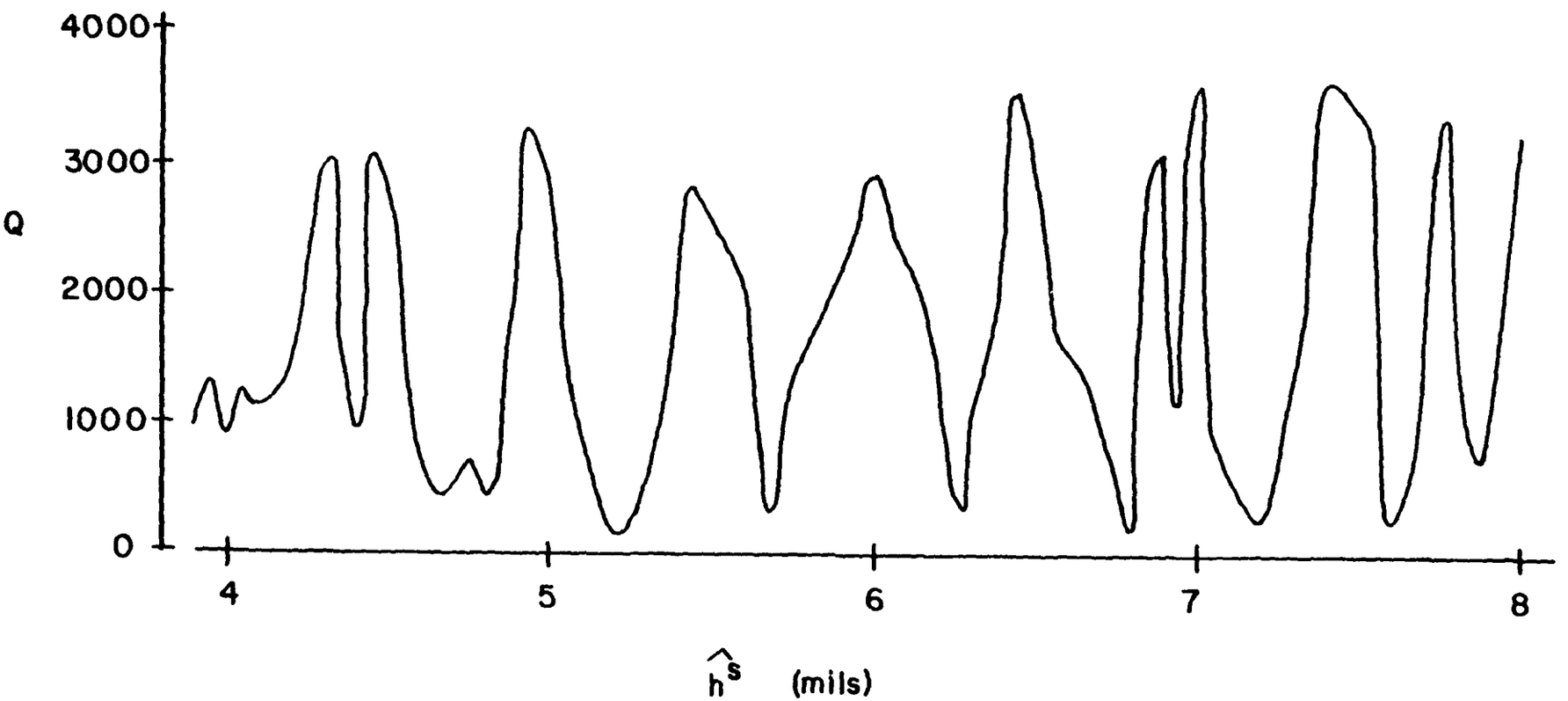

Figure 6

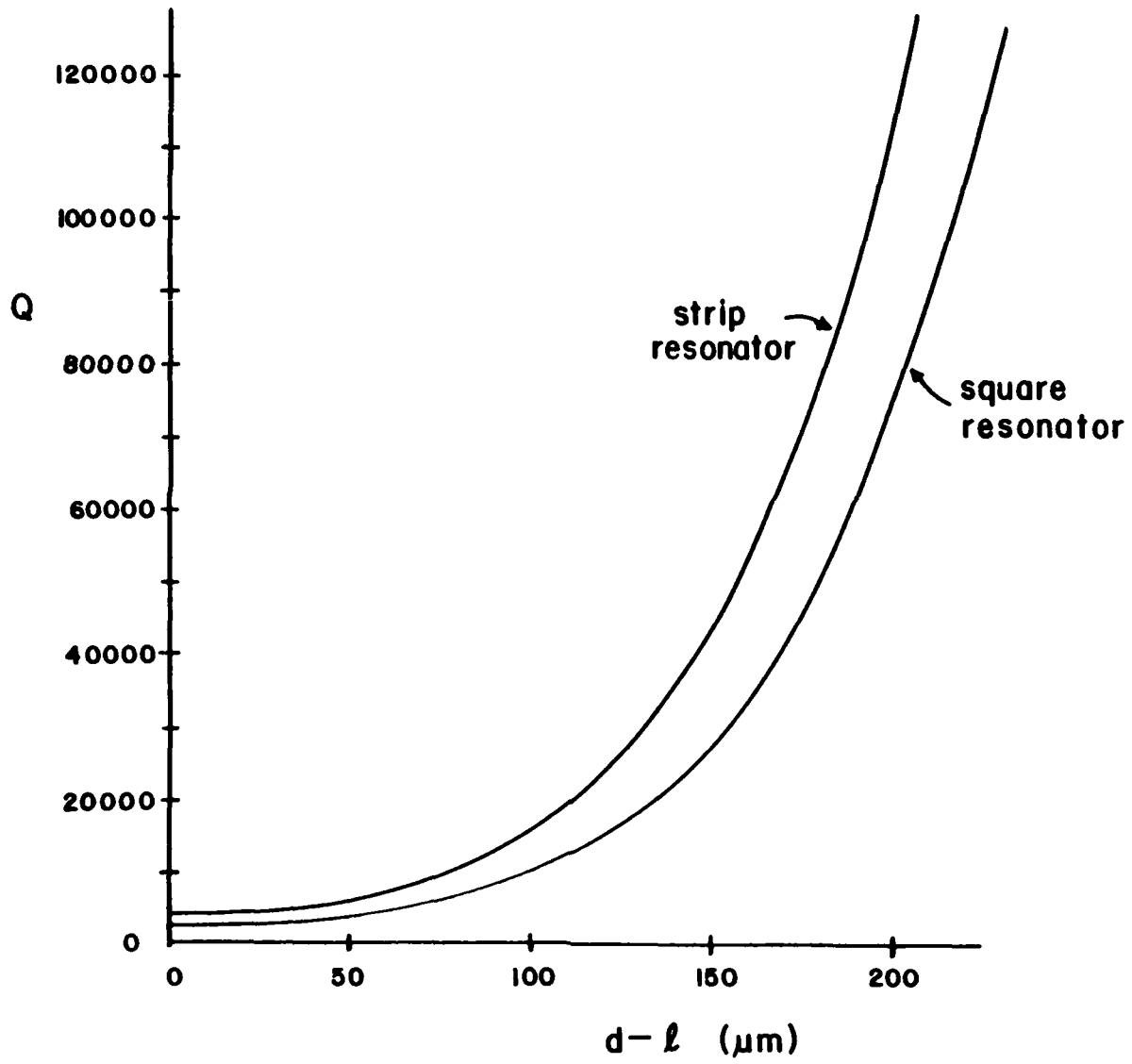
120000
100000
Q
80000
60000
40000
20000
0
0
50
100
150
200
d − ℓ (μm)
strip resonator
square resonator

Figure 7

END

12-87

DTIC